January 2021

Electrospray Deposition of ZnO Nanostructures for Nanoscale Electronic Applications

David Hooks

ELECTROSPRAY DEPOSITION OF ZNO NANOSTRUCTURES AND THEIR APPLICATIONS TO NANOSCALE ELECTRONIC DEVICES

A Thesis

Submitted to the Graduate Faculty of the
Louisiana State University and
Agricultural and Mechanical College
in partial fulfillment of the
requirements for the degree of
Master of Science in Electrical Engineering

in

The Division of Electrical and Computer Engineering

by
David Michael Hooks
B.S., University of Louisiana at Lafayette
May 2021

Dedicated to my Mom and Dad, Pam and Ryan Hooks

Acknowledgments

I would like to thank Dr. Daniels-Race for allowing me to conduct research in the field of semiconductor electronics and also for all of her help throughout my years as a graduate student, constantly encouraging me and helping me along the way.

I would also like to thank each member of my committee: Dr. Feldman, Dr. Park, and Dr. Vaidyanathan for allowing me their time to defend my research.

I am also very appreciative of all of the help in the lab from fellow group-member Alex Young for working closely with me in the lab and making suggestions to help improve my experiments.

I would also like to thank Mr. Christopher O'Loughlin, whose help was paramount in completing this work. He helped me in many facets throughout the project, I am extremely grateful for his help and friendship.

Lastly, I would like to thank my family, for their constant encouragement and understanding.

TABLE OF CONTENTS

LIST OF TABLES

LIST OF FIGURES

Abstract

Modern technology is ever-evolving and as more emphasis is placed on faster, more sensitive electronic devices, advancements in the field of electronics are as important now as they ever have been. To meet the need for more sensitive devices, it is important to study new semiconducting materials and the applications in which they pose a potential advantage.

The field of electronic materials research falls at the intersection of physics, chemistry, materials science, and electrical engineering. Zinc Oxide (ZnO) is of particular interest in modern electronic devices for its uses in sensing applications, high-powered transistors, and LED technology. ZnO has been compared to Gallium Nitride (GaN) which is a common compound semiconductor used in high-powered transistors because of its high bandgap energy. Most techniques for depositing ZnO films are heavily dependent on high vacuum, temperature-controlled environments. However, electrospray deposition has shown potential to be a way of depositing ZnO films removed from highly controlled environments.

Zinc Acetate dihydrate (ZnAc) is a common precursor material used to form ZnO thin films. This research investigates the formation of ZnO nanostructures from the aforementioned precursor and the delivery of the material via electrospray deposition onto silicon substrates. Several different spray modes were studied over the course of this project, with each being quantified by their onset characteristics and their resultant nanoparticle size. The effect of substrate rotation was observed and quantified by their resultant film thickness and surface coverage.

Raman spectroscopy was the method by which it was observed that ZnO was successfully deposited and scanning electron microscopy was used to characterize nanoparticle sizes and surface thicknesses. For observation of the spray modes used, a Sony RX-II camera was used to capture images of the resulting meniscus deformation.

CHAPTER I. OVERVIEW OF CHAPTER CONTENT

The purpose of this chapter is to lay out the outline of the chapter content in the chapters to follow.

Chapter 2: “Research Motivation” will discuss the underlying motivations for undertaking the research that was subsequently carried out. The primary goal for the research was to demonstrate that electrospray deposition was a viable method for depositing ZnO films onto silicon substrates. In addition to studying the electrosprayed films, the characteristics of the nanostructures formed under different heating conditions was also studied. The depositions under different spray modes were also observed, as well as the conditions under which the depositions occurred.

Chapter 3: “Background and Overview of ZnO” provides a literature review spanning the fundamentals of ZnO, to techniques for achieving thin films and nanostructures, and the subsequent characterization of these films and nanostructures.

Chapter 4: “Background and Overview of Electrospray Deposition” lays out a framework for the deposition technique used in this research via studying the fundamentals of electrospray and the applications of electrospray deposition in the realm of electronic materials and devices.

Chapter 5: “Development of Novel Electrospray Setup” discusses the various subsystems of the electrospray setup used and their subsequent integration into a cohesive piece of equipment. Of those subsystems, a motor-driving printed circuit board was constructed for substrate rotation for the purpose of achieving a controllable, uniform deposition pattern. The frame was constructed from metal t-slot with custom-mounting for installing the motor normal to the syringe-pump.

Chapter 6: “Experimental Results and Discussion” details the research carried out over the course of the project. A detailed discussion is provided on verifying that ZnO was successfully obtained from annealing the ZnAc (Zinc Acetate dihydrate) precursor, the size and characteristics

of the nanostructures formed under various annealing conditions and under different spray modes, the formation of the meniscuses under different voltages and flow rates, and the films thicknesses obtained under different rotational velocities.

Chapter 7: “Future Work” provides a discussion on potential future avenues for this project. One such area is for the fabrication of gas sensors, electrospray can be employed to rapidly achieve semiconducting, chemosensitive layers for the detection of various target gases.

CHAPTER II. MOTIVATION AND RESEARCH GOALS

Zinc Oxide (ZnO) is a wide bandgap semiconductor with properties that have brought about comparisons between it and GaN, a compound semiconductor used in high-power transistors. ZnO has shown promise in recent years for its use as a semiconductor, a chemosensitive layer, and in LED and TCO (transparent conducting oxides) technologies. LEDs are of particular promise given ZnO's high room-temperature exciton binding energy. Due to the highly-controlled conditions typically used to deposit ZnO films, electrospray poses a unique advantage in that it does not need to be conducted in such environments. To uncover the feasibility of using electrospray for depositing ZnO films, experiments need to be conducted in order to quantify these depositions under different rotational speeds and with differing needle diameters (effecting spray mode onset).

To understand the impact of rotating the substrate during deposition and its impact on film thickness, experiments were carried out to quantify this effect. Before the effect of the substrate rotation could be studied, a stable ZnO suspension needed to be obtained. After several iterations of different suspensions, ZnAc suspended in a solvent of ethanol, polyethylene glycol, and NaOH resulted in the highest quality depositions. After successfully depositing ZnO precursor onto silicon substrates, characterization of these samples and sprays were conducted via scanning electron microscopy (SEM), Raman spectroscopy, and a high-speed camera (Sony RX-II).

The primary goal of the following research was to provide a method of depositing ZnO films via electrospray and to show the effect of substrate rotation and post-depositing annealing on nanostructure size and formation, as well as film thickness and surface coverage. Secondary to the former goal was to quantify the effects of flow-rate and applied voltage on the formation of the Taylor Cones that form during the deposition process. Attaining an understanding of this effect allows one to further control the depositions.

CHAPTER III. INTRODUCTION AND LITERATURE REVIEW OF ZNO

3.1. Basic Properties of ZnO

Zinc Oxide (ZnO) is a well-known semiconductor with a myriad of applications ranging from electronics to additive manufacturing in printed GHz devices [1], 3-D metal-oxide structures [2-4], and flexible photodetectors [5] to sunscreen agents [6]. This II-VI compound is inherently n-type with a direct bandgap of 3.3 eV and high exciton binding energy of 60 meV at room temperature. [7] ZnO exhibits both opto-electronic and piezoelectric properties with the added benefit of being readily available. Thus, in recent years ZnO based research has been fairly extensive. The compound's wide bandgap has potential application to high power transistors while its optical properties have been studied with respect to light-emitting diodes and laser technologies such as strain-sensitive LED-arrays for pressure sensing and pn junction excimer lasers. [8,9]

As engineering researchers have focused upon the electrical and optical device applications of ZnO, an interesting point of contention exists among many studying this material with respect to its inherent n-type nature. The most widely held view is that ZnO is n-type due to oxygen vacancies and zinc interstitials in the crystal lattice. [10] Electron mobility as high as 2000 cm^2/Vs at 50^o K has been reported for ZnO crystals grown from bulk material [11, whereas this figure drops to as low as 205 cm^2/Vs at room temperature. [12] ZnO nanoparticles exhibit electron mobility of approximately 5×10^{-3} cm^2/Vs for nanoparticles of about 3 nm in diameter. [13] There is comparatively little information on p-type doping. With respect to optical properties, the photoluminescence of ZnO is a promising characteristic for the aforementioned LED and laser applications. A strong emission peak at 380 nm [14-15] is attributed to the radiative recombination of holes and electrons. [16] A green (electromagnetic spectrum) emission peak has been observed via PL spectroscopy at approximately 500 nm due to oxygen vacancies in the lattice structure.

These visible spectra characteristics demonstrate that ZnO can be used for LED and laser technologies. ZnO/GaN heterojunctions have been used for the creation of white LEDs via their annealing-dependent emission characteristics. [17] ZnO has been investigated greatly in LED technologies primarily because of its high room-temperature exciton binding energy (60 meV) relative to its thermal energy at room temperature conditions.

ZnO has been shown to exist in three primary crystal structures as follows: cubic rock-salt, hexagonal Wurtzite, and cubic zinc-blende. Cubic rock-salt cannot be stabilized for growth as an epitaxial layer to serve as a substrate. Hence, the discussion here will be limited to hexagonal wurtzite and cubic-zinc blende. For stability of the cubic zinc-blende stage, [12] ZnO must be grown on the surface layer of a cubic crystal substrate such as Si, GaAs, or SiO_2. The wurtzite structure is characteristic of defect-laden substrate mismatched depositions. Figure 3.1. shows a visual representation of the different morphologies.

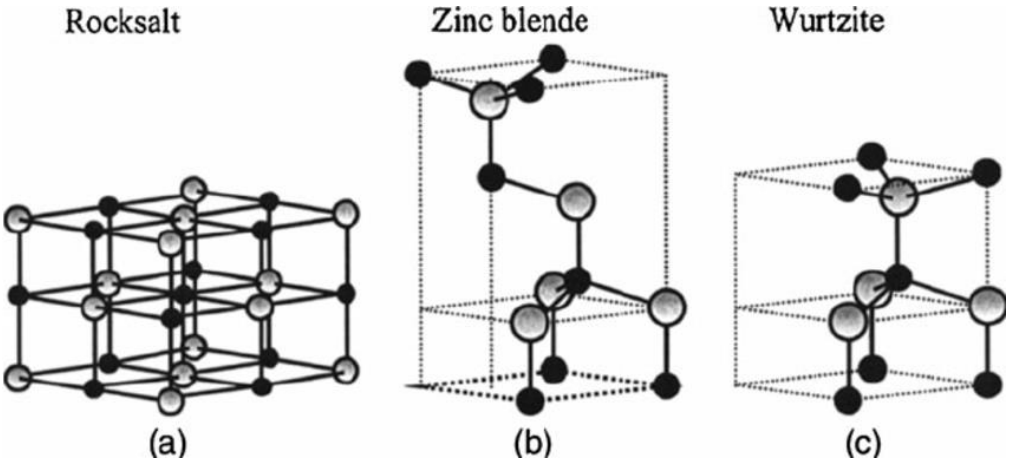

Figure 3.1. Three different ZnO morphologies, reprinted with permissions from [12]. Copyright 2008, Wiley & Sons

The native n-type doping, as previously mentioned, has been largely attributed to oxygen vacancies and zinc interstitials. Oxygen vacancies occur when particular oxygen atoms are absent from the

lattice structure. Zinc interstitials occur when the zinc atoms do not "sit" exactly where they should in the crystal lattice and instead exist outside of the lattice position that they should normally occupy. For each oxygen vacancy, two free electrons are left behind via dangling bonds from zinc atoms. [18] Zinc interstitials occur when excess zinc atoms move into vacant (interstitial) sites. In ZnO, two electrons are pulled in from neighboring atoms to compensate for the two acceptor states carried by the zinc atom. Though still the most widely held convention, there has been considerable contemporaneous literature arguing that the n-type nature of ZnO cannot be attributed to the native crystal defects [18] but instead to the incorporation of hydrogen into the lattice structure [19-20]. Hydrogen is widely known as an amphoteric dopant which indicates that it can behave as an acceptor or a donor. In ZnO, the hydrogen acts exclusively as a donor. [20]

3.2. ZnO Growth and Preparation Techniques

Zinc Oxide has been grown via many different techniques considering that research into ZnO has been prevalent since the early 2000's. These techniques include but are not limited to: Chemical Vapor Deposition (CVD), Molecular Beam Epitaxy (MBE), Thermal Physical Vapor Deposition (T-PVD), Atomic Layer Deposition, Magnetron Sputtering, Electrophoresis (EPD), and Electrospray Ionization (ESI). In the following subsections, the techniques of CVD, MBE, ALD, Magnetron Sputtering, and Sol-Gel techniques will be discussed.

3.2.1. Chemical Vapor Deposition

Chemical vapor deposition (CVD) is a high-vacuum deposition technique which involves injecting vaporized material into a deposition chamber where molecules adsorb onto a target substrate, with the waste gases filtered out of the chamber. [21] Some CVD processes are carried out at atmospheric pressure (AP-CVD), with others at low-vacuum (LV-CVD) (~ 10^{-6} Pa) and ultra-high vacuum (UHV-CVD) (~ 10^{-8} Pa). CVD techniques have been used extensively in the

deposition of ZnO. [22-25] CVD typically involves the use of volatile precursor materials. However, CVD methods using soluble materials instead of volatile precursors have been developed such as Aerosol Assisted CVD (AA-CVD). [26] ZnO thin-film depositions usually involve a Zn based precursor material interacting with some dopant material inside of the reaction chamber [16,17]. Special care must be used when considering which chambers should be proximal to one another and which should be separated. If one were introducing gaseous donors and acceptors, sufficient care would need to be given to keep the two separated. Once the desired chamber conditions are met, the constituent gases are pumped into the chamber with N_2, the substrate is then heated until the precursors have been exhausted and the waste gases have been pumped out. N_2 serves the dual purpose of pumping out any remaining gases and cooling the substrate. Successful deposition and control of ZnO surface morphology have been demonstrated using AP-CVD with increased film quality when heating substrates to temperatures greater than 450^{o} C. [17] Metal-Organic CVD (MO-CVD) has been used for the deposition of ZnO and the creation of ZnO nanostructures on silicon substrates [18,19], which involved heating of p-type Si to temperatures exceeding 500^{o} C for the growth of nanorods [18] and $350\ ^{o}$ C for thin films containing quantum dots. [19]

3.2.2. Molecular Beam Epitaxy

Molecular Beam Epitaxy (MBE) is a deposition technique involving the precise control of temperature and pressure inside the deposition chamber, with pressures ranging from high-vacuum (10^{-6} to 10^{-8} torr) to the ultra high-vacuum (UHV) range (as low as 10^{-11} torr). [26] Samples are loaded into an MBE system via a load lock that requires bringing this portion of the MBE chamber up to atmospheric pressure (i.e. up-to- air). The load lock is then “pumped down” to the high vacuum range. At the opposite end of the MBE system is the growth chamber. The load lock and

growth chamber may be separated by a single gate valve or, more likely, one or more of a series of preparation and/or analysis chambers, each of which may be atmospherically isolated from one another. The growth chamber contains effusion cell, also known as Knudsen cells which hold the source materials used in the growth process. [26] These Knudsen cells are a type of effusion evaporator where solid source materials are heated and then sublime (from solid to the gaseous phase) into the deposition chamber. Effusion itself is a process whereby a small hole is introduced into an otherwise sealed container of gas. If the diameter hole is smaller in size than the mean free path of the gas molecules, a pressure difference is created, and the molecules begin exiting the container through this hole. Once the gas molecules begin to exit the Knudsen cells, they flow into the growth chamber, which contains the substrate, where they are adsorbed onto this substrate (desorption can also occur). This adsorption then leads to the creation of small islands that eventually grow and spread across the substrate (growth) surface. The UHV environment, positioning of the Knudsen cells (with respect to the target substrate), and temperature settings (source material, substrate) in MBE allow for precise control of the deposition rate. Carrier gases are not needed to move the sublimated gas molecules to the substrate, and thus low impurity levels are achieved. For the MBE deposition of ZnO, zinc is placed into a Knudsen cell alongside any additional dopants placed in their own respective Knudsen cells. Aluminum for instance is a common dopant and has been used as such in ZnO depositions [27] with the oxygen component coming from an RF controlled oxygen radical beam. The quality of the deposition is monitored via a RHEED system (Reflective High-Energy Electron Diffraction) where a beam of electrons is aimed at at a shallow grazing angle incident to the substrate surface. The reflected (or arguably refracted) beam then impinges upon a detector. The intensity of the reflected beam changes as

more material gathers on the substrate surface and these changes are used to generate an image indicating the surface features.

3.2.3. Atomic Layer Deposition

Atomic Layer Deposition (ALD) is a process involving the deposition of individual layers of material by feeding in precursor materials (volatile liquids, gases, or solid materials [28]) in sequences onto a pre-functionalized substrate (hydroxyl groups are formed). ALD allows for precise layer control at low temperatures (< 350^{o} C) and pressures (< 1 torr) [29] by depositing materials one monolayer at a time. After the initial monolayer is formed on the functionalized surface, a metal-oxide layer is formed. Following this initial step, the chamber is then purged of the waste and unreacted gas-phase molecules to prepare for the next stage of deposition which follows the same procedure as the first. Each subsequent stage is set for the next material to be deposited, and this process is repeated as necessary. ZnO monolayers have been developed using this technique and because of the precise control of the layer growth, other factors have been able to be studied in detail. It has been determined, for example, that in thin film transistors (TFT's) the deposition temperature of the ZnO channel layer in ALD has a profound effect on the channel conductivity of the device. [30] It was observed that for temperatures varying from 100 to 170^{o} C at 1 V applied across the drain to source, the current was increased by approximately 4 orders of magnitude in the case of 170^{o} C. [30] ALD is a proven, robust technology that can be used for highly controlled, precise ZnO based depositions.

3.2.4. Magnetron Sputtering

Magnetron Sputtering (MS) is a subset of the broader Plasma Vapor Deposition technique. Plasma-based sputtering, in general, involves a plasma, a target, a high voltage source, and a substrate. Inside the deposition chamber, a large potential difference is applied between the target

and the plasma. As this potential is established, electrons begin to flow from the lower potential to the higher potential (cathode to anode) and for sufficiently high voltages, the electrons begin to ionize the gas molecules in the chamber. Once the gas molecules become ionized, positively charged, they begin to flow toward the cathode where they collide with the target. Upon collision, atoms from the target are knocked loose, as are secondary electrons. These atoms from the target are then sent via collision and negative pressure toward the substrate where they are deposited. [31] The contribution of the magnetron comes in that it entraps electrons on the target. Traditional Magnetron Sputtering is limited to applications involving a conductive target, because without there being an electrical connection established, no current can flow. This led to the creation of Radio Frequency Magnetron Sputtering (RF-MS). RF-MS involves a sinusoidal voltage in the RF frequency regime, typically at about 13.56 MHz. [32] For a time-varying voltage, during the negative half-cycle, electrons travel from the target to the electrode which in turn causes the gas ionization and moreover the same process as described above. In the positive half-cycle, electrons flow toward the target, where they become entrapped on the target surface by the magnetron. This charging and discharging pattern on the target allows for non-conductive substrates to be used, as well as, conductive ones. There are 3 main control parameters associated with RF-MS which are input power, pressure, and temperature.

RF-Magnetron sputtering is often used for ZnO deposition onto insulating substrates such as glass or semiconducting substrates such as silicon. [32] In these cases, ZnO is used as the target materials and deposition takes place as the chamber is filled with Argon gas to facilitate the adsorption of the ZnO molecules onto the substrate.

3.2.5. Sol-Gel Method

A common issue with the deposition of ZnO thin films is the creation of a highly uniform colloidal suspension that readily adheres to the substrate. Sol-Gel's are composed of two parts: the sol, which is often the colloidal solution and the gel which is the gelatinous by-product of the process prior to post-treating with heat. There are three primary steps in the Sol-Gel method: hydrolysis, condensation, and drying. [33] The "Sol" is formed by the hydrolysis reaction with the precursor materials. In the case of ZnO, one of the most commonly used precursors is zinc acetate-dehydrate. When the zinc acetate dehydrate is combined with a solvent (combinations of alcohols and deionized water are common) to cause the hydrolysis reaction resulting in the "Sol". The sol is then deposited onto the substrate by whichever method the user chooses. This sol condenses onto the substrate as a heating pre-treatment is applied to the substrate resulting in solvent evaporation and formation of the "gel" or more specifically, the xerogel component. The final component of the Sol-Gel is the post-deposition annealing step used for drying which results in a crystallized, dense deposition. [34]

3.3. Properties and Applications of ZnO Nanostructures

ZnO nanostructures have interested researchers for decades and has recently had a resurgence because of its photoluminescent properties as well as applications with sensor technologies and power-transistors. The primary hurdle for wide-spread use of ZnO in power transistors is the lack of ways to effectively impose p-type doping. Heavily n-doped ZnO (usually Al doped ZnO) shows extensive promise as a Transparent Conducting Oxide (TCO) that may eventually "dethrone" Indium Tin Oxide (ITO) as the primary TCO. Recent studies have also examined the use of ZnO as a piezoelectric layer and its use in additive manufacturing. [35, 36] ZnO is widely produced,

cost-effective, and readily available in a variety of forms for purchase from various vendors thus making it a candidate for thin-films and nanoparticle-based depositions.

Characterization of ZnO nanostructures is most widely performed via Scanning Electron Microscopy (SEM) and Atomic Force Microscopy (AFM) for morphological studies and X-Ray Diffraction (XRD) for crystallographic studies. Spectroscopic studies give insight into the nature of the depositions and associated impurities and are typically done via Raman spectroscopy and fluorescence spectroscopy. As previously discussed, ZnO typically comes in two crystal structures. Hexagonal zinc-blende occurs in lattice matched depositions between the ZnO and substrate. The wurtzite occurs in non-lattice matched and impurity-laden depositions.

The photo-luminescent (PL) emission spectrum of ZnO ranges from the visible spectrum down to the near-visible UV wavelength range (~370-380 nm) where a strong emission peak exists. [37] The PL emission spectrum of ZnO can be shifted based on impurities in the solution or deposition, often described by the color of the wavelength range (e.g. red-shifted for spectra that are closer to the red end of the visible spectrum). There are several characteristic peaks in ZnO and each can be attributed to different physical processes. Some of the most commonly observed emission peaks occur in the following wavelength regions and can be ascribed to the processes as follows: UV (~ 380 nm) is due to excitonic recombination of excitons [37], green (~ 530 nm) is attributed to lattice vacancies of either zinc or oxygen, orange (~ 630 nm) is attributed to interstitial oxygen atoms, and red (~ 730 nm) is due to the incorporation of carbon into the lattice. [38] The large room-temperature excitonic binding energy (60 meV) is very promising for light-emitting semiconductor technology (e.g. LED's and photodetectors), measuring at over a factor of two larger than that of GaN (~ 25-28 meV). [31]

The piezoelectric properties of ZnO are also of great interest, as the piezoelectric coupling is high for zinc oxide (the ratio between the mechanical energy produced to the electrical energy applied). The piezoelectric coupling of ZnO is high because of the low symmetry of its wurtzite structure phase. [40] Piezoelectricity is a function of the balance of dipole moments in a crystal structure. Inducing a deformation upon the lattice results in a change in polarization that occurs due to an imbalance in the dipole moments. This deformation and thus change in polarization is what is described as piezoelectricity. Piezoelectric materials are often piezoelectric in specific directions depending on orientation which is to say that crystal structures tend to be piezoelectric along some axes, but not others. In the case of ZnO, this low-symmetry wurtzite structure requires less energy to change its polarization and essentially vibrate given its pre-disposition to being deformed. These properties make ZnO a good candidate for resonator technologies and acoustic sensors.

3.3.1. Applications of ZnO Nanostructures

ZnO is a ubiquitous semi-conducting material with several noteworthy properties that encompass many fields and industries. The wide bandgap of ZnO is widely noted for (3.37 eV) which is great interest for power applications and can be heavily n-doped such as in ITO (indium tin oxide) which is used in devices such as touchscreens for smart phones to high-definition monitors and screens in LCDs. The chemosensitive properties are well-documented in literature, in the form of sensing technologies and the resulting visible spectrum light emission of the chemosensitive layer can be advantageous for use in opto-electronic devices. Its mechanical properties, such as its great piezoelectricity, can be used for frequency-devices such as different types of RF devices (e.g. SAW/BAW filters). In the subsection below, these applications will be expounded upon.

3.3.2. Thin Film Transistors (TFT's)

Thin Film Transistors (TFT's) have risen to popularity in modern times for their use in liquid crystal displays. [43] TFT's differ from typical transistors in that instead of being deposited onto a substrate such as silicon, the deposition usually takes place on a non-conductive substrate such as glass. [44] ZnO has been widely studied as a conductive channel for TFT's given its wide bandgap and ability to be deposited at room temperature in its amorphous or polycrystalline phase. [45] Deposition of ZnO is more commonly done using RF magnetron sputtering where the thickness is controlled as a function of time. It was exhibited that increased layer thickness corresponds to a decrease in channel resistance [46], which leads to an increase in leakage current when the transistor is in its "Off" state when used as a switch. In other applications such as transparent TFTs (TTFT) [46, 47], ZnO is used because of its high transmissivity given that it is essentially transparent in the visible spectrum (84% transmissivity [46]). An example of a generic ZnO TFT topology is shown below (Figure 3.2.)

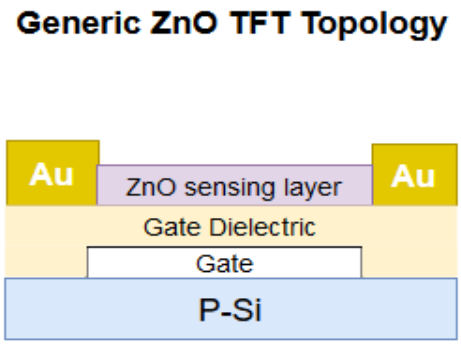

Figure 3.2. Cross-Sectional View of a generic ZnO TFT

3.3.3. Gas Sensors

For a given area of semiconducting sensing material, the sensitivity is directly affected by the grain size, as decreasing the grain size to will increase the resolution of the sensor response. In

effect, by breaking a particle into many smaller parts, the sensors ability to detect smaller analytes will increase. While the exact physical mechanisms behind ZnO's sensing ability are not totally understood, it is believed to related to the adsorption of oxygen atoms onto the surface prior to introduction of the target gases. These oxygen atoms that deposit atop the ZnO take an electron from the conduction band and become reactive oxygen atoms. The electron transfer to the surface layer oxygen atoms created a surface charge depletion layer, increasing the resistance of the sensor. [41-42] Once the gas analytes of interest are introduced, they interact with the charged oxygen atoms which then release their additional electrons back to the conduction band resulting in a decrease in the depletion layer resulting in reduced resistance. [42] Lastly, operating temperature is another factor of great importance in gas sensing devices. Oxygen-sensing at room temperature can be achieved by ZnO, however, this is subject to change for different gases. Heat is required, in many instances, to facilitate interaction between the adsorbed atoms and the chemosensitive layer. Producing chemo-sensitive performance for a given target-gas can be achieved by looking at the van der Waals force that exists between the gas-sensor and the adsorbed atoms. A generic gas sensor topology is shown below in Figure 3.3.

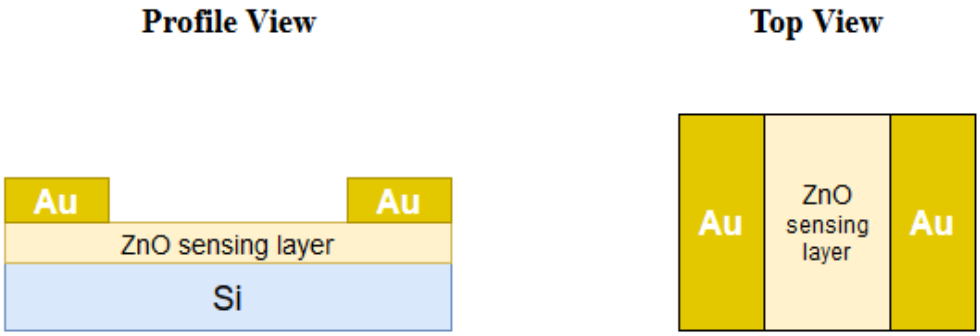

Figure 3.3. Figure 3.3. Profile/Top View of a Generic ZnO Gas Sensor Topology

3.3.4. Transparent Conducting Oxides

Transparent Conducting Oxides (TCO's) are a group of compound semiconductors used extensively in devices including solar cells and displays. TCO's consist of an oxide, as well as, a metal or group of metals that have a high transmittance of light in the visible spectrum. The most commonly used TCO is Indium Tin Oxide (ITO) which is widely available and features high conductivity and transmissivity, however, in recent years ZnO has been investigated as a potential successor. Given that TCO's must exhibit high conductivity, ZnO is typically further n-doped by aluminum ($Al_xZn_yO_z$) as in AZO such that the desired conductivity can be reached [40]. The properties of AZO are subject to change based on various factors including the crystallinity of the substrate, the deposition time, the gases present during deposition, and the post-deposition annealing process [40]. While ITO is still generally favored, there are applications where AZO is more favorable such as transparent, conductive contacts. [49]

3.3.5. Light Emitting Diodes

Light Emitting Diodes (LED's) have revolutionized lighting as their efficiency far surpasses that of conventional light bulbs and the like. LEDs emit light when a sufficiently high voltage is applied such that the pn junction is forward biased. For a semiconductor to emit light, it must be a direct-bandgap semiconductor such that excitonic recombinations can occur and release photons as a result. In this regard, ZnO can be said to be an electro-luminescent (EL) material. ZnO has shown to be a promising competitor to GaN given its much higher exciton binding energy 60 meV vs. the 25 meV at room temperature. This energy corresponds to the brightness of the light output from the LED, thus at room temperature ZnO can glow significantly brighter than GaN LEDs.

ZnO has been used in both homojunction and heterojunction-based LEDs. In the case of ZnO heterojunctions, the most commonly used substrates are sapphire, GaN, and silicon carbide (SiC)

with the lattice mismatch for each being 46.5%, 1.8%, and 4.6%, respectively. [50] Heterojunctions consist of several semiconducting materials of different doping concentration, whereas a homojunction typically consists of the same semiconductor materials cascaded together at different doping concentrations. ZnO heterojunctions are less prone to lattice-mismatch issues than their homojunction counterparts. Because of the ionically bonded nature of ZnO, the potential wells are spherical vs. the anisotropic potential wells in covalently bonded semiconductor homojunctions. [51] Thus the potential well energy is less sensitive to changes in atomic arrangement, this indicates that lattice mismatch issues will be less prevalent in the case of ZnO and the substrate it is being deposited onto. The electro-luminescent properties of ZnO depositions onto GaN have been shown to improve when a layer of aluminum is placed at the GaN-ZnO interface. [52] This Al buffer-layer is used because of a mismatch in the bandgap/lattice structure and to suppress the formation of an oxide layer atop the GaN before the ZnO deposition, resulting in a thin layer of GaO. For ZnO depositions onto aluminum-oxide substrates, magnesium doped GaN buffer layers have been reported. [52] Without the presence of the buffer layer, LEDs prove even less efficient as there is a corresponding increase in non-radiative recombinations. [52] Heterostructure ZnO LEDs are plagued by the inability of ZnO to be effectively p-doped.

It has been hypothesized that a ZnO homostructure would be more efficient than their heterostructure counterparts. Homojunctions require both p-type and n-type doping of the same material to form the desired pn junction, however, being that they consist of the same material, they do not suffer from lattice mismatching. P-type doping of oxide-based semiconductors has been a notorious issue, especially in the case of ZnO. Though not nearly as efficient or high-performing as the n-doped ZnO case, p-type doping has been achieved by some groups using high-vacuum deposition techniques such as MBE and CVD. Most techniques for p-type doping of ZnO

involve using additional dopant elements to manipulate the Fermi level, however there are other simpler techniques as well. One of those methods involves depositing ZnO directly onto a GaAs substrate then annealing at temperatures between 500 and 600^{o}C. This heating step has been shown to result in p-type doped ZnO. [53] One suspected reason for this is that the arsenic atoms diffuse into the ZnO and act as shallow acceptors thus changing the doping profile. [54] It is further noted in [54] that increasing the annealing temperature beyond 600 ^{o}C results in a change back to n-type ZnO.

3.3.6. Photodetectors

Photodetectors, are in many respects, similar to the technology used in that of LEDs, however these detectors use photons to facilitate an electrical signal, rather than the inverse. When a photon imparts its energy onto an electron that is greater than the electronic bandgap of the material, an electron-hole pair is generated. This is referred to as carrier generation. Some forms of photodetectors, such as photoconductors, rely upon the amplifier-based circuitry due to their poor room temperature gain. [55] Wide bandgap semiconductors, and particularly ZnO, show promise in this area due to the lack of need for amplifier circuits. Metal-Semiconductor-Metal (MSM) photodetectors share the same carrier generation working-principle as photoconductors, however, these devices make use of back-to-back diode setups that can conduct in either direction (e.g. npn/pnp). The responsivity of these devices is in many cases limited by the barrier height of that metal (e.g. work function of Au/Cu as electrodes). [55] Comparative studies of the performance of photodetectors created from different ZnO based nanostructures were conducted in. [56] It was determined that ZnO nanoparticle-based photodetectors yield a higher photo-voltage (voltage generated on device output from incident photons) and higher response time than detectors created with ZnO nanosheets and nanoflowers respectively. This comes at the cost of a much longer turn-

off time than either case by over an order of magnitude. This turn-off time is attributed to the readsorption of oxygen atoms onto the surface of the ZnO after exposure has been completed. Prior to exposure, oxygen atoms adsorb to the ZnO layer over time, leaving behind a free electron on the surface. When the light incident toward the ZnO detector has energy greater than the electronic bandgap, electron-hole pairs are created, and the holes combine with the free electron left by the oxygen atom causing desorption from the surface and hence a narrowing of the depletion region of the device. This narrowed depletion region is the mechanism by which the conductivity increases. Once the exposure is completed and the source is no longer emitting photons, oxygen atoms slowly begin to readsorb onto the surface which is the cause of the slowed relaxation, or turn-off, time. [57, 58]

3.4. Characterization of ZnO Nanostructures

ZnO is commercially available material that can be purchased in the form of various nanostructures, as well as, bulk material. These nanostructures can also be synthesized from precursor materials that are also commercially available (e.g. Zinc Acetate ZnAc). These nanostructures, nanoparticles in this case, can often vary in size from < 10 nm to some agglomerations in the order of > 100 nm. This range gives us insights into what sorts of instruments will need to be used for sufficient characterization of these depositions. In this case those are Scanning Electron Microscopy (SEM), Atomic Force Microscopy (AFM), and Fluorescent Spectroscopy.

3.4.1. Scanning Electron Microscopy (SEM)

SEM rose to prominence when the minimum feature sizes of integrated circuits fell below the optical diffraction limit.[59] In the modern study of semiconducting materials, nanostructures and the like fall far below this regime thus necessitating the ability to observe smaller features. Optical

microscopes are widely used, available, and capable of imaging a wide range of structures and organisms, however, their imaging capability (resolution) is limited by the Abbe diffraction limit. [59] The equation for the Abbe diffraction limit is given by $R = \frac{\lambda}{2NA}$; where NA = n sin (α), with n being the refractive index and α being the half angle of the spot size. Thus, when NA = 1, we are limited to R = λ/2 or half of a wavelength, and being that the visible range spans from approximately 400 – 700 nm, the resolution limit is fixed to approximately 200 nm. Because the mechanism by which the SEM works is the deflection of electrons, and not based on the refraction and convergence of beams of visible light, the achievable resolutions are much smaller (< 1 nm).

Two primary parameters of SEM are the working voltage [1-30 kV] [59] and the distance to substrate. Higher applied voltages correspond with an increase in sample penetration, and decrease sample penetrate in lower applied voltages. The penetration depth of the sample is not only governed by the applied voltage at some fixed distance, but also on the atomic number of the element(s) being imaged. Elements with high atomic numbers tend to suppress penetration given the increased number of particles that can oppose it [60], with the opposite being true for atoms with lower atomic number. SEM can produce images from the detection of several surface interactions and are listed here, from the interactions most proximal to most distal from the electron beam: Auger electron interactions, secondary electron interaction, backscattered electron interactions (BSE) , characteristic x-ray interactions, cathodoluminescence-transmitted electrons, and absorbed current. [60]

The images that give structural information about the sample are the secondary electrons, the BSE, and the characteristic X-rays, while the others provide chemical information.

The two primary detection methods for structural information are secondary electrons and backscattered electrons. Secondary electrons provide better surface information about the sample,

where backscattered electrons are better at penetrating and producing images deeper in the deposition. In many instances, BSE images can show better contrast than images using secondary electrons at the cost of lower resolution (1 μm vs. 10 nm). When the beam of electrons is sent incident to the surface via the electron gun, these electrons interact with the surface atoms of the sample. If a sufficiently large accelerating voltage is used, these incident electrons ionize the surface atoms and the result of this collision and subsequent ionization are low-energy electrons (~ 3 – 5 eV) [60] that displace in the order of individual nanometers. This slight displacement dictates the resolution of the secondary electron-based image. The image is produced via a scintillator that converts the secondary electrons (attracted to the low-voltage biased faraday cage) into electrons which then travel through a photomultiplier tube then converted back into electrons prior to forming the image. This photomultiplier tube acts to essentially serve as the brightness control of the image. BSE's based imaging relies on interactions between the incident electrons with the atomic nuclei of the sample. This interaction with the nucleus forces electrons back out from the surface at much higher energies than secondary electrons (order of magnitude). The reflected electrons maintain over half of their energy after the collision(s) inside the sample, and hence penetrated further into the bulk of the deposited material. The image extraction here is like that of the process for secondary electrons, however, the Faraday cage is negatively biased to provide a repulsive force to secondary electrons attempting to enter. Only the electrons directly incident to the detector are received in this case and thus the contrast here is much higher than in secondary electron images.

Some additional considerations when using SEM are the conductivity of the deposited material to be examined and the focal distance of the image on-screen. For more conductive samples, electro-static charge may build-up on the sample causing an image blur and thus careful

consideration must be given to obtain a useful image. In some cases, one can adjust the accelerating voltage and the charging effects on the image will be mitigated, and in other cases it becomes necessary to deposit a very thin layer (< 5 nm) of a metal (e.g. gold). The application of the thin layer provides a barrier between the deposition and the source thus preventing charge build-up on the desired sample. A diagram of a standard SEM system is depicted below in Figure 3.4.

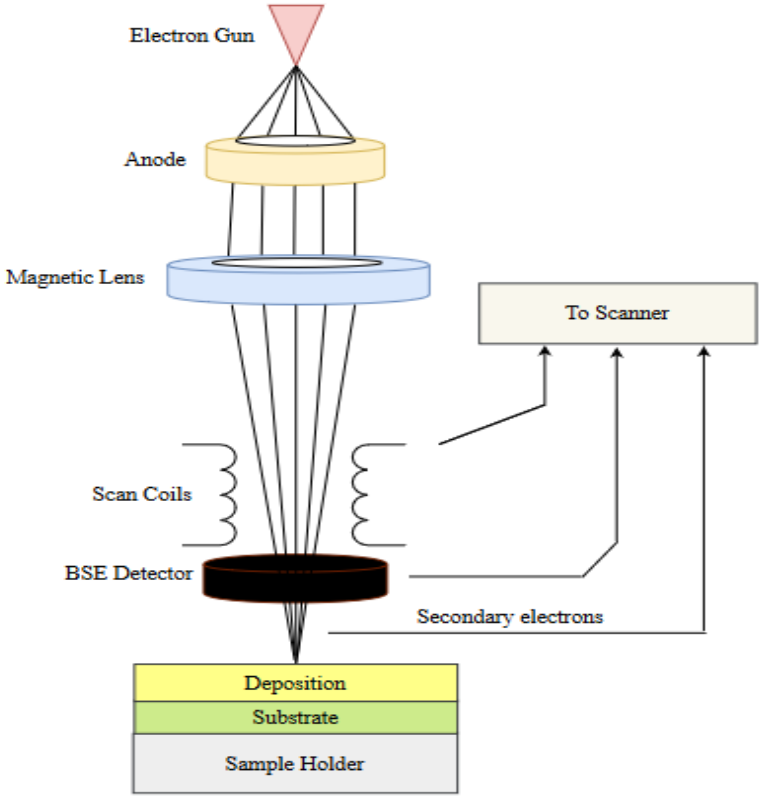

Figure 3.4. Standard SEM Layout

3.4.2. Atomic Force Microscopy (AFM)

AFM was invented by Gerd Binnig in 1986, coming on the heels of his work on the Scanning Tunneling Microscope (STM). He postulated that high-resolution images could be obtained using force measurements, which would allow for imaging of insulating materials, as opposed to current-

based measurements of devices like the STM which did not allow for imaging of insulating materials. [61] The working principal of AFM is that a cantilever with a force less than that of inter-atomic forces (and thus spring constants) could be used as a highly effective means to measure nm-scale features. Today, AFM is a widely utilized means of characterization in areas from nanoelectronics to biological applications.

The working-principle of AFM is that a small, piezoelectric cantilever with an extremely fine tip (single atom wide to several nm) [62] is rastered across the surface of a sample, generating topographical information about the sample. This piezoelectric sensor then converts the mechanical forces experienced from the deflection along the surface to an electrical signal which is then fed back via control circuitry to the tip where it compensates this deflection; the cycle repeats along the path of the probe-tip. Extensive filtering techniques are employed in the control circuitry as AFM is especially vulnerable to noise in its measurements which manifests via a combination of flicker noise and white noise on the output signal. [63] The probe, in the scenario described above, physically contacts the surface, in the repulsive region of the sample. This need not be the case, the previous example is known as "Contact Mode", there are other methods of AFM that do not involve this direct, physical contact with the surface. These other two modes are subsets of "Vibrational" mode (or "Oscillating" mode); they are referred to as "close-contact" and "intermittent contact". [64]

Vibrational Mode involves having the tip located at some distance above the sample surface. As it moves along the length of the surface, the tip is vibrated up and down such that the tip experiences a variance in attractive and repulsive forces. The interaction of the surface and the tip can generate a change in phase, and this information is passed through the feedback circuitry that converts this change to a proportional voltage to be sent to the output. [65, 66]

Close-Contact Mode involves having the probe tip sufficiently far from the surface such that it does not experience any repulsion of the tip from the surface (experienced in Contact-Mode), but close enough for the attractive forces to be experienced by the tip. The tip must be relatively stiff, as it is vibrated in and out of this attractive field causing the phase-shift described in the paragraph above. [67] This mode is susceptible to interactions with contaminant layers that may act as a barrier between the substrate and the tip, with the contaminants interacting with the tip more than the desired material, thus causing poor surface imaging. In some instances, if the user has knowledge of the contaminant layer, one can have the probe tip vibrate inside of the contaminant layer, near the surface. This allows for better imaging performance but is much more difficult as information must be known about the contaminant layer.

Intermittent-Contact Mode is essentially a combination of Contact and Non-Contact modes respectively. The probe tip is vibrated through the contaminant layer and attractive/repulsive fields until contact with the surface is made. Since the tip is being oscillated and moving along a line, the tip is moving into and out of contact. This constant oscillation allows the tip to mitigate any lateral stresses on the tip. The tip also experiences less ware over time, thus increasing its lifetime. [65] A diagram depicting the lateral motion is given below in Figure 3.5.

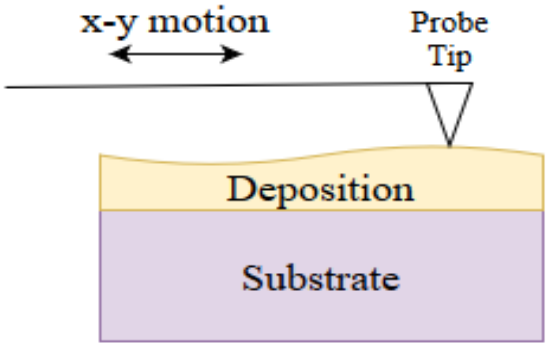

Figure 3.5. AFM Contact-Mode

Deciding which mode to use depends on the needs of the user. If one were to employ Contact-Mode on a soft sample, the tip would be prone to scratching off some portion of the sample. Another consideration when using the AFM in this mode is the lifetime of the tip. The difference between the non-contact and intermittent contact modes are depicted below in Figure 3.6.

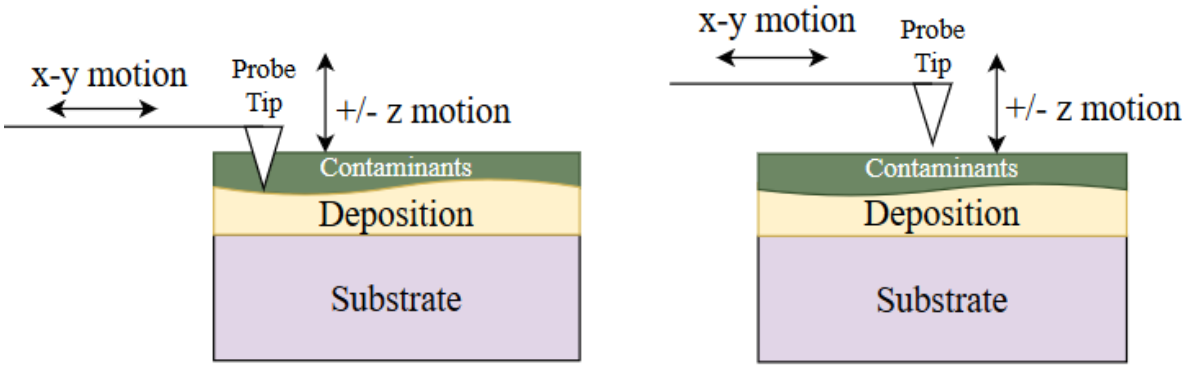

Figure 3.6. **(**a) AFM Intermittent-Contact Mode (b) Non-Contact Mode

If the tip were used exclusively in this mode, where it is constantly in contact with surface, the tip would eventually begin to ware. Non-Contact mode may tend to minimize ware on the tip, but in the case of a very hard sample, would inevitably suffer some loss of image quality as compared to Contact Mode. Intermittent-Contact mode is a combination of both contact and non-contact. One must be sure to have a probe-tip of sufficient stiffness such that excess deflection can be avoided.

3.4.3. Photoluminescent Spectroscopy (PL)

PL is another widely used technique in the study of semiconductor to characterize wavelengths of interest in a material, which can give indication as to the impurities present in the crystal structure based on where sample luminesces. These peaks also reflect the electronic bandgap of the material and give information about possible recombination mechanisms inherent in the

material. An attractive feature of PL is that it is a non-destructive method of observing these characteristics. [67]

The operating principle of PL Is simple, a lamp (typically Xenon) is used provide a range of wavelengths to an emission monochromator which then produces a singular excitation wavelength incident to the sample. When this excitation hits the sample, the light is absorbed by the sample and causes electrons to move into their excited higher-energy states. After the excitation is ended, the electrons transition back into their low energy states causing the emission of light at different wavelengths. These wavelengths are sent to the emission monochromator which sweeps the wavelengths increments one at a time and send this information to the detector. [67]

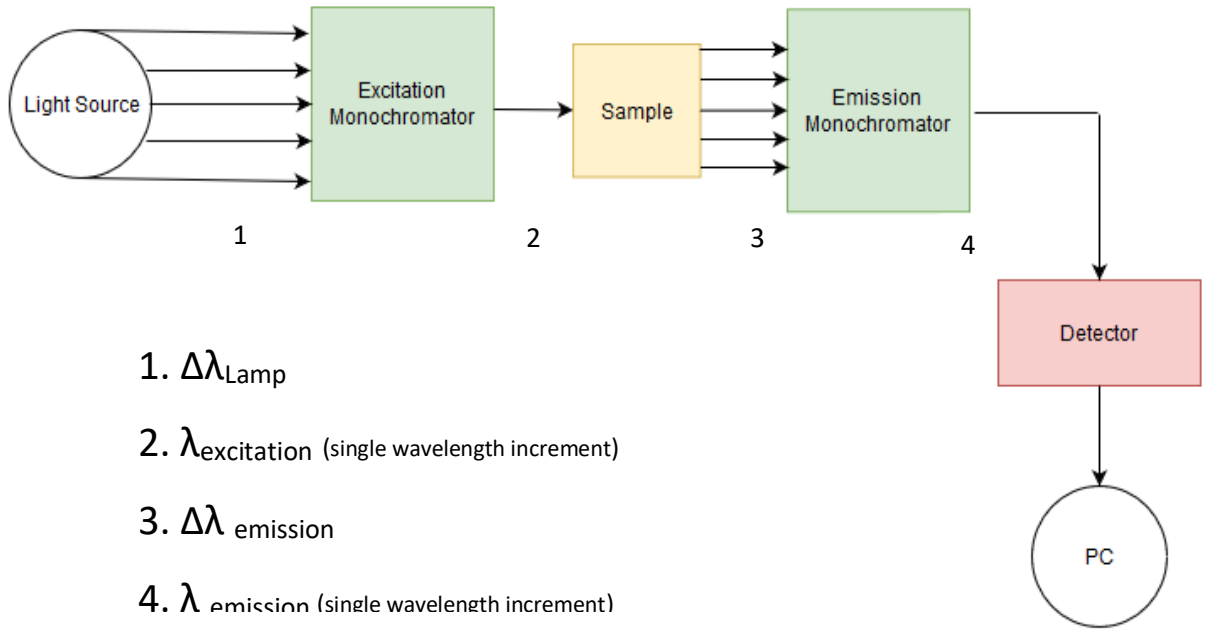

Figure 3.7. PL Schematic Diagram

3.4.4. Raman Spectroscopy

Raman Spectroscopy is a technique used for characterizing materials in a variety of applications in the realm of materials research. A laser beam in the visible or near-visible spectrum is sent through a monochromatic lens which then sends the beam incident to the material being examined. The photons then scatter inelastically and cause vibrations in the crystal-lattice of the material and exit with equal energy, more energy, or less energy than the initial incident beam. A notch filter (band-reject) is then employed such that the desired wavelengths can be observed in higher detail. For Raman to be applicable to a material, the incident photons must be able to cause a change in the rotational or vibrational state must occur. [68] The Raman intensity is thus proportional to the change of rotational or vibrational state given a photon of a certain energy and wavelength.

The aforementioned change of energy of the exiting photon or lack thereof is how the particular scattering event is described. If the energy and wavelength remain unchanged, the scattering is characterized as “Rayleigh Scattering”. If the frequency of the photon exiting is higher or lower, the scattering event is characterized as either anti-stokes or stokes respectively.

In typical Raman Spectroscopy setups, the laser aperture can be adjusted to allow for a more intense or less intense beam to enter into the lens. The beam is then focused through a microscope objective and shone onto the sample. The scattered photons then travel back through the objective lens into a beam splitter which then route the photons through a notch filter and the desired, frequency-shifted photons then arrive at the spectrometer through a diffraction grating. The general setup for a Raman spectrometer is depicted below in Figure 3.9.

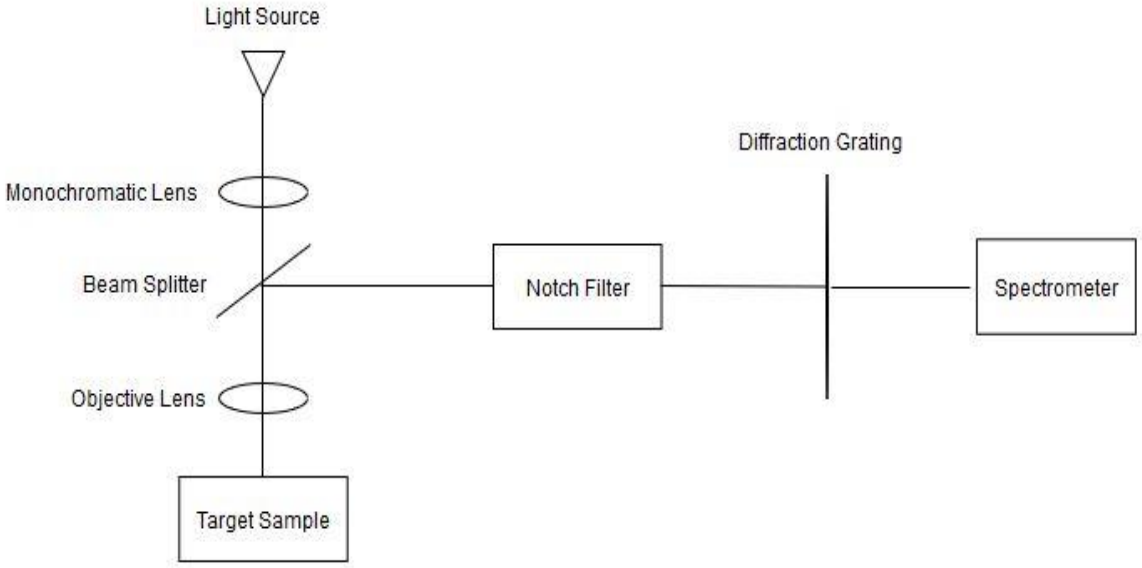

Figure 3.8. Standard Raman Spectroscopy Setup

CHAPTER IV. ELECTROSPRAY DEPOSITION AND LITERATURE REVIEW

The research conducted for this thesis was in large part made possible through the technique of electrospraying and the use of a custom-designed system for electrospray deposition. Thus, a review of the literature and a description of this technique is in order.

Electrospraying is a technique that has been used to form Taylor cones in liquids as early as the 16th century, beginning with physicist William Gilbert (electrospray of water). [70] A Taylor cone is a stream of charged droplets that originate at the tip of a liquid meniscus that forms under a sufficiently large electric-field. After the work of Jean-Antoine Noillet (electrospray of blood) [71], in the 19th century Lord Rayleigh was able to quantify the maximum amount of charge in a droplet, thus identifying what came to be known as the "Rayleigh Limit". [72] The cone-like shape, originally documented under the observations of Gilbert, were studied in the later 20th century by Sir Geoffrey Ingram Taylor who, in turn, coined the term "Taylor cone" for the droplet spray phenomenon. Electrospraying has recently experienced a rebirth given its amenability to room temperature operation and comparably lower production costs. [73]

The application of sufficiently large electrostatic force across a small capillary with an outward flowing liquid can induce the characteristic Taylor cone involved in Electrospray deposition. As the voltage applied is increased from 0, the shape of the droplet begins to change as the electrostatic force deforms it. The single droplet can only "hold" so much charge before the potential created becomes greater than the droplets surface tension. This charge threshold is also referred to as the "Rayleigh Limit" [71] as described above. Upon the surface tension being exceeded, the single droplet now undergoes Coulombic fission where smaller droplets form and further repel each other. This repulsion is the mechanism for the generation of smaller droplets and what end up

causing the plume, as it is referred to in literature. [74] The formation of the Taylor cone is dependent not only on the applied voltage but also the flow rate and the separation distance between the nozzle and the substrate. With this dependency comes a variety of different "modes" encountered during electrospray, all of which have characteristic behaviors and some, their own, unique applications.

4.1. Fundamentals of Electrospray

Prior to the formation of the Taylor cone, the droplet undergoes considerable deformation unto the point of the Rayleigh limit. The following equations and parameters appear as described by Jaworek. [75] The Rayleigh limit is defined as $Q_R = 2\pi\ (16\sigma_l\acute{\epsilon}_0\ r^3)^{1/2}$, where σ_l is the liquid's conductivity (the solutions being deposited), $\acute{\epsilon}_0$ is the permittivity of free space, and r is the radius of the droplet. Similarly, the electric field as experienced by a single droplet can be described as: $E_{SD} = Q_D/(4\pi\acute{\epsilon}_0 r^2)$ where Q_D is the amount of surface. The plume of the electrospray jet can be described as a function of the mass flow rate and the time constant (mass/unit-time) which can be written as $c_d\,(1/T)^{-1} = q$ where q is the flow rate. Once the electrostatic force from the applied voltage can overcome the surface tension of the droplets in the nozzle, the Taylor cone is able to form as shown in Figure 4.1.

At the onset of the meniscus, the droplets within the liquid stream become much smaller and hence the droplets leave the nozzle more frequently. Upon the formation of the Taylor cone, several interesting phenomena are observed, namely: The cone will be unstable. Since the voltage is right at the threshold for forming the Taylor cone, the meniscus is constantly being shaped into a cone then collapsing and falling back into the micro-drip. This instability in the shape of the meniscus results in an instability of the spray itself and given its unstable nature, the cone may form and reform at different points along the meniscus. This results in an oscillating spray that

may move in different directions with respect to the collector. Further increasing the voltage at the nozzle induces a stable spray, as the emitter is biased such that it is well beyond the threshold between micro-drip and an unstable cone. If the voltages continue to be increased, further instability is observed as different points along the meniscus begin to form small jets (multi-jet mode). The voltage can be modulated in multi-jet mode such that control of the number of jets can be obtained, as well as, the spray angle, essentially multiplexing the spray. Instability remains an issue in this mode, as very precise high voltages must be applied.

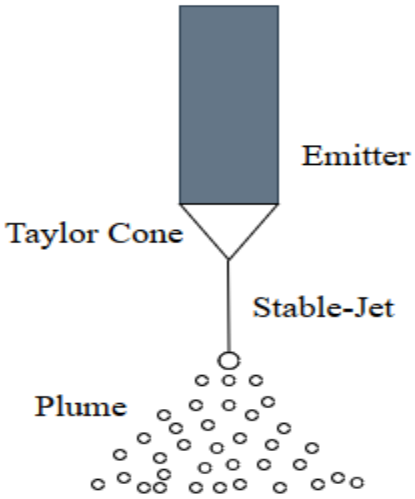

Figure 4.1. Stable Cone-Jet with Taylor Cone

The prediction of the radius of the droplets at the Rayleigh limit, by which gas-phase ions are produced from progeny droplets (the iterative creation of smaller droplets produced from their parent droplet) in electrospray has been mathematically described by two separate models that are both typically employed in different scenarios. One of these models, introduced by Dole [76] describes the formation of gas-phase analytes from larger droplets where the charge of the analyte

originates from the surface charge of the initial droplet prior to the evaporation of the solvent. This model is referred to as the "Charge-Residue" Model. The second of the two models are used more in the description of very small droplets (< 10 nm) and is referred to as the Ion Evaporation Model which was introduced by Iribarne and Thomson. [77] Here, coulombic fission is no longer the chief mechanism by which these gas analytes are formed, but rather it is direct ion emission. For droplets over 10 nm, coulombic fission dominates, however, below this threshold an attractive force exists between the gas-phase ion and the droplet surface at sufficiently small distances. The "transitional" state, where one model becomes more appropriate than the other is the point at which the charges are equal for a certain droplet radius. [78]

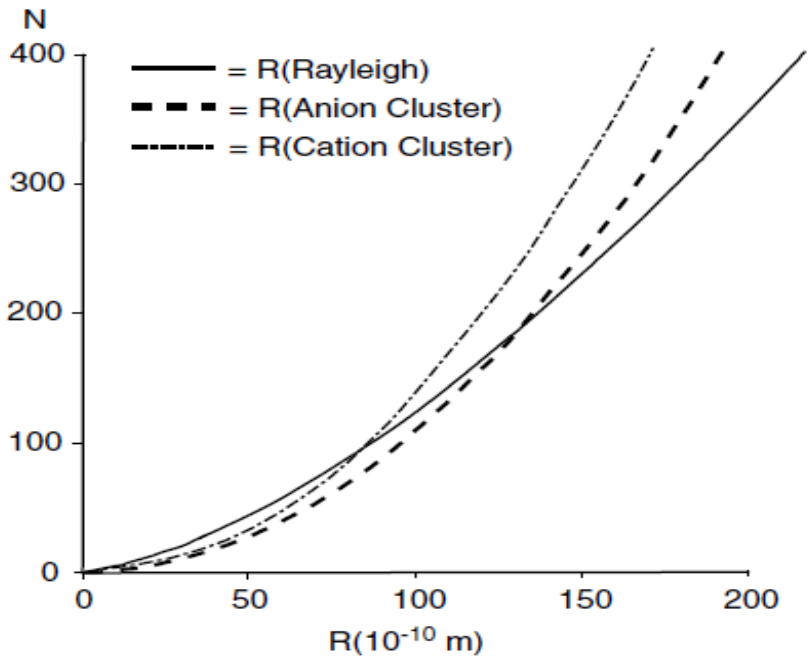

Figure 4.2. Elementary Charge vs. Droplet Radius (leftmost-IEM, middle-CRM) reprinted with permissions from [78]. Copyright 2010, Wiley & Sons

Figure 4.2. shows a plot where R(Anion Cluster) represents the Charge Residue Model (CRM) while R(Cation Cluster) represents the Ion Evaporation Model (IEM) with the intersection

(transition point) being at 8 nm, which is in the range of the 10 nm cutoff that was previously mentioned.

4.1.1. Electrospray Modes

As previously discussed, there are several "modes" in electrospray deposition. Prior to the onset of micro-dripping mode, no meniscus is forming. Thus for this discussion dripping mode will not be considered as a true "mode" but rather as a pre-requisite to obtaining modes. This logic suggests that micro-drip is the first true mode and so it will be discussed first in the sections to follow. To provide a visual representation of the spray modes, Figure 4.3 demonstrates several.

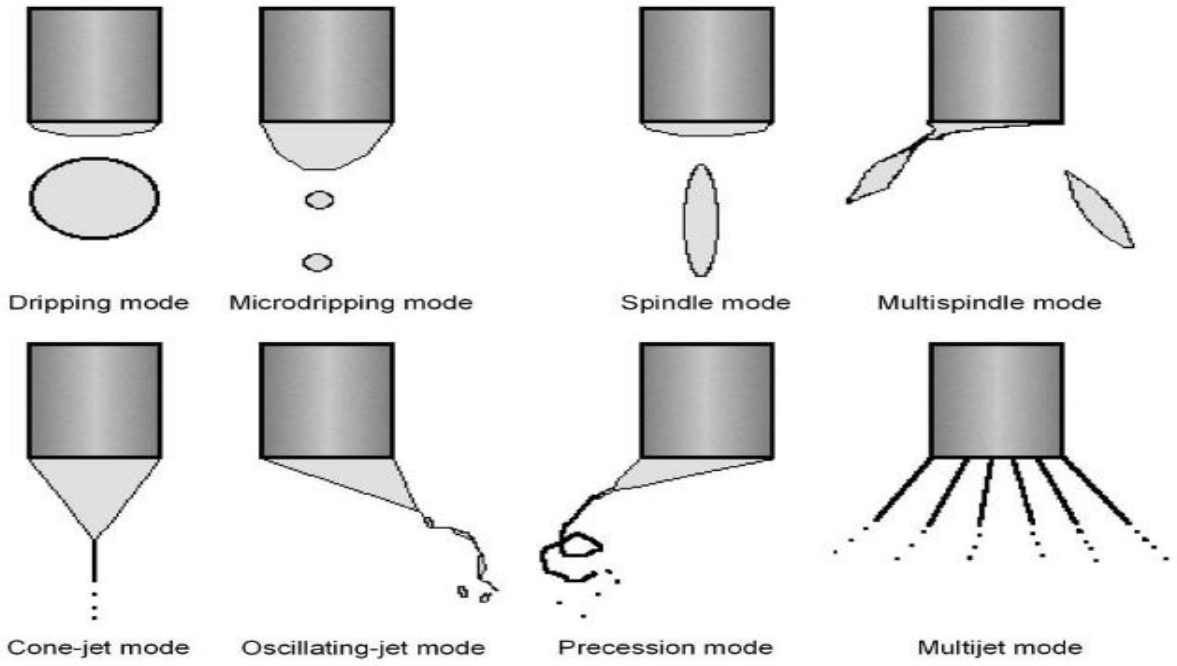

Figure 4.3. Visual Description of Several Jet-Modes reprinted with permissions from [79]. Copyright 1998, Wiley & Sons

4.1.1.1. Dripping Modes

As a voltage is applied to the needle of the syringe, and gradually increased, it is observed that the droplets leaving the needle come out smaller and at a higher rate than those without any applied potential. In dripping modes, large droplets can form and as they reach a critical size they begin to separate from the meniscus. As this separation occurs, the middle region between the meniscus and the droplet elongates and separates after the main droplet has fallen. [80] This is referred to as the "secondary droplet". This can be observed in both dripping and micro-dripping modes, where the micro-drip further exacerbates this phenomenon. One key differentiator between micro-dripping and any Taylor cone associated mode is that the particles will not get smaller after leaving the emitter (needle tip). [81] The E-field is not sufficiently strong so as to reach the Rayleigh-limit and achieve coulombic repulsion of smaller droplets. The resulting reduced particle size is due to the reduction in size of the meniscus caused by the stresses induced upon it via the applied electric field.

4.1.1.2. Spindle Modes

Spindle-based modes are a subset of the dripping modes, however, with higher flow rates. The small droplets are coming out fast enough such that reform into longer "spindles". These modes occur when the voltage is sufficiently increased passed the onset of micro-drip and can reach instability at voltages further along. Oscillating spindles are also sometimes referred to as oscillating jet modes which involve the Taylor cone forming briefly then collapsing in on itself which creates an oscillatory, lateral deposition pattern on the substrate. [80] This oscillation can be attributed to changes in momentum due to collisions of positively charged ions colliding with the gas molecules surrounding the tip. [81]

4.1.1.3. Oscillating Jet Mode

Oscillating jets are caused by instability in the meniscus of liquid at the tip of the emitter. There are two primary mechanisms of this instability: varicose instability and kink instability. [82] In varicose instability, the oscillating meniscus is deformed into a jet on the maxima of the surface wave causing the droplet disintegration necessary for a jet. At all other points along this oscillatory pattern, no droplet disintegration occurs, and the droplets remain incident to the center of the track. Kink instability involves a lateral movement of the spray pattern, as the jet itself is unstable due to inertial and electrical forces present on the emitter. This results in a pattern that moves laterally along the collector in a single direction orthogonal to the emitter. [83] This mode can often overlap with "Spindle Mode" which was not covered in the previous subsection.

4.1.1.4. Stable Cone-Jet Mode

Stable Cone-Jet mode is the most widely used method for the deposition of materials using electrospray. A stable cone-jet is formed when the applied voltage overcomes the surface tension and a sufficiently fast flow-rate is used such that a stable meniscus and thus a stable Taylor cone can be formed. Stable Cone-Jet mode allows for the most uniform deposition pattern given its stability, and is used in nearly every application of electrospraying given its highly controllable nature. As the ionized droplets travel through the jet, coulombic repulsion causes the "plume" where the small, charged droplets spread out across the grounded substrate. To obtain a highly directed spray, a metal ring that surrounds the needle-based emitter is often used, as first reported by Jaworek et al. [79] The ring-shape helps evenly-distribute the electric-field around the needle, thus effectively centering the Taylor cone and thus the spray. One issue with depositing materials in this mode is the concern of scalability. If one were to attempt to run many simultaneous depositions with needle-based emitter in this mode, interactions between the charged needles

would affect the quality and characteristics of the depositions. With this concern came an increase in the study of electrospraying in its next mode, multi-jet.

4.1.1.5. Multi-Jet Mode

Multi-Jet modes occur when increasing the applied voltage sufficiently past that required to obtain the stable cone-jet, and increasing the flow rate also further facilitates this occurrence. The number of jets present scales with voltage per the flow-rate. Control of the multi-jet modes is an issue, as the onset of these jets tends to come with increased instability causing oscillating jets. One method for increased control is the use of a needle with several grooves cut into it. [84] These grooves allow for the onset of several, stable jets that form at each groove. Investigations into the characteristics of these multi-jet sprays were conducted in [85] where it was determined that the individual jets were capable of producing very similar droplet sizes. Despite these small individual jets, the number of jets formed were highly unstable and their positions along the emitter were increasingly variable with applied voltage. The multiplexing action of the multi-jet mode makes it more promising that the stable cone-jet mode in terms of scalability, however, the variable nature of the spray positions is the limiting factor.

4.1.2. Electrospray Parameters

There are several experimental “process” parameters that determine the characteristics of the spray pattern and mode of operation. The most widely hailed of these parameters are the following: the applied voltage on the emitter, the flow-rate of the liquid into the emitter, and the distance between the nozzle to the substrate. Care must be given to best optimize these parameters, or a desired spray pattern may not be achievable.

4.1.2.1. Flow-Rate

The flow-rate (Q) plays as important a role in the formation of desired jetting modes as does the applied voltage. For flow-rates that are too fast, a stable Taylor cone is never able to form and thus a stable cone-jet is rendered impossible. Similarly, if the flow-rate is too low, the meniscus is never able to fully form resulting in a sub-optimal spray pattern that can have issues with instability as well. As one increases the flow-rates, the modes begin to be increasingly unstable where multi-jet reaches instability first followed by instability in the cone-jet mode and then the spindle mode. Optimizing the flow-rate to the applied voltage is very important for the proper formation of the various spray modes in electrospray.

4.1.2.2. Applied Voltage

The voltage applied to the emitter is the mechanism by which the Taylor cone is established, assuming a sufficient flow-rate. This applied potential is what causes the deformation of the meniscus as the electro-static force overcomes the liquid's surface tension. For this reason, the voltage has a profound effect on the induced spray mode. The application of the emitter potential also greatly influences the characteristics of the spray. If, for example, a single alligator clip connector is used on the needle, the uneven electric-field distribution will cause the spray to deviate greatly from its center point and in some cases induce instability into the meniscus resulting in an oscillating jet pattern. Often times, a guard plate or metal ring is placed around the emitter such that the applied electric field is evenly distributed which effectively centers the spray and can stabilize the meniscus, as first suggested by Jaworek. [75] Varying the potential at the guard plate such that it is constant with respect to the voltage applied to the emitter has also shown several interesting features, namely, the constant guard plate-collector voltage has resulted in more

uniform droplet distribution and charge [86, 87], which in turn gives a wider range for stable-cone jets and increased uniformity of the droplet distribution.

4.1.2.2. Nozzle-Substrate Distance

The nozzle to substrate distance is the third of the aforementioned three most common process parameters in electrospray. The distance between the nozzle and the substrate must be sufficiently close such that the electric field is high enough to induce the ions from the liquid to travel to the ground plane. This, in turn, affects the required potential at the emitter to obtain the various spray modes.

4.2. Alternative Electrospraying Techniques

Aside from the more conventional approach to electrospraying, needle-tip situated several cm from collector with applied voltage in kV range, there are other methods such as Near-Field Electrospraying (NFES) and Faraday Spraying (mechanically excited meniscus, needleless). Needleless electrospraying is a field-of-study that is attempting to increase the scalability of electrospraying given the limitations presented by obtaining a single stable cone-jet per needle whereas NFES is used for direct-writing of patterns on various substrates using electrospray at very short distances using adjustable x-y stages.

Electrospinning is technically a different deposition technique than electrospray, however, this difference is subtle. Electrospinning is used to deposit long strands of material such as nanofibers whereas electrospray which is used in the deposition of nanostructures such as nanoparticles or nanorods. Despite this difference, the physical mechanisms of each remain effectively the same as they rely upon the formation of a Taylor cone under sufficient voltage bias and flow-rate. For this reason, techniques that are applicable for electrospinning applications are often also applicable for electrospray techniques.

4.2.1. Near Field Electrospraying

Near-Field Electrospraying is a technique employed to achieve direct-write patterns on various substrates using vastly decreased nozzle-substrate distances that are capable of fast depositions over large surface areas. The technique was first used in electrospinning systems to serve as an intermediate step between inkjet printing and dip-pen nanolithography (DPN). [88] NFES has been used extensively for gas sensor fabrication employing a heated substrate and a moveable x-y stage. [89, 90] The decreased distance from emitter to collector comes with a decrease in the spread of the particles due to coulombic repulsion, resulting in narrower patterns. This allows for very precise depositions on targeted regions of a substrate. The smallest achieved feature-size of this writing technique is reported to be 38 nm. [91] Another notable effect of the decreased collector-emitter distance is the corresponding decrease in the necessary applied voltage for the stable cone-jet. Since the distances are, in some cases, as small as only 1 mm, the reported voltages are in the order of several 100's of Volts, with Zheng reporting < 2 kV for the onset of the stable jet. [89]

4.2.2. Needleless Electrospray

Unlike standard electrospraying, where a needle is used as the medium by which the spray is dispersed, needleless electrospray employs a piezoelectric transducer to provide a mechanical stimulus to a liquid container that is then given an applied potential large enough to induce a Taylor cone. The piezoelectric is set to provide a mechanical stimulus such that a standing wave is formed that is on the threshold of liquid atomization. This threshold is where the inertial forces and the surface tension are equal. At this point the sufficiently large applied voltage causes the Taylor cone to form and thus electrospraying occurs. [92] The instability of the individual jets is one major concern in needleless electrospray. This jet instability is induced by the constantly shifting surface waves and hence controllability of the individual droplet size is difficult.

4.3. Applications of Electrospraying

Electrospraying shows great promise as a deposition technique in many industries and applications given its facile nature and ability to operate at room temperature and ambient pressures. The potential for quality depositions at these conditions has prompted its use in semiconductors, sensors technologies, and solar cells.

4.3.1. Semiconductors

Electrospray Deposition has found extensive applications in semiconductor applications with a great deal of effort being placed to use ESD as a means of fabricating TFTs and Organic Field-Effect Transistors (OFETs). Electrospray demonstrates several advantages in the realm of OFETs given its room temperature/pressure operation, as well as, its ability to quickly deposit and not necessitate the use of toxic chemicals. For patterning, Electrospray can also make use of shadow masks which allow for different deposition geometries without the use of any true photo-lithographic processes. [93] FET-based applications using electrospray deposition are often targeted toward depositing semiconducting materials dispersed in organic-solvents that offer increased electron mobility. One common combination used is of ZnO and TIPS-pentacene, which is typically used to form a thin, organic film. Specifically, electrospray is used to deposit a channel layer, where the portions of the FET are deposited via lithographic processes. As with most thin films, in-situ substrate heating impacts and influences the surface morphology. In the case of OFETs, it has been shown that this substrate heating impacts the electron mobility demonstrating the tunability of electron mobility in OFETs. [93] Though this heating step tends to increase the electron mobility, it also can induce surface defects such as cracks and gaps in the deposition, as well as, the well-documented Coffee Ring Stain Effect (CRE). [94]

4.3.2. Solar Cells

The increased research interest into solar cells has generated increased discussion on how to quickly deposit films for the creation of highly-efficient perovskite solar cells. Electrospraying has been used as a method to deposit Electron Transport Layers (ETLs) and Hole Transport Layers (HTLs) on perovskite solar cells to increase efficiency. [95, 96] Dye Sensitized Solar Cells (DSCs) are an alternative solar cell technology that utilizes electrospraying. DSCs incorporate photosensitive layers atop TCO layers to improve the light capturing ability of the surface layer for increased efficiency. [97] Solar cell technology currently relies heavily upon spin-coating methods which hinders its scalability. Electrospraying has demonstrated that large area, uniform depositions are attainable. Hence the utilization of it and other aerosol-based deposition methods are expected to increase in use moving forward.

Partially-wet electrosprayed depositions are the preferred type when attempting to produce uniform films as the collection of wet droplets eventually merge together to form a continuous layer. [98] If complete desolvation occurs, a dry-deposition is the result. Dry depositions yield less uniform collections of nanoparticles across the dry substrate which results in a less uniform film. Field-uniformity is of great importance in solar cell technology as the layers of each heterojunction need to be finely controlled to ensure uniform electrical performance. The contact angle of the droplets presents another sensitive parameter than can alter the quality of the deposition. It was observed by Jiang [98] that for contact angles of approximately 18^{o}, the post-deposition annealing process changes the contact angle. This change in contact angle is due to the Marangoni effect as the droplets tend to evaporate more in the middle and less around their edges. This results in an uneven layer, with the color of the material being more profound in the thicker areas, and less on the thinner ones where more of the liquid evaporated. For initial contact angles > 18^{o}, the wet-

layer tended to evaporate more uniformly resulting in a more even layer. When compared with spin-coated layers, shorter working-distance sprays demonstrated comparable uniformity and thickness.

Due to the desolvation of electrosprayed droplets in electrospray, it poses an advantage over conventional deposition methods in its ability to remove excess solvent prior to the arrival of the nanostructures to the substrate. Whether the deposited material is in the form of a partially-wet layer or a dry one, the concentration is markedly reduced as compared to spin-coating or dip-coating techniques. This makes the deposition of multi-layered films quicker and given the room-temperature conditions electrospray allows, it serves as a viable alternative to spin-coating.

4.3.3. Sensors

Many different types of sensors have been fabricated by use of Electrospraying. The study of gas sensors has been studied closely by Zheng [89] [98] [86] and surface acoustic wave sensors by Jasek [97] and Go. [99] Once again, the favorable operating conditions of ESD and the relative uniformity are the chief reasons that it is a highly promising technique for sensor-based depositions. This is especially true when feature sizes range from 100s of nanometers to 100's of microns. Zheng demonstrated in [89] that the efficacy of depositing ZnO precursor materials via ESD then annealing to form the desired sensor performance. Jasek conducted a detailed look at the frequency response of SAW sensors and their use in humidity detection and quantification. [99] Go provided a comprehensive review of sensing technologies fabricated from aerosol-based deposition methods such as electrospray. [97] In these applications, Electrospray is used to deposit the sensing layer, or chemo-sensitive layer that the target molecules adsorb to.

CHAPTER V. INSTRUMENTATION AND DESIGN OF EXPERIMENTAL SETUP

5.1. Standard Electrospray Setups

While different sorts of electrospray setups exist, they rely upon several, fundamental components: a high-voltage power supply (applied to the emitter), a fixed flow-rate system (typically a syringe-pump), and a grounded substrate (collector). Differences in the formation of the Taylor cone and the deposition qualities are studied when variations are introduced into the operation of these respective components (e.g. changing the flow rate, substrate-nozzle distance, applied voltage). As the field of electrospraying has matured, the setups have become more complex, with some setups introducing components including, but not limited to: substrate heater elements [44], guard plates around the nozzle to increase the stability of the spray [75], NFED [95] and custom-machined needles. [79] A fifth component, substrate rotation, has also been studied [98] which demonstrated increased deposition uniformity. This increased uniformity due to substrate rotation is a technique used in spin-coating and magnetron sputtering systems. Thus its integration into electrospray setups is promising.

5.1.2. Conventional Electrospray with Temperature-Controlled Substrates

Electrospray deposition systems involve a liquid source, a high-voltage potential, and a substrate. In many cases, a heated substrate is used for in-site heating which facilitates solvent evaporation resulting in dry, uniform films. The heat directly affects the grain size of the crystallites, and with increased substrate-temperature comes a reduction in the reported grain size. [99]

5.1.1. Near-Field Electrospray Deposition Systems

NFED is a relatively recent development in the field of electrospray. In contrast to conventional electrospray, which takes place with a nozzle-substrate distances of centimeters to tens of

centimeters, NFED takes place with nozzle-substrate distances of only millimeters. Li [96] demonstrated successful electrospray deposition with a nozzle-substrate distance of only one millimeter. NFED can also differ from traditional electrospray via removal of the syringe-needle arrangement entirely. In lieu of using the syringe to drip material into the needle, a probe is dipped into the liquid to be deposited and then the potential is applied to the probe. As there is no continuous source of liquid, deposition times are drastically reduced as there is only a finite amount of liquid bound to the probe-tip that is to be sprayed. This deposition-time limitation also led some groups to instead opt for the more traditional needle-syringe combination while still utilizing millimeter-range depositions. NFED has been used for the development of direct-write patterns via a movable, computer-controlled x-y stage. Direct-write NFED has been used to achieve line widths in the range of 10's of microns. [86] The line-widths are achieved depend strongly on the flow-rate of the liquid, with higher flow-rates resulting in an increase in satellite droplets due to the disintegration of the larger, primary droplets. Direct-write patterning via NFED is especially promising in scalable sensor fabrication as the introduction of a template or grid on the movable substrate holder could facilitate rapid depositions of chemo-sensitive layers atop the substrate. Conventional direct-write techniques offer smaller line-widths, but at the cost of achieving rapid, large area depositions.

5.2. Development of Electrospray Setup

Upon beginning the task of setting up an electrospray experiment, there was originally some debate about whether the spray should be incorporated vertically or horizontally. Horizontally oriented setups do not have to worry about any residual dripping from the needle tip either before the Taylor cone has been established or afterward where the applied potential goes to 0 V such as in the vertical orientation. Despite posing this advantage, questions about uniformity were raised

given that any residual liquid build-up on the substrate would tend to “bleed” off of the substrate slowly due to the effects of gravity. The most common arrangement is vertical given the ease of centering the spray and introducing standing equipment such as guard plates. Due to the number of instruments involved, a custom-built frame was constructed for housing the equipment used such that equipment could be appropriately mounted and spaced. The next addition to the setup was made by introducing a collector plate that was mounted onto a DC motor with tunable RPM via a custom-built integrated circuit. The overall, original setup is presented in Figure 5.1. below. It was observed that, in this configuration, a stable cone-jet was unattainable due to instability in the formation of the meniscus. The applied voltage was placed onto the needle tip via an alligator clip connector and a laterally offset cone was observed. To combat the instability and lateral offset, a guard plate was made to be placed around the needle itself with the applied voltage on it as well as on the needle.

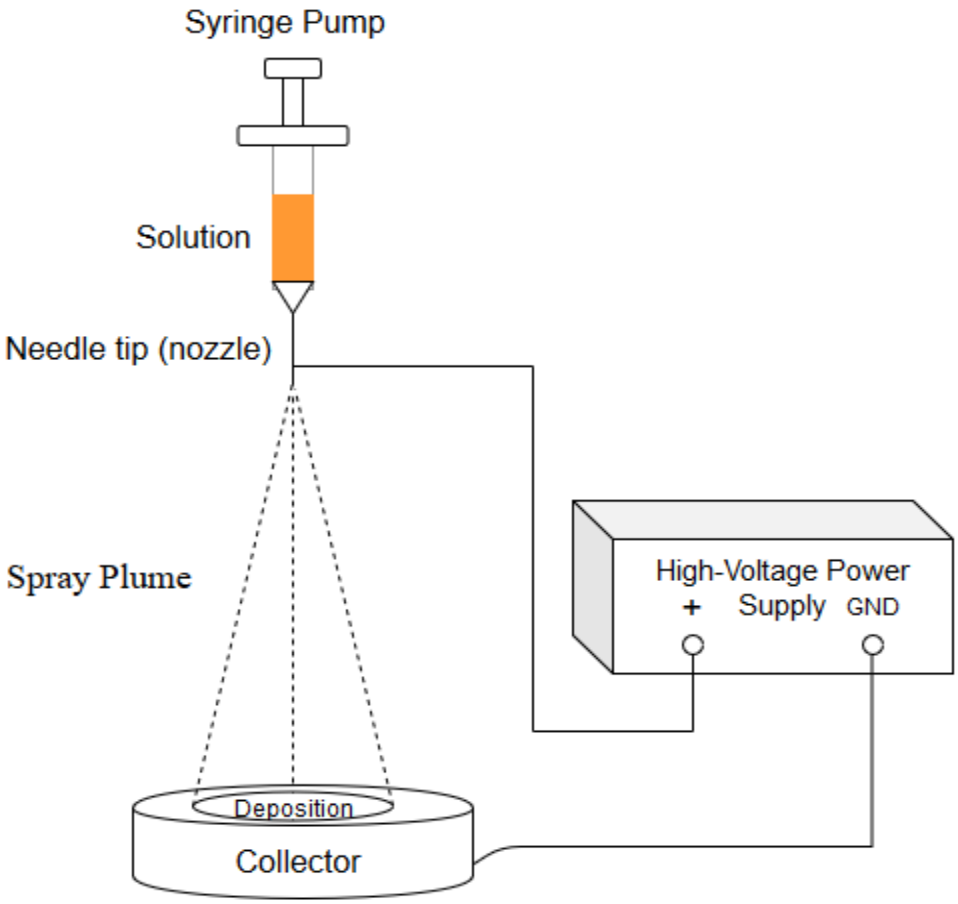

Figure 5.1. Initial Electrospray Setup

This guard plate acted to evenly distribute the electric field which resulted in a centered, stable Taylor cone. In many cases, in-situ substrate heating is used as a mechanism to promote solvent evaporation and the formation of an oxide layer. To address this, heating elements were added to two sides of the collector plate which are controlled via soldered connections to a Variac transformer. The final electrospray setup is seen below in Figure 5.2.

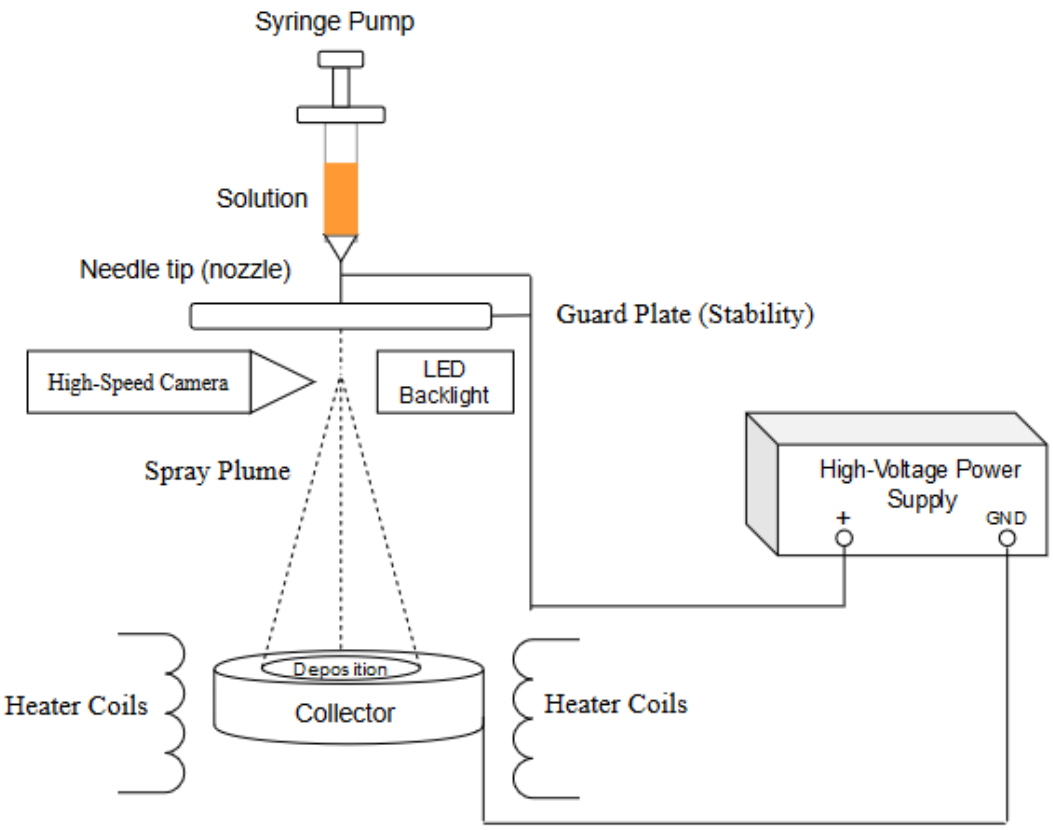

Figure 5.2. Final Electrospray Setup

The motor driver-pcb was constructed using a 555 timer in its astable multivibator mode using an additional bypass diode and a potentiometer to achieve a tunable PWM waveform to drive the motor. The output of the 555 timer drives current into the base of the transistor (npn Darlington), which then drives current through the motor connected on the collector of the transistor. The gain of the tip122 transistor is about 250 at the collector-emitter saturation voltage. Thus it was a suitable transistor for motor-driving applications. The potentiometer forms and RC input load that sets the duty cycle on the output. Thus adjustments could be made for the desired RPM. An optical tachometer was then used to verify the RPM at different collector-emitter voltages, as well as different supply voltages. A reverse-biased diode was added in parallel to the motor to prevent

excessively high voltages from forming on the collector of the transistor during the PWM from the timer IC. The schematic of the circuit is as shown below in Figure 5.3. and the final wiring diagram of the entire setup is shown in Figure 5.4.

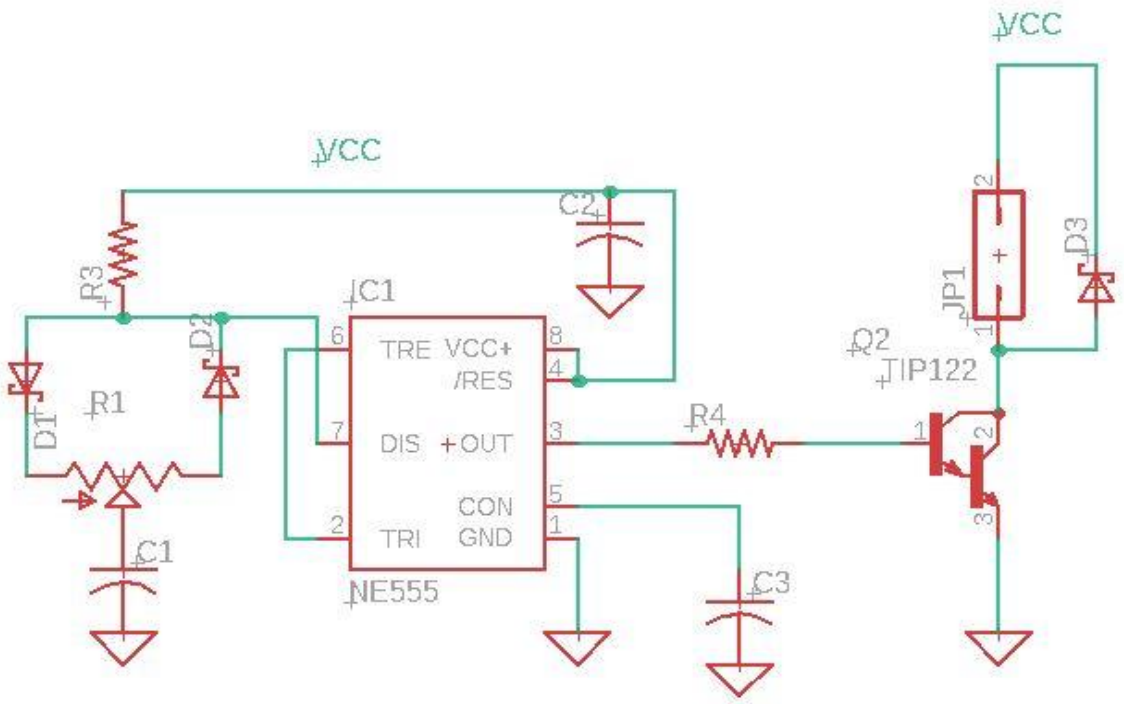

Figure 5.3. Motor Driver PCB Schematic

To provide a DC path for the current to flow from the DC power-supply, a high-powered resistor was utilized to allow the full supply voltage to form on the needle-tip (approximately 10 MΩ). The collector plate was made from aluminum plating such that a solid ground connection could be established via the chassis of the motor and the electrospray frame. A 150 W power-supply was used to power the motor-driver PCB which could then be tuned for the desired RPM. The chassis was grounded via the low-side of the high-powered resistor being connected to a screw terminal on the mount that the motor was screwed into.

The voltage was applied to the emitter via a connection to the interface of the needle and syringe to ensure stability of the needle's position relative to the collector.

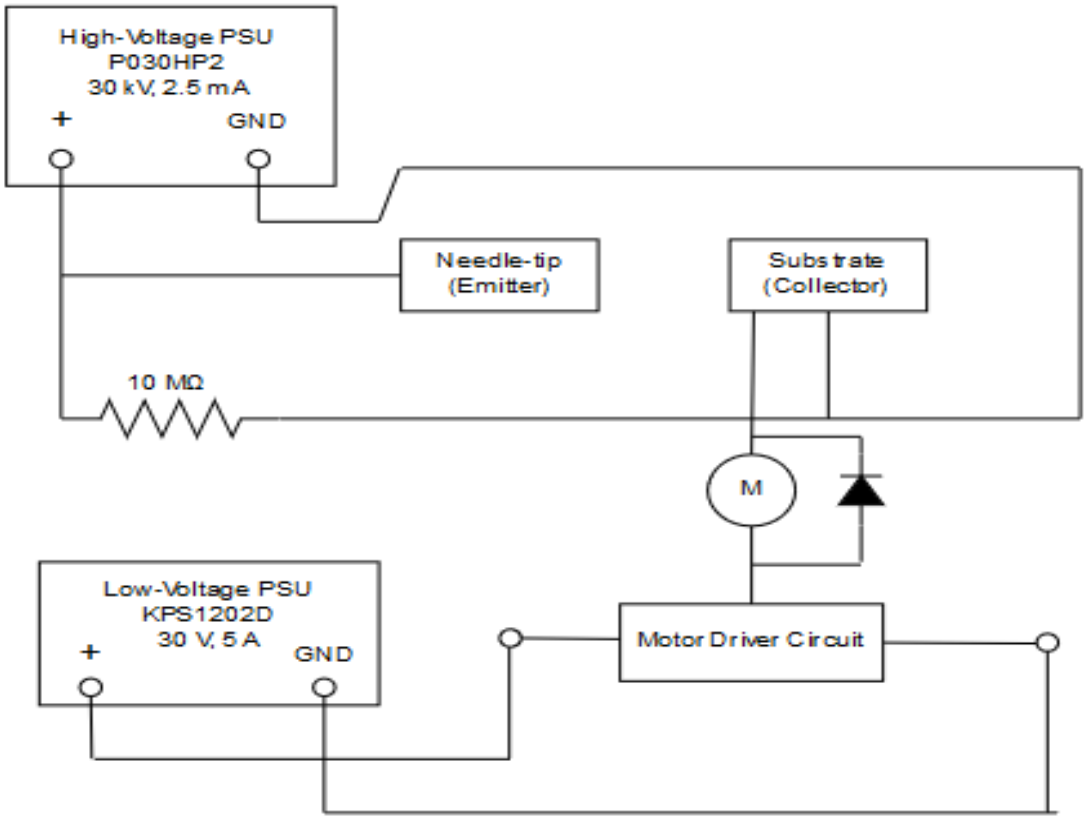

Figure 5.4. Wiring Diagram of the Electrospray Setup

Stability was of great importance as the deposition could only evenly-spread across the sample when sprayed exactly normal to the collector. Any lateral offset in the needle can potentially compromise the deposition pattern as the material would unevenly spread over the surface of the sample. The decision was made to use a stainless steel needle here for the aforementioned reasons pertaining to stability. The needle came pre-blunted which ensures that the voltage is uniformly distributed over the tip of the needle which in-turn allows for more controllable spray mode patterns.

CHAPTER VI: DEPOSITION OF ZNO NANOSTRUCTURES VIA ELECTROSPRAY DEPOSITION

ZnO's wide-bandgap and optoelectronic characteristics have made it a promising material in a wide array of applications in recent years. Producing rapid, quality ZnO depositions for semiconducting layers is a highly attractive venture for those in the realm of electronic devices as this would inherently increase the scalability of device production. In this research, it was decided to study the deposition of ZnO precursor material and its subsequent decomposition into ZnO nanostructures through the electrospray deposition technique. The ZnO precursor, Zinc Acetate Dehydrate (ZnAc) was dispersed in a solvent consisting of ethanol, polyethylene glycol, and NaOH. This suspension was then deposited onto p-type silicon substrates and annealing to form ZnO. The subsequent characterization was done via SEM and Raman spectroscopy.

6.1. Preparation of ZnO Precursor Suspension

The solvent consisting of ethanol and polyethylene glycol was prepared in the quantity of 200 mL with 180 mL of ethanol and 20 mL of polyethylene glycol. Upon the preparation of this solvent 17 g of ZnAc dehydrate nanopowder was added to this solution and placed on a magnetic heater/stirrer at 60^{o} C and stirred at the rate of 1000 rpm. At this point, the pH of the suspension was 4 and then NaOH was added pellet wise until the pH approached 7. The resulting suspension was then tip-sonicated over a 30-minute period for 2 minutes on the 2 minutes off. The pH was then recheched to ensure that it remained at 7 after any residual NaOH would have dispersed. Subsequent to this, the solution was allowed to sit for approximately 18 hours. The resulting suspension is pictured below in Figure 6.1.

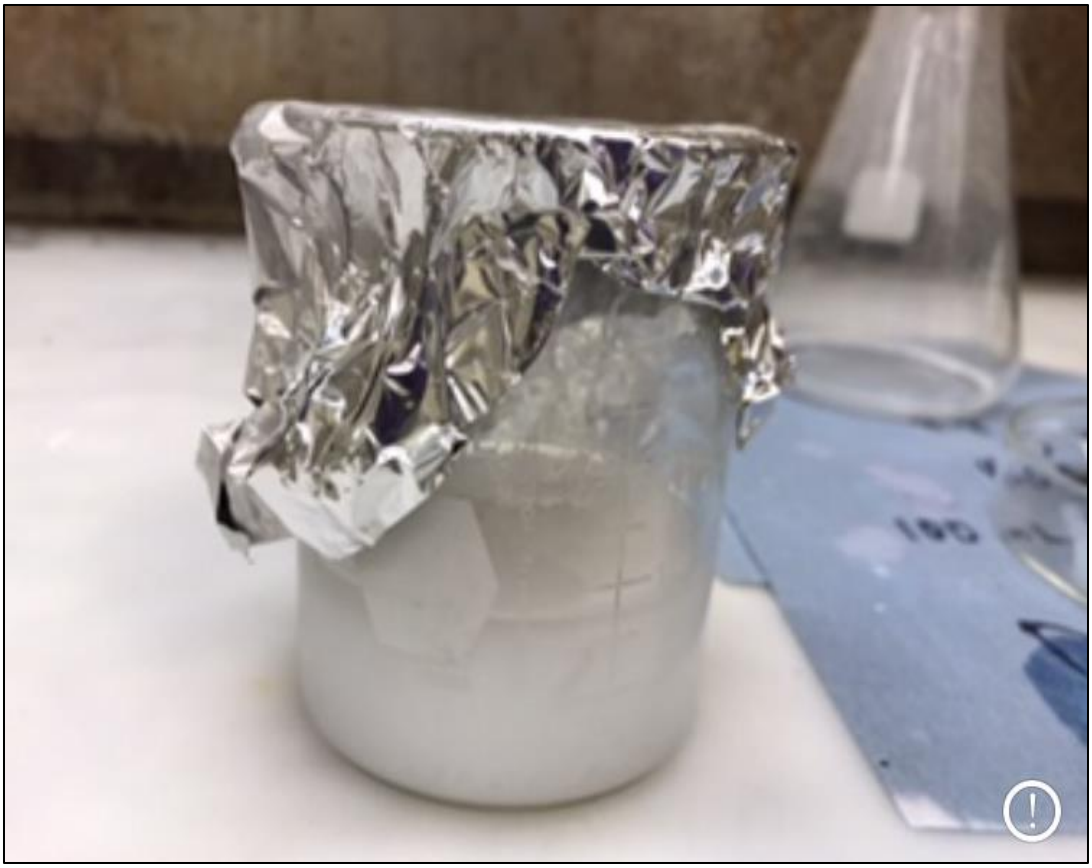

Figure 6.1. ZnO Precursor Suspension

6.2. Electrospray Deposition of ZnO Precursor

The ZnO precursor material was then deposited on silicon substrates via electrospray. The intended spray mode for this deposition was the cone-jet mode, and thus the formation of the different spray regimes was studied in detail. The needle was fixed on the Harvard Apparatus 22 dual syringe pump 2 inches above the grounded collector plate. Flow rates of 10 μL/min to 50 μL/min were examined, and their spray modes were noted for different applied voltages at each flow rate from 10 μL/min to 50 μL/min at 10 μL/min steps. Aside from the voltages and flow-rates, the diameter of the needles also affects the formation and transition of these modes. Thus needles of 18, 20, and 22 gauge diameters were used. The needles were bought pre-blunted to

ensure uniform electric-field over the entire needle. Prior to deposition, all silicon substrates were cleaned via acetone, isopropyl alcohol, and then rinsed with deionized water. Each mode characterized can be seen in the following Figure 6.2.

The 18-gauge needle (outer/inner diameter: 1.27/1.054 mm) resulted in the following images (Figure 6.2 - 6.3 respectively):

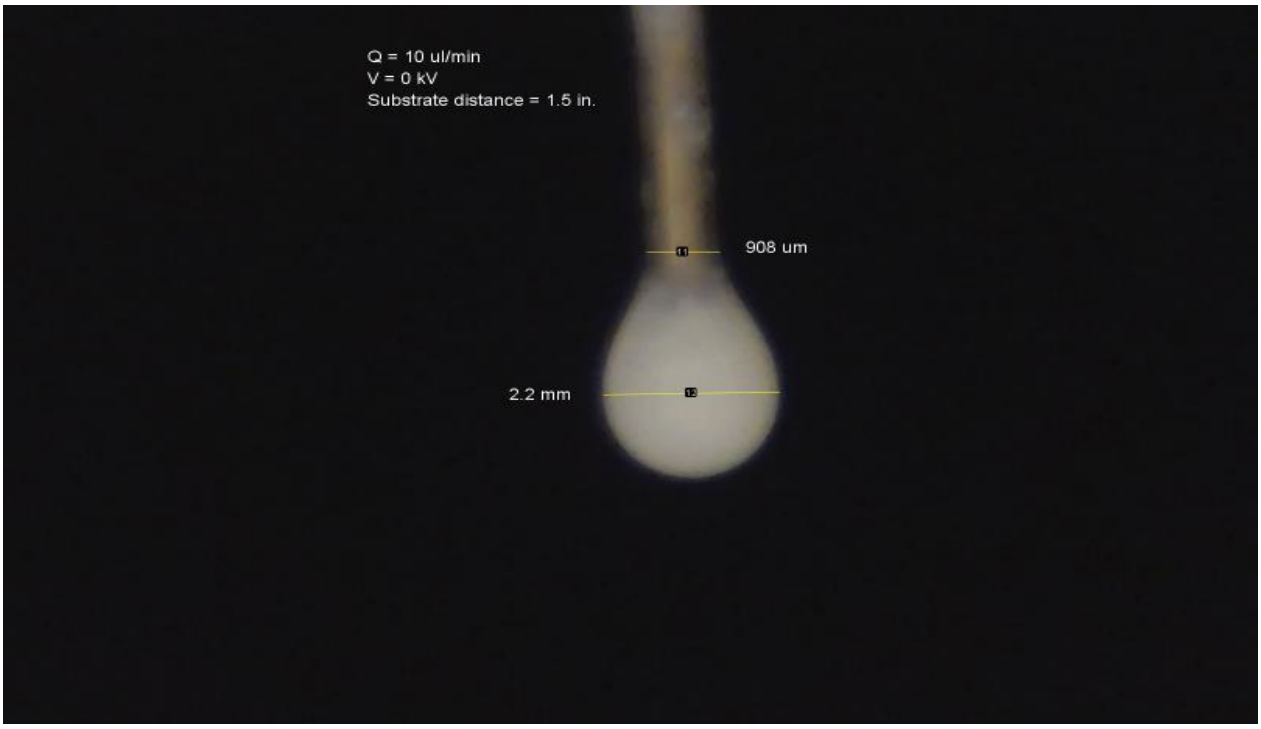

Figure 6.2. Electrospray Droplet Mode

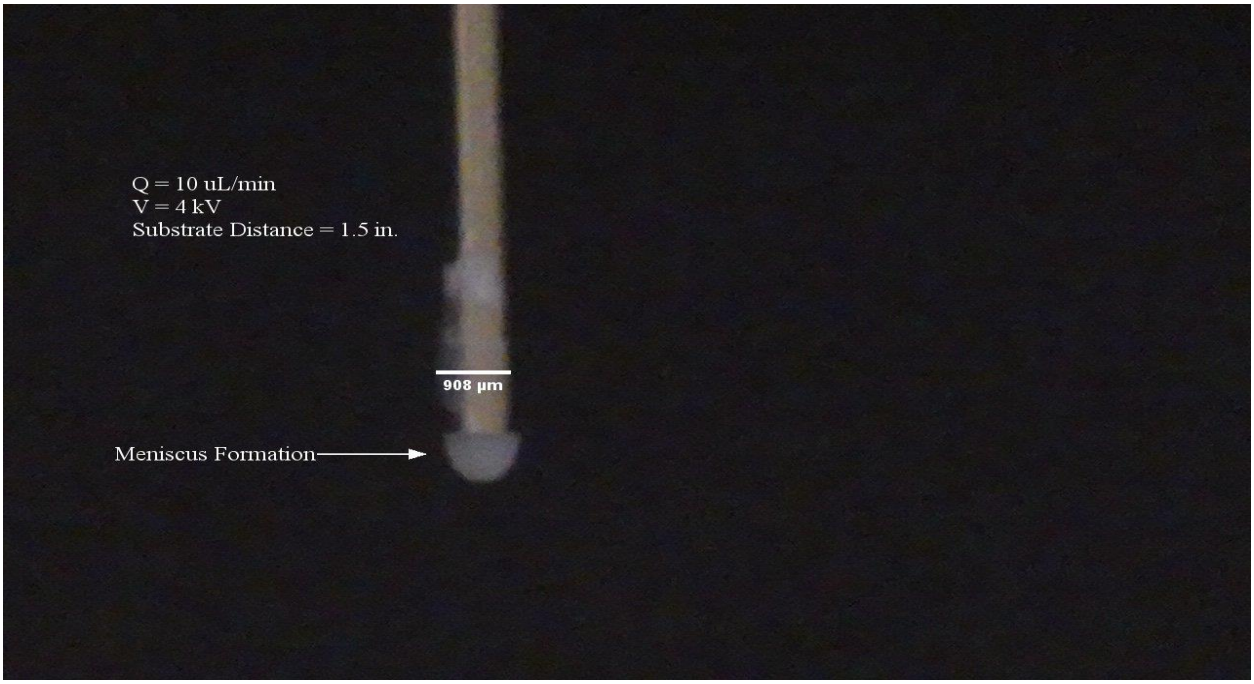

Figure 6.3. Electrospray Microdroplet Mode

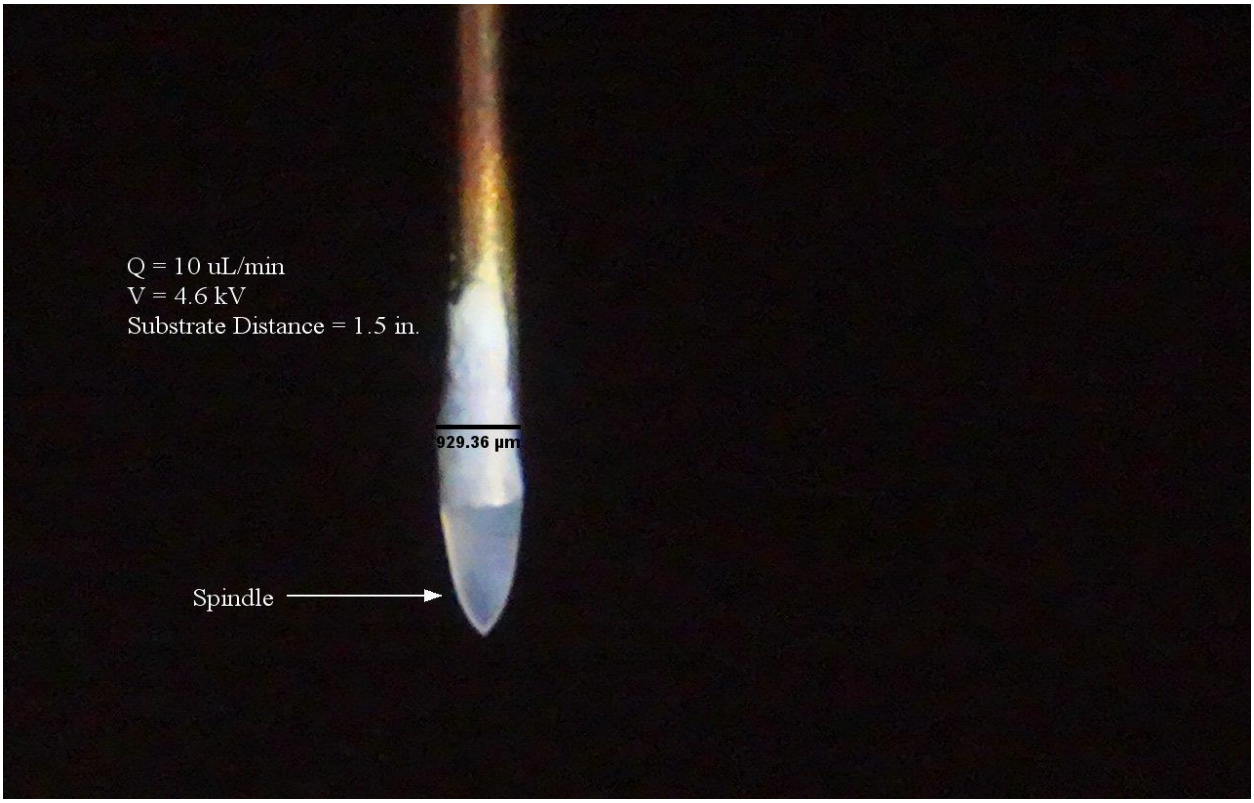

Figure 6.4. Electrospray Spindle Mode

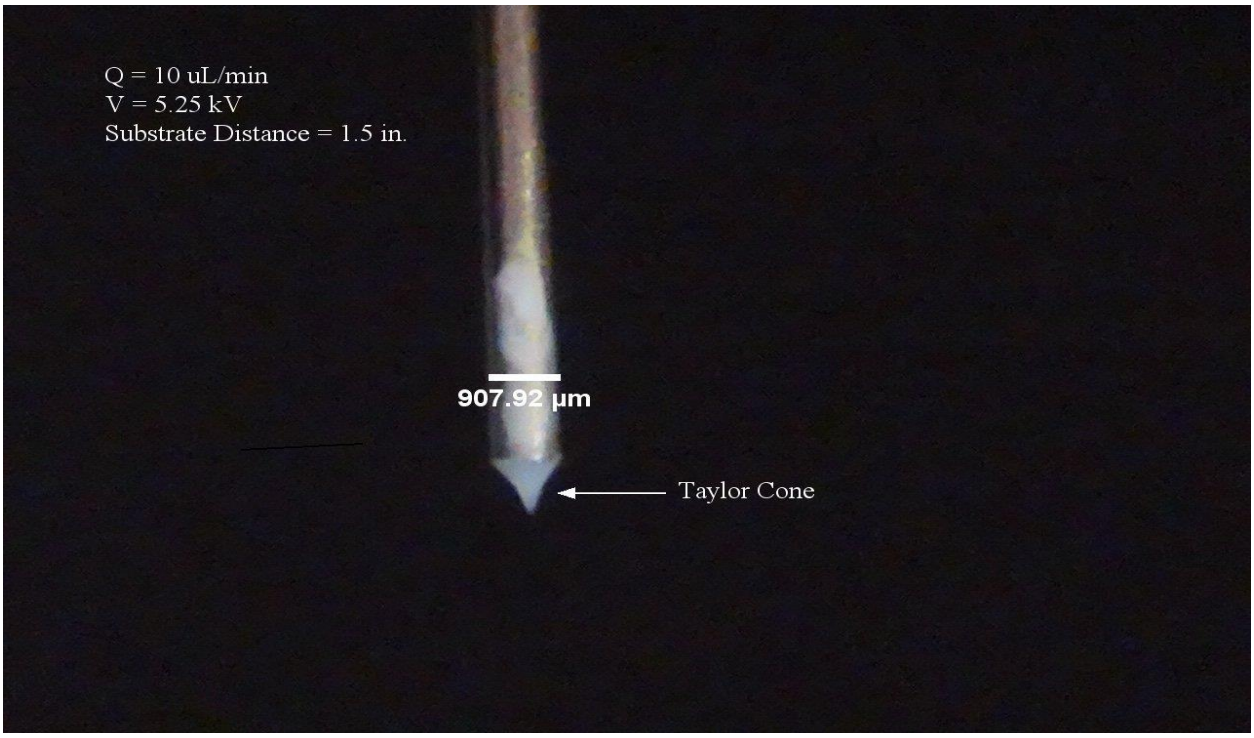

Figure 6.5. Electrospray Cone-Jet Mode

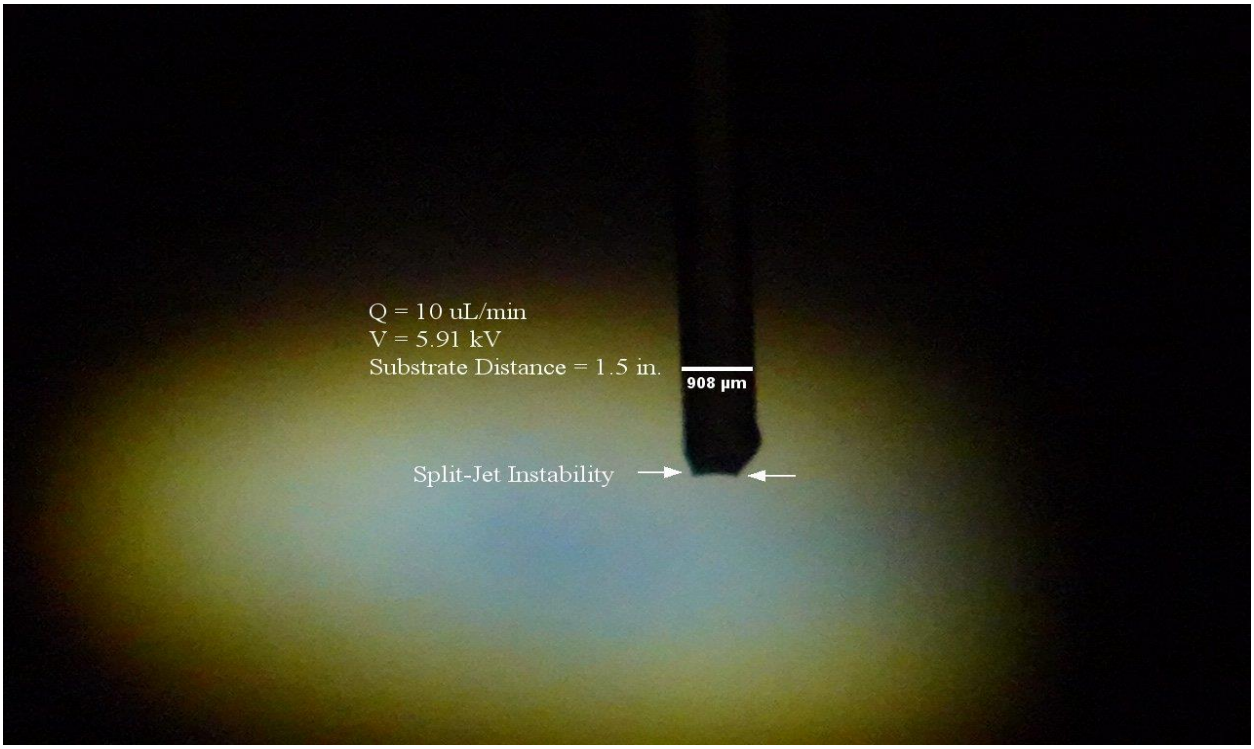

Figure 6.6. Electrospray Multi-Jet Mode

6.3. Characterization of Electrospray Mode Formations

As mentioned in 6.2, the applied voltage vs. the flow-rate was plotted to characterize the spray mode transitions per increase in flow-rate. The flow-rates were increased at a step size of 10 uL/min from 10-50 uL/min for 3 different needle sizes. These plots can be observed below in

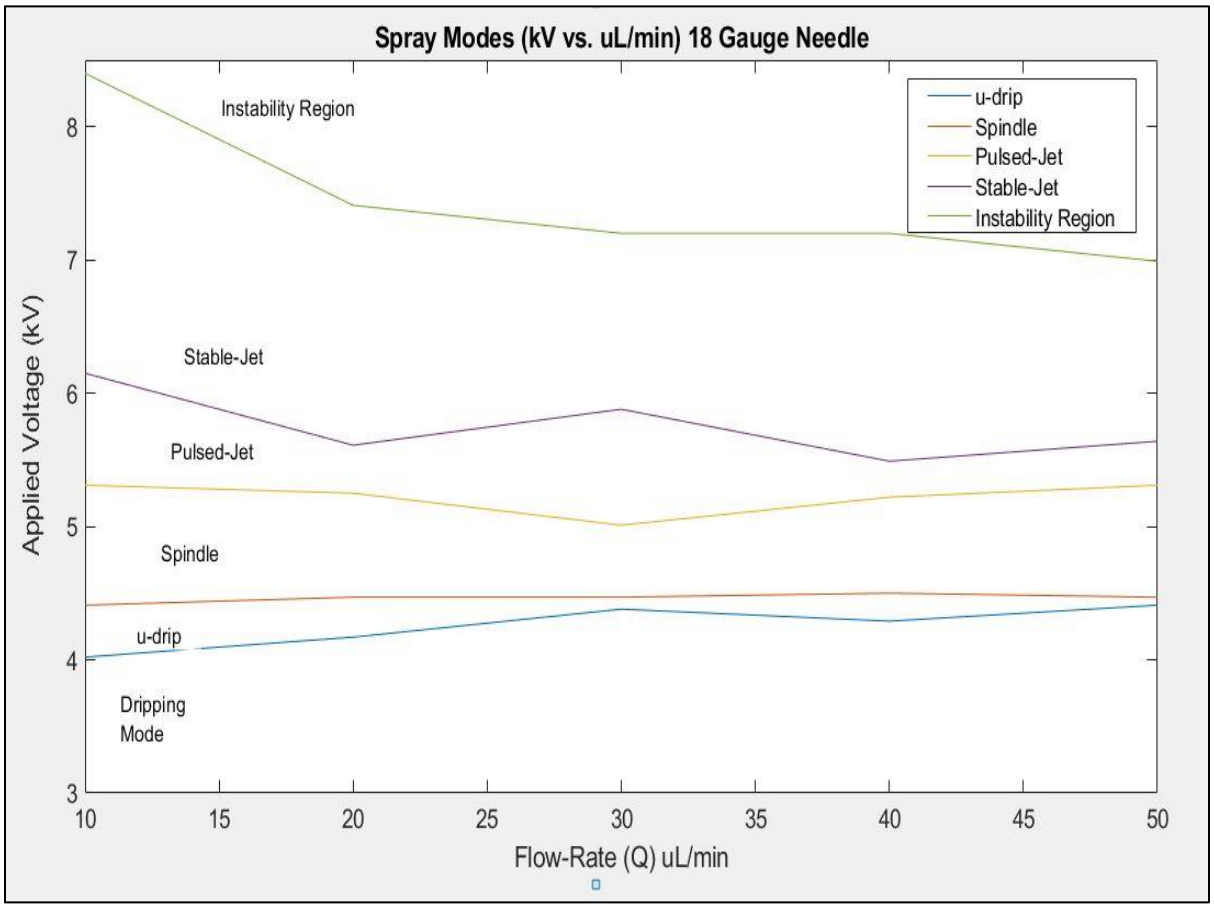

Figure 6.7. Plot of Applied Voltage vs. Flow Rate (18 gauge needle)

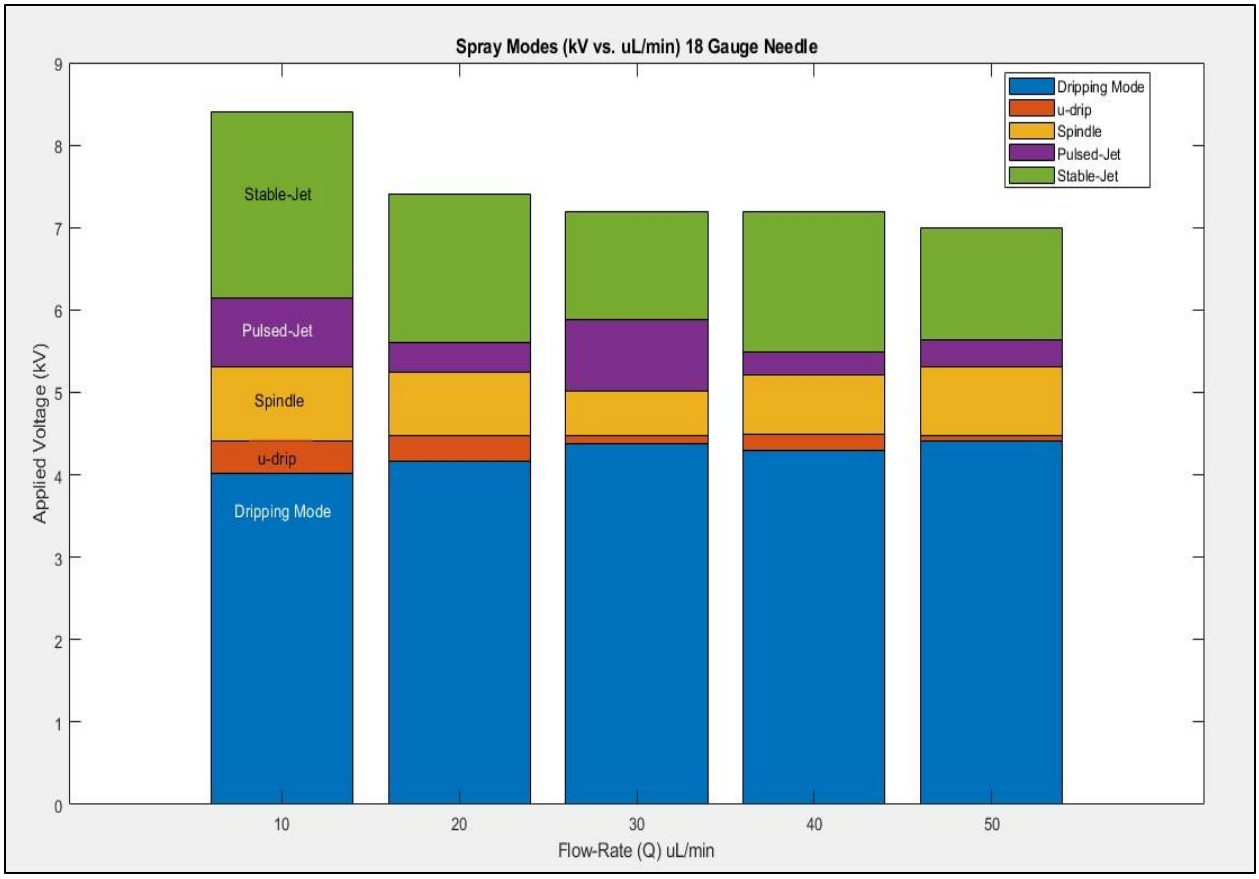

Figure 6.8. Equivalent Bar Graph Representation of Figure 6.7.

The space between the lines on the plot are the corresponding regions in which they are stable. From the above, it can be noted that for increasing flow-rates, the regions in which the modes are stable tend to become smaller. The same experiment was carried out two more times for the 20 gauge and 22 gauge needle respectively resulting the following:

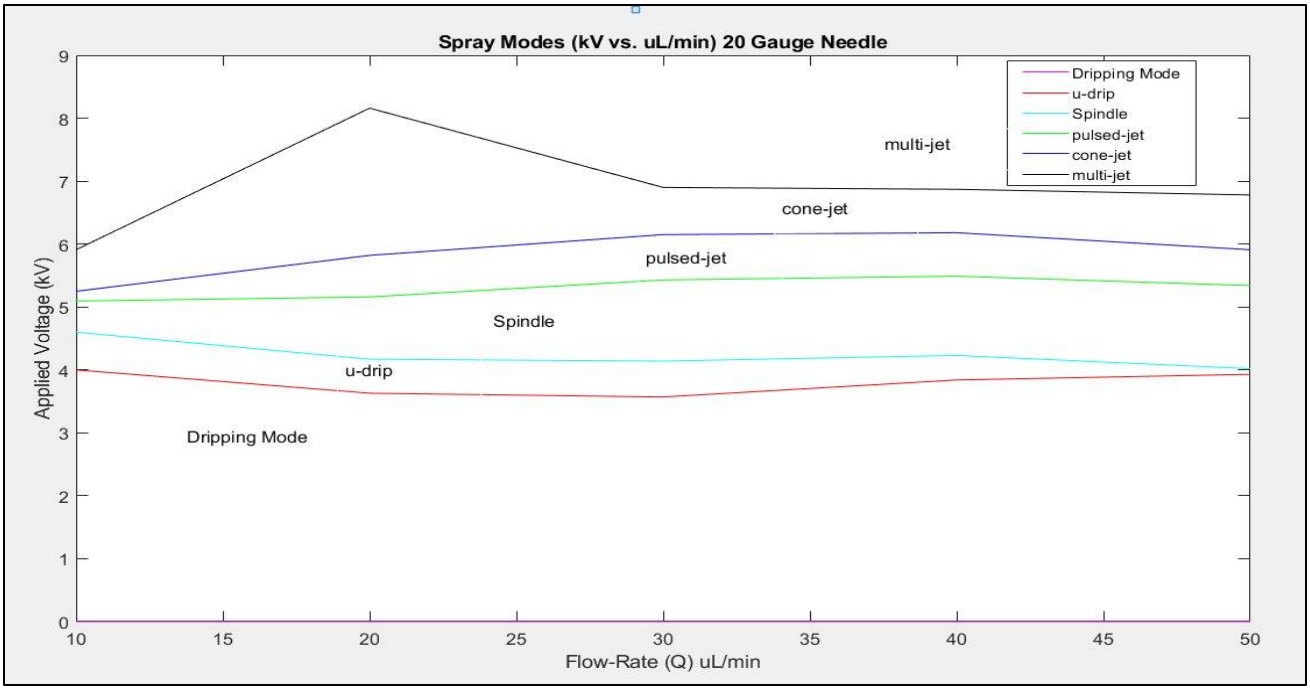

Figure 6.9. Plot of Applied Voltage vs. Flow Rate (20 gauge needle)

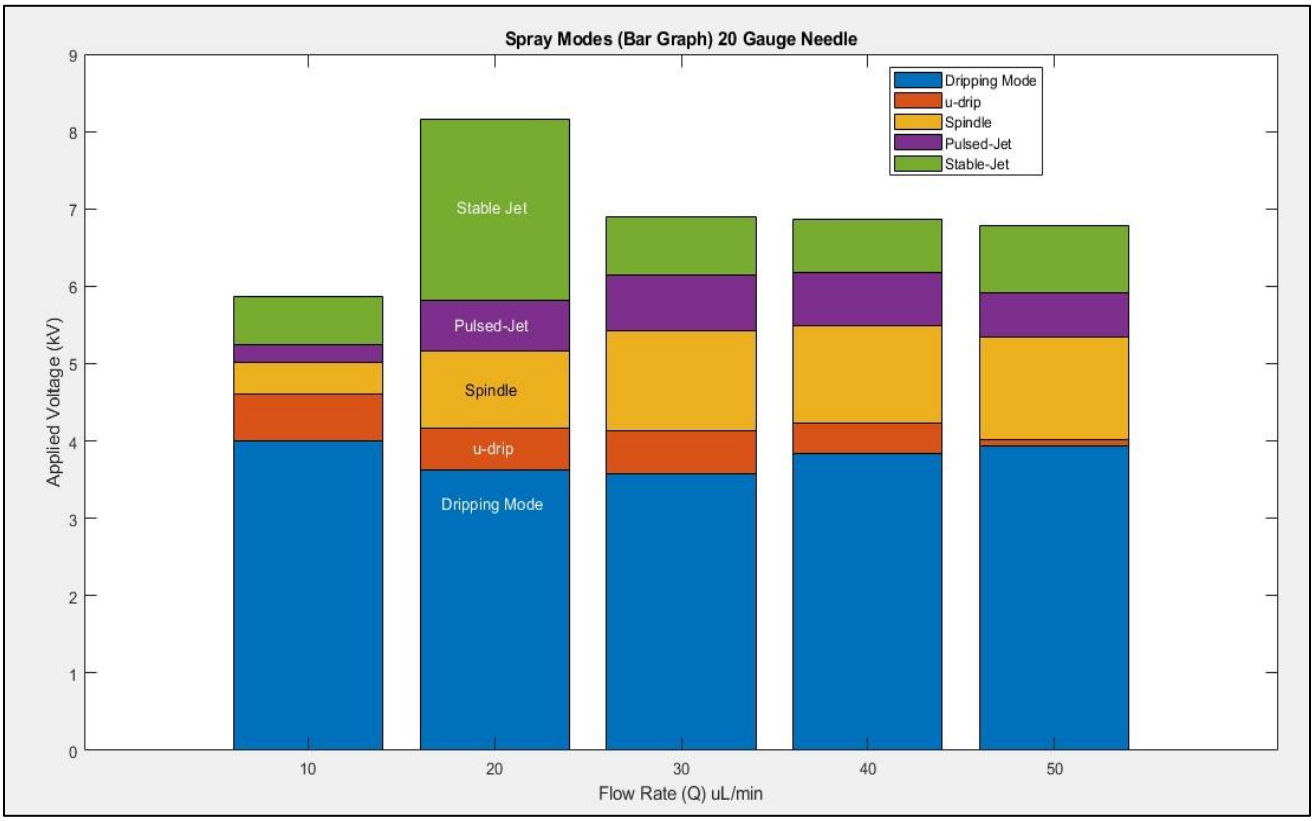

Figure 6.10. Equivalent Bar Graph Representation of Figure 6.9.

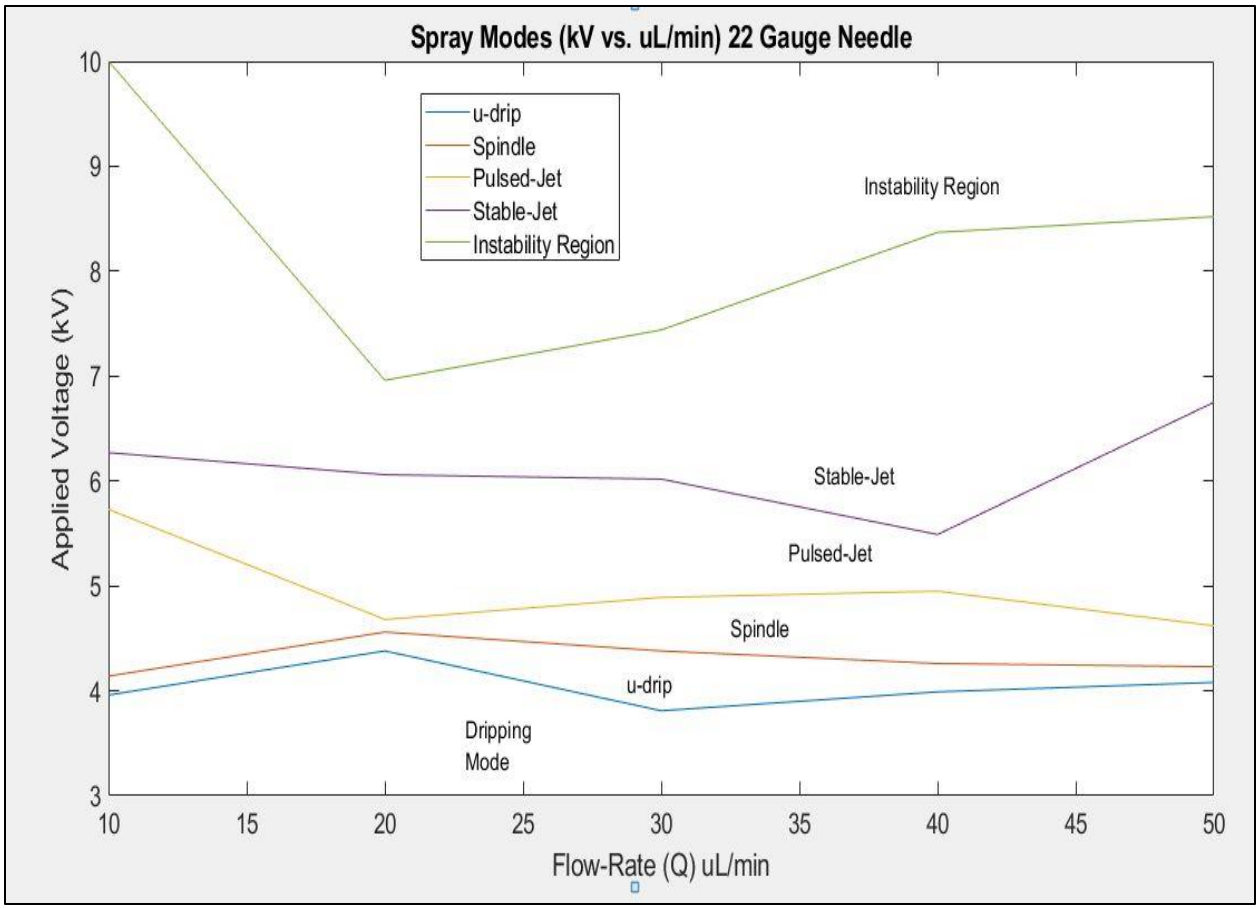

Figure 6.11. Plot of Applied Voltage vs. Flow Rate (20 gauge needle)

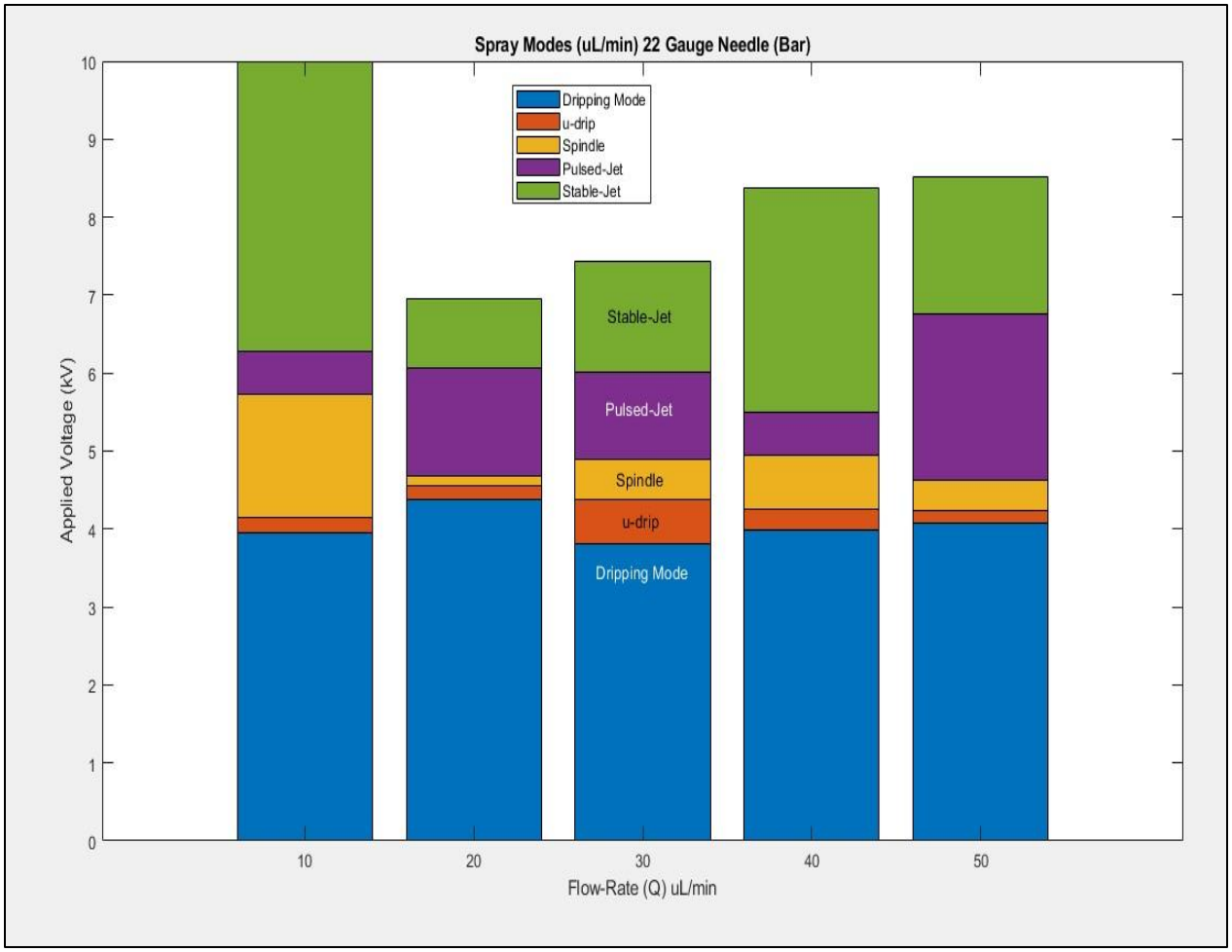

Figure 6.12. Equivalent Bar Graph Representation of Figure 6.11.

Several deposition modes were carried out and the subsequent nanostructure sizes were studied in detail. The jet-mode is the most common mode used for the depositions because of the better nanostructure distribution obtained and this was observed experimentally here. The 20 gauge needle was used in all subsequent depositions because its stainless steel frame was the most stable and provided the highest quality depositions.

6.4. Characterization of ZnO Depositions

Upon obtaining the silicon coated ZnO precursor material, the substrate was then annealed at 605ºC for 1 hour. Upon the thermal decomposition of the precursor coated silicon substrate, the following Raman spectrum was obtained (Figure 6.13).

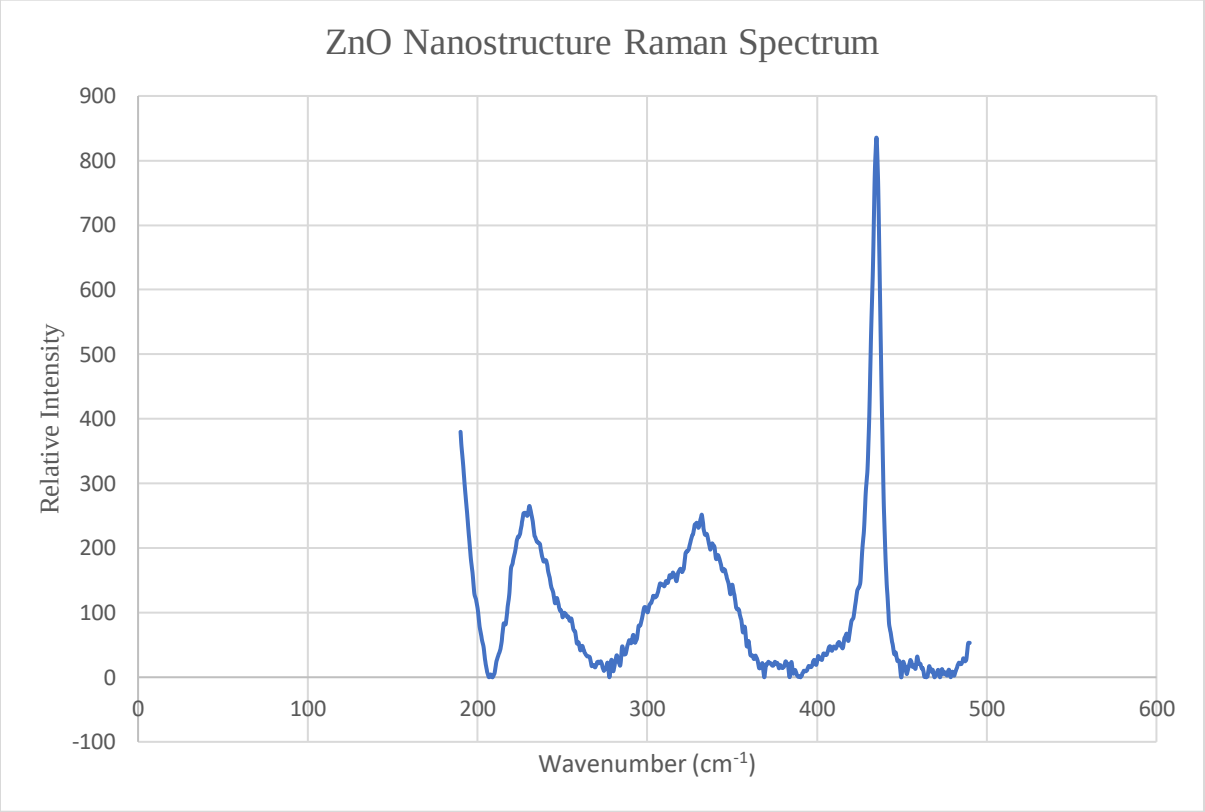

Figure 6.13. Raman Spectrum of ZnO (lower spectrum)

The relative intensity of the spectrum peaks is represented along the y-axis while peak wavenumber (in cm^{-1}) is shown along the x-axis. The primary peaks observed were at 231 cm^{-1}, 332 cm^{-1}, and 434 cm^{-1} respectively. The 332 cm^{-1} peak is categorized as the 2E2 with the 434 cm^{-1} categorized as the E2 mode. The 434 cm^{-1} peak is commonly associated with ZnO nanorods hence the above plot demonstrates that the precursor was successfully decomposed into the desired ZnO

nanostructure film. Another, higher peak was observed at 1097 cm^{-1} which is also characteristic of ZnO nanostructures. The resulting spectrum can be observed below in Figure 6.14.

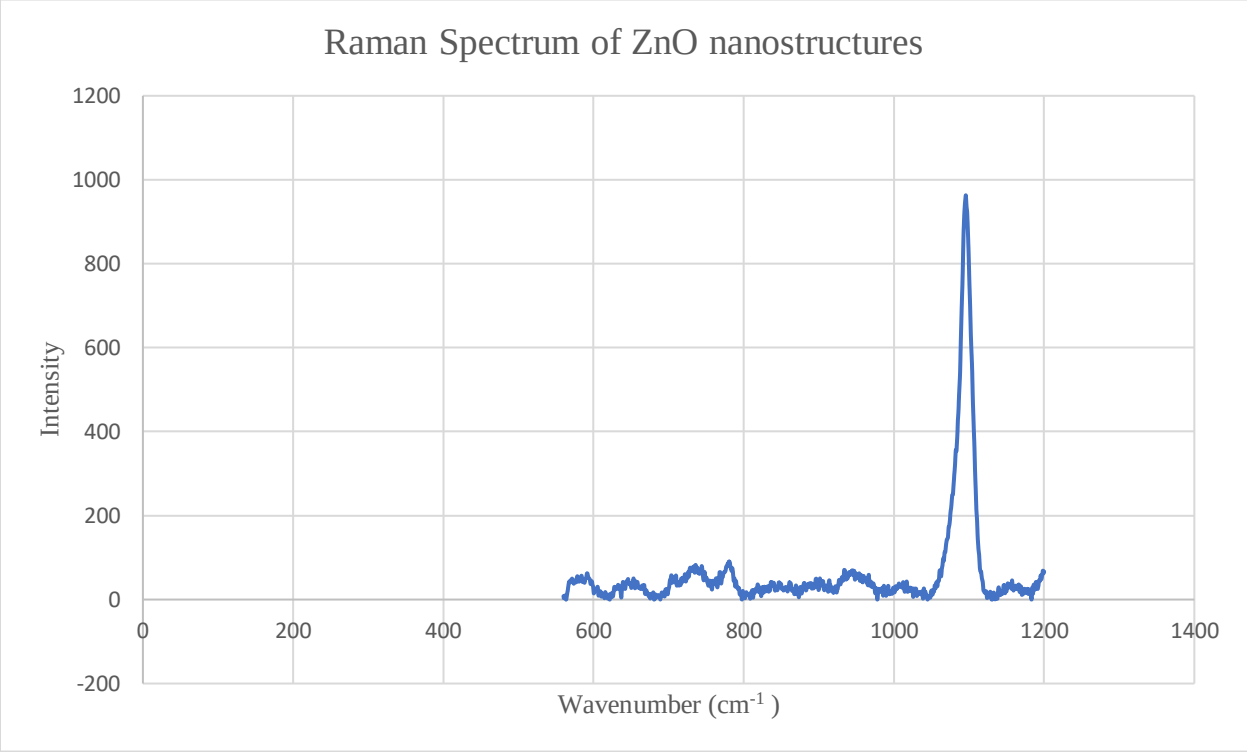

Figure 6.14. Raman Spectrum of ZnO from 580 to 1200 cm^{-1}

Upon confirmation that ZnO nanostructures were obtained the deposition was then observed through an SEM. The first step to the characterization was to determine the film thicknesses obtained in the various spray modes. The first mode used was droplet mode, the ZnO was dripped at 50 ul/min for 2 minutes at 0 rpm. The deposition was then annealed at 605ºC for 1 hour then imaged via SEM. These parameters were held constant through u-drip, and cone-jet.

The average film thickness by mode is depicted in the bar-graph below, where the thinnest film is obtained via the cone-jet mode at approximately 1.3 um.

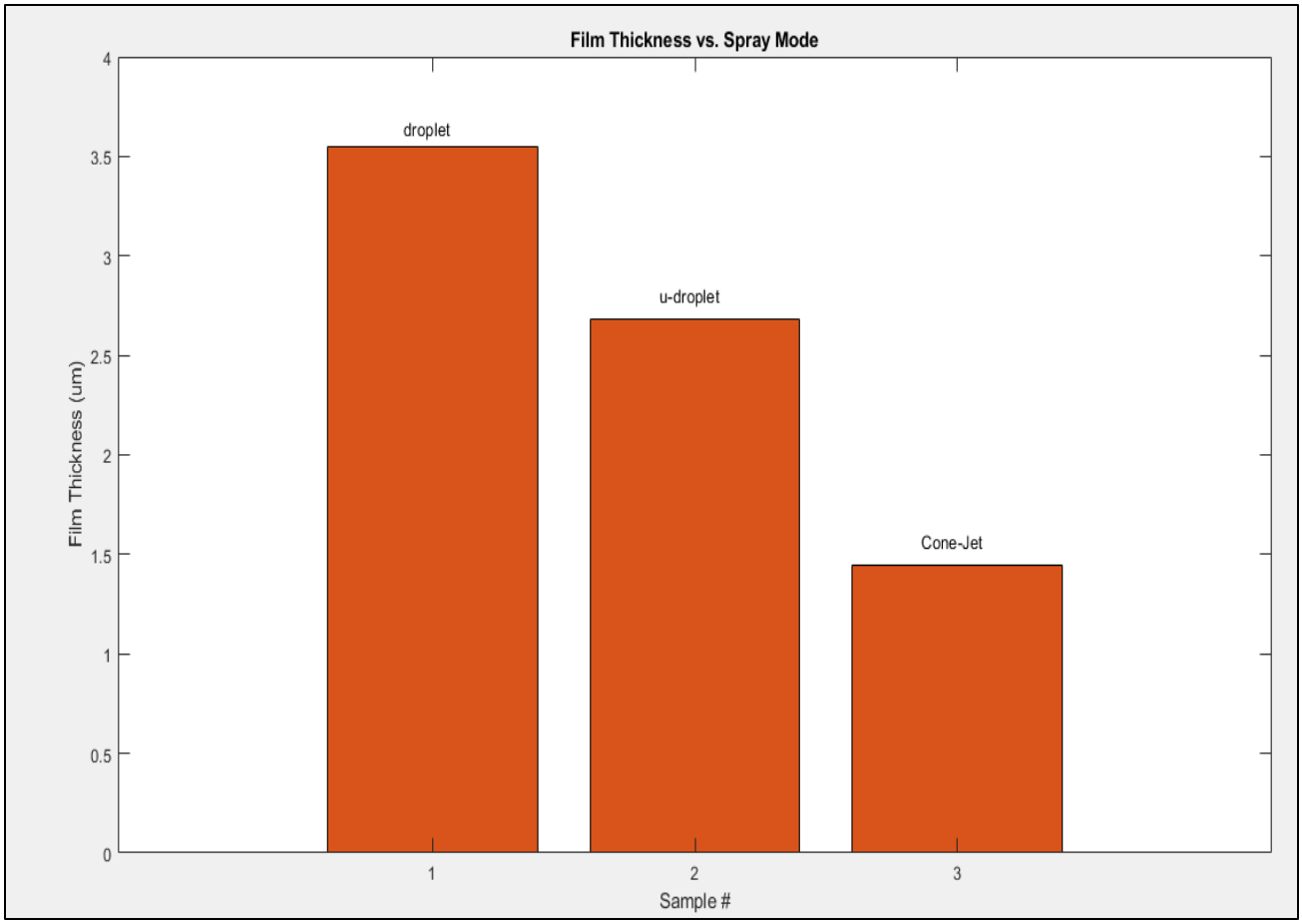

Figure 6.15. Average Film Thickness per Spray Mode

As expected, the cone-jet mode showed the best film thickness thus this was the mode chosen to carry out the future depositions. The weight of the sample pre-anneal and post-anneal was also noted during the experiment (table below).

Table 6.1. Sample Weight & Film Thickness per Spray Mode

Spray Modes	**(1) droplet**	**(2) u-droplet**	**(3) Cone-Jet**
Sample Weight	0.802 g	0.749 g	0.790 g
Sample Weight (Post-Anneal)	0.805 g	0.758 g	0.798 g
Film-Thickness	3.546 um	2.682 um	1.448 um

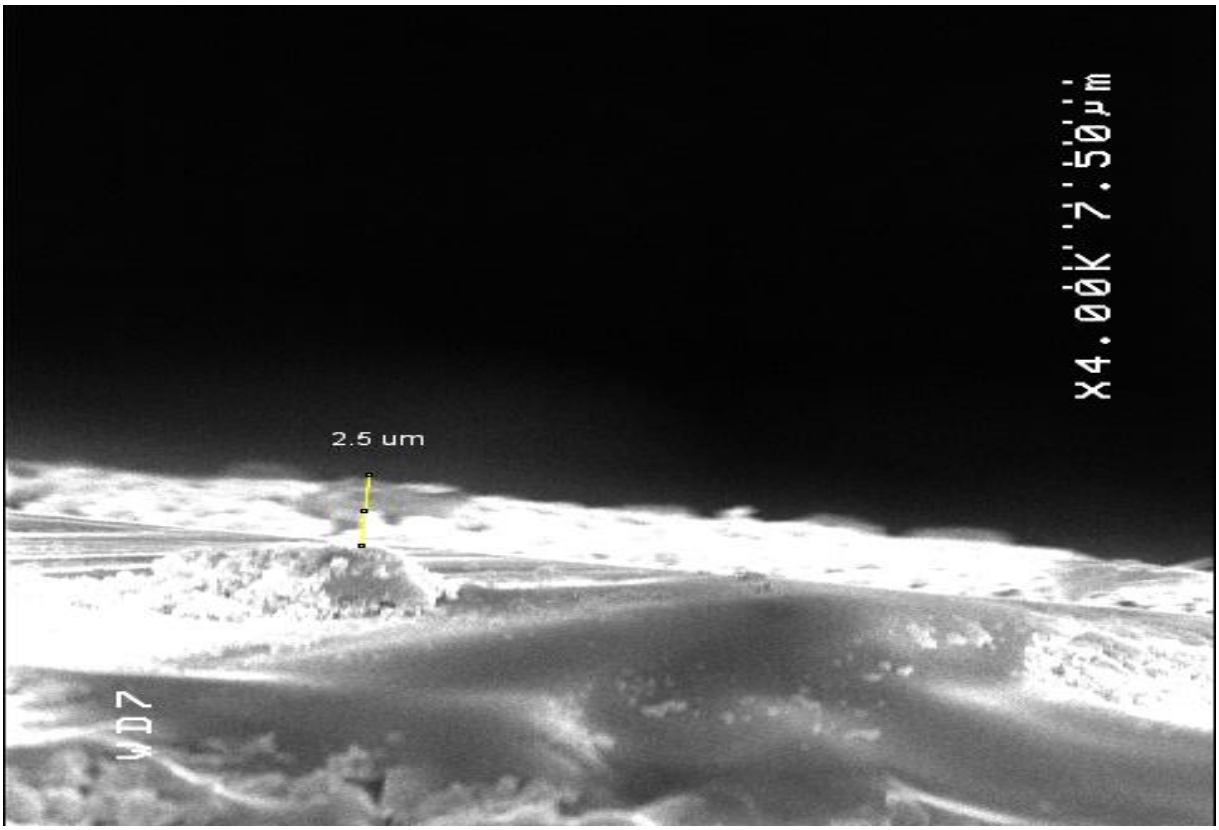

Figure 6.16. Droplet Mode Film Cross-Section

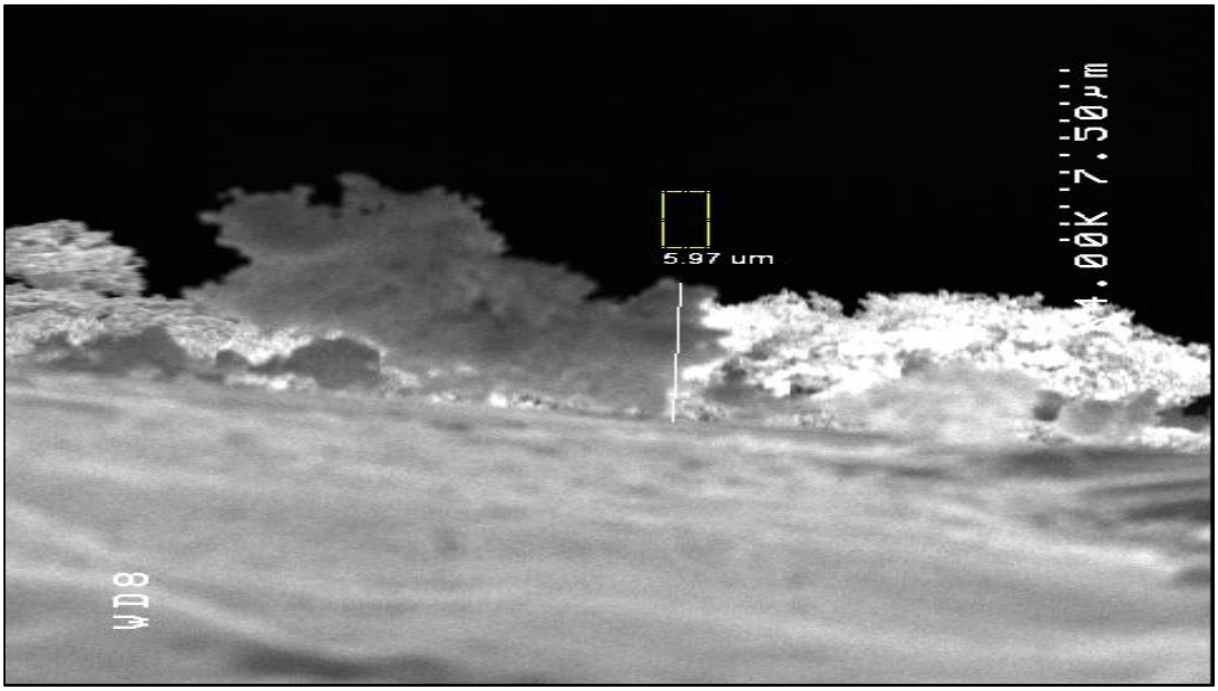

Figure 6.17. Droplet Mode Film Cross-Section (thicker region)

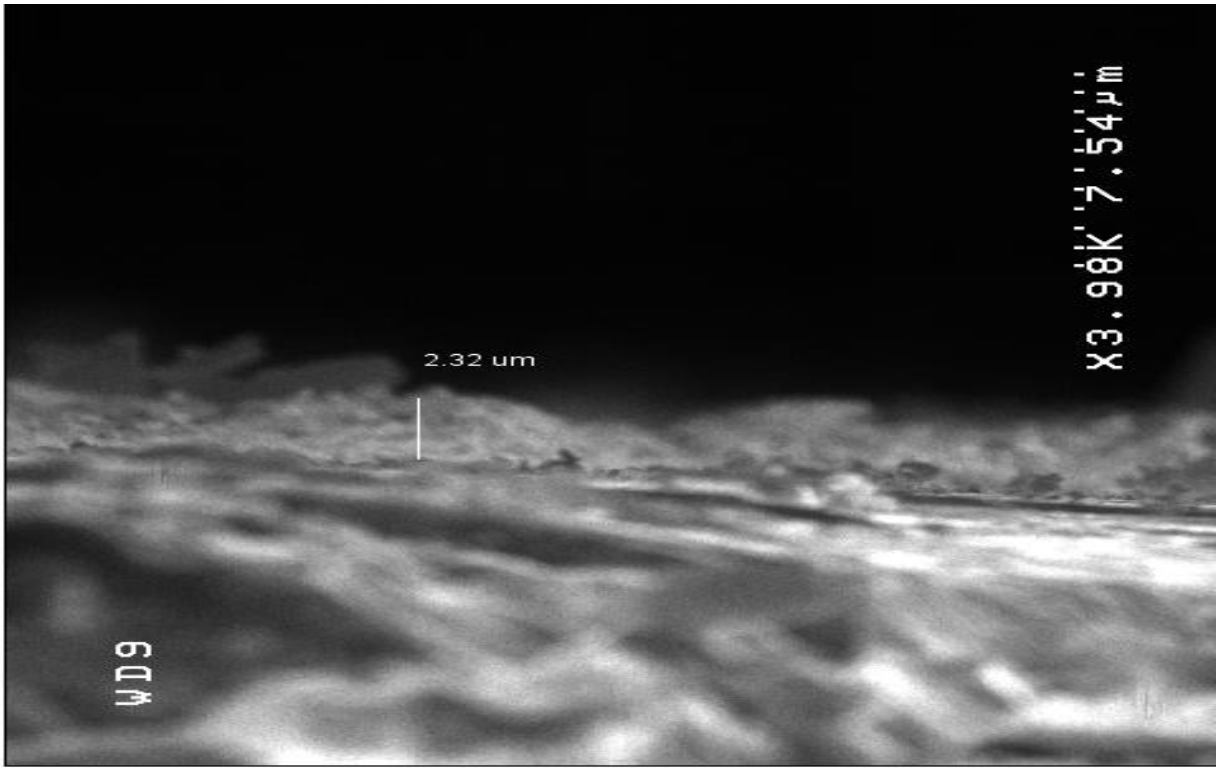

Figure 6.18. Micro-dripping Mode

The film remains closer to 2.5 – 3 µm, however there are more non-uniform regions that have significantly thicker regions as seen in Figure 6.19. The next spray regime, u-drip, has fewer outlier regions than that of the droplet mode.

The microdripping mode shows noticeably thinner regions of deposition than the droplet regime. The deposition, in this case, seems less continuous across the cross-section. This can be attributed to the droplet evaporation occurring over a smaller area and each successive droplet displacing more of the already deposited semi-dry liquid. The final mode observed was the jet-mode which was used in all subsequent experiments due to its even thinner films due to the effect of coulombic repulsion and resulting more uniform distribution of droplets and thus nanostructures.

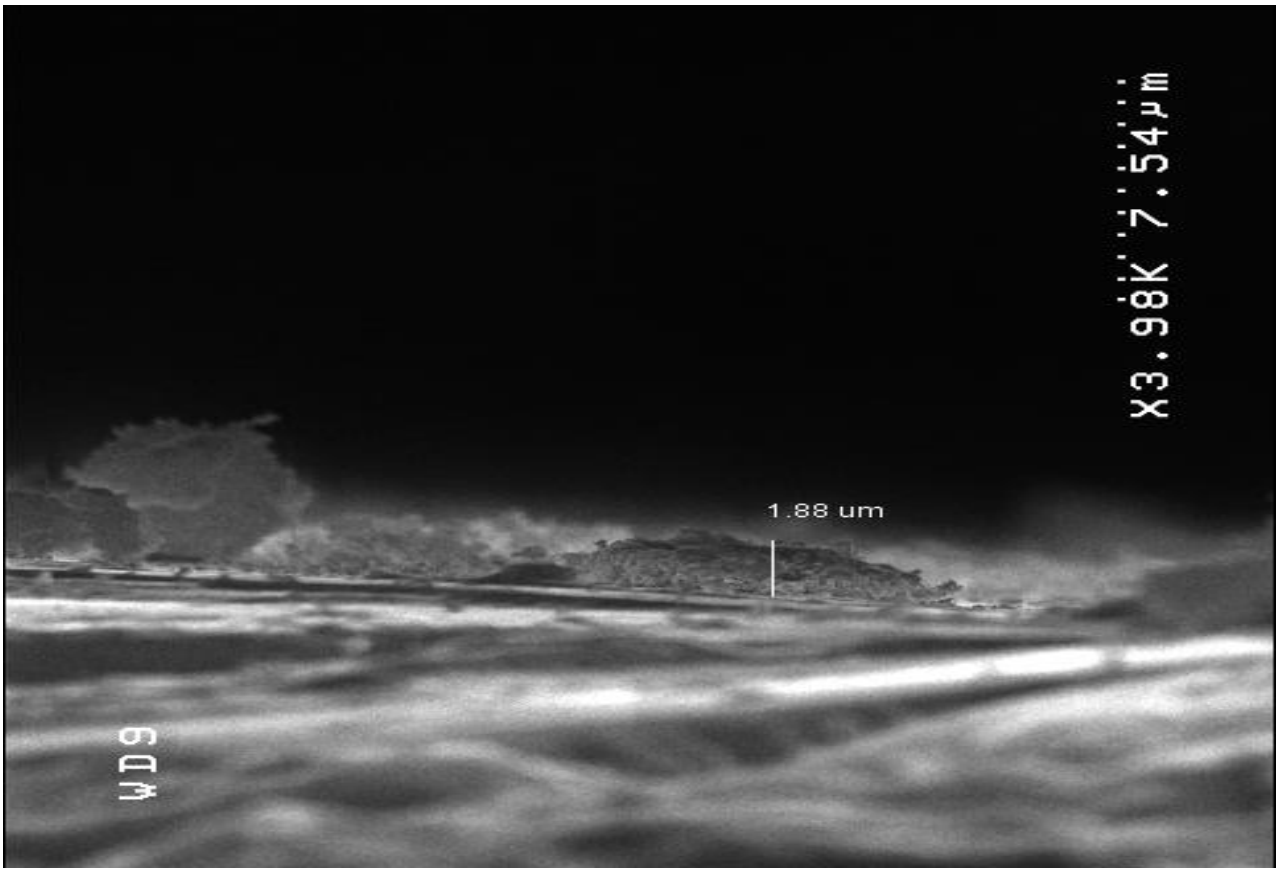

Figure 6.19. Micro-dripping Mode Cross-Section

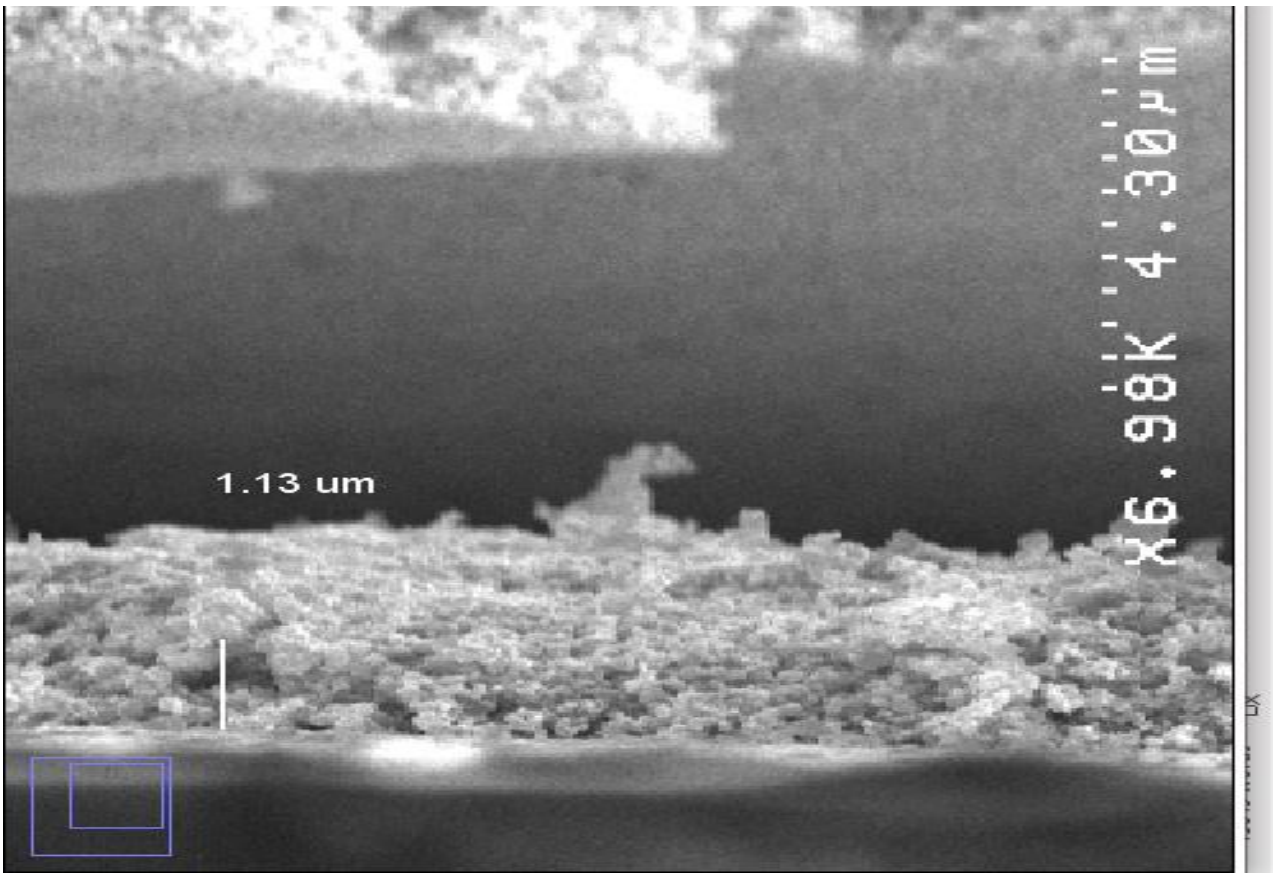

Figure 6.20. Cone-Jet Mode Cross-Section

The final mode observed was the jet-mode which was used in all subsequent experiments due to its even thinner films due to the effect of coulombic repulsion and resulting more uniform distribution of droplets and thus nanostructures. The cone-jet demonstrated the thinnest films with the average thickness being approximately 1.5 μm. In the image above a thickness of slightly over 1.1 μm was observed. This also proves that the electrospray regime can conceivably be used to obtain true sub-micron thin films. The subsequent steps were to observe the effect of varied-temperature and varied-deposition time on the nanostructure size and formation. Each deposition was prepared in the same fashion, deposited for 2 minutes at 0 rpm and a flow-rate of 50 ul/min. The subsequent steps were to observe the effect of varied-temperature and varied-deposition time on the nanostructure size and formation.

Each deposition was prepared in the same fashion, deposited for 2 minutes at 0 rpm and a flow-rate of 50 ul/min. Upon completion of the deposition, the samples were then pre-heated for 10 minutes at 150^{o}C for 10 minutes then annealed at 605 ^{o}C for 30 minutes, 1 hour, and 2 hours in each case. This same procedure was then repeated for annealing temperatures of 405 ^{o}C and 505 ^{o}C. The resulting samples were then imaged via SEM to determine the size and type of the nanostructures formed. The plot below summarizes these relationships (Figure 6.21). For higher annealing temperatures, the excess surface energy on the film causes an increase in the resulting particle size as the effect of nanoscale agglomeration increases with increased surface temperature. The nanostructure type was predominantly nanorods, however, in some instances nanothorns and nanoflowers were also observed on the sample. Temperatures in excess of 600 ^{o} C
are more commonly used in literature, hence this is the temperature used as the default for most of the deposition studying film thickness.

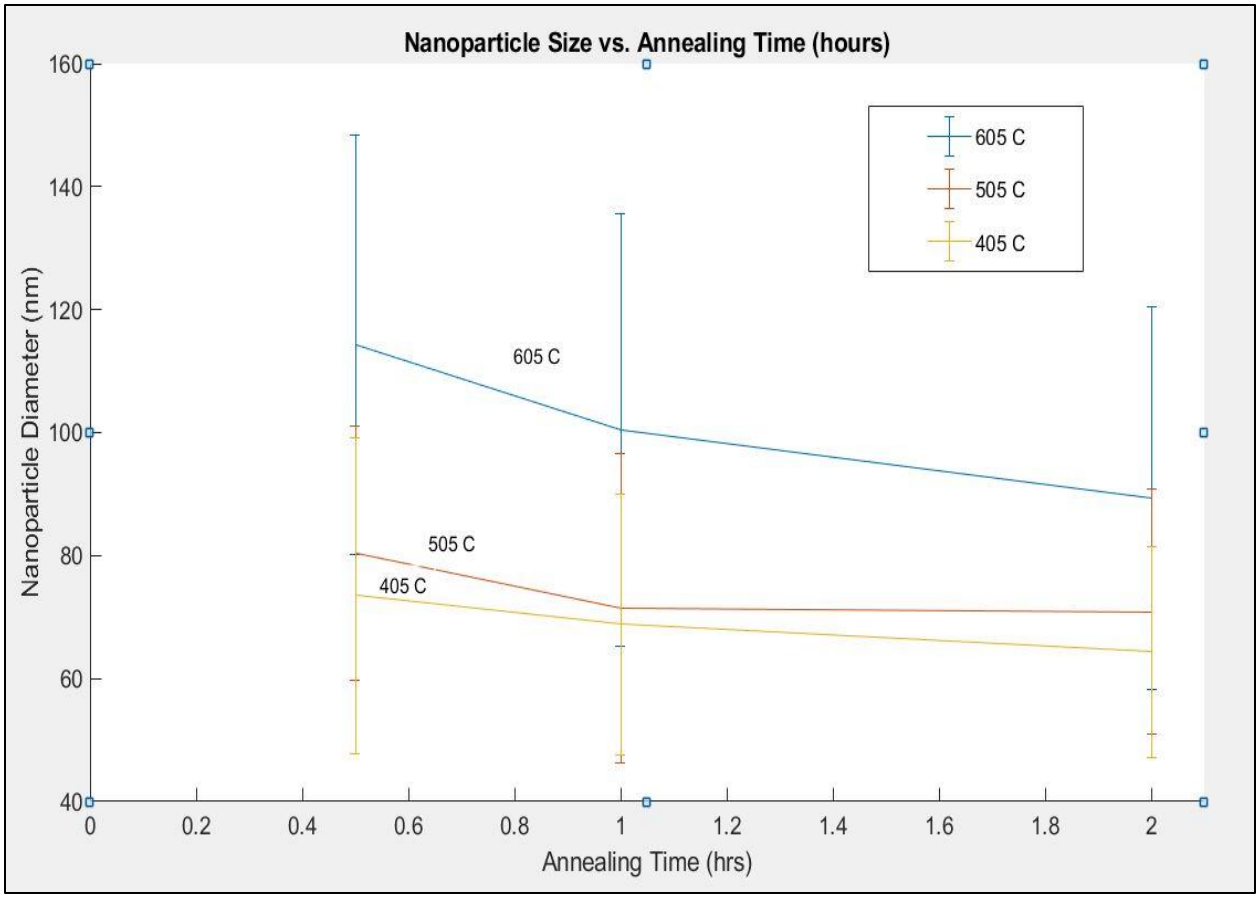

Figure 6.21. Nanostructure size vs. Annealing Time (405 ^{o}C, 505 ^{o}C, and 605 ^{o}C respectively)

Table 6.2. Nanorod Size vs. Annealing Time for 405^{o} C, 505^{o} C, and 605^{o} C respectively

Annealing Time	**405°C**	**505°C**	**605°C**
0.5 hr	73.471 nm	80.347	114.32 nm
1 hr	68.778 nm	71.484	100.326 nm
2 hr	64.309 nm	70.885	89.373 nm
Standard Deviation (avg)	21.322	21.887	33.54

The average nanoparticle size for 1 hour at 605 ^{o}C was just below 100 nm hence successful formation of ZnO nanorods.

6.5. Effect of Controlled Substrate Rotation on Film Thickness

After demonstrating that the cone-jet mode was the optimal mode for thin-film regime depositions and that 1 hour of annealing at 605 ^{o}C produced ZnO nanorods, the attention of the research was turned to the effect of substrate rotation on film-thickness. Previous research from [89] showed that substrate rotation had a thinning effect on electrospray deposited sample, however with carbon nanotubes, and thus we set out to quantify this effect with ZnO as the material used. Prior to finding the appropriate solvent concentrations, depositions that were spun at different rotational velocities all had an empty circle in the center of the deposition with the material all being concentrated in ring-patterns on the outer regions of the sample (Figure 6.22). A similar effect is also observed in spin-coated films with very low-viscosities as the evaporation of the solution, in effect, pushes out the material as the center evaporates away. Once the polyethylene glycol was added, this vacant region of the substrate was mitigated, and the resulting depositions were more uniform across the entire sample. Upon obtaining the improved surface coverage, the effect of the substrate rotation was studied in detail. The rotational velocities set were 3200, 5500, and 9000 rpm, respectively. Each of these were compared to the case of depositions at 0 rpm. In addition, the RPM effect was studied on depositions carried out for 2 minutes, 5 minutes, and 10 minutes.

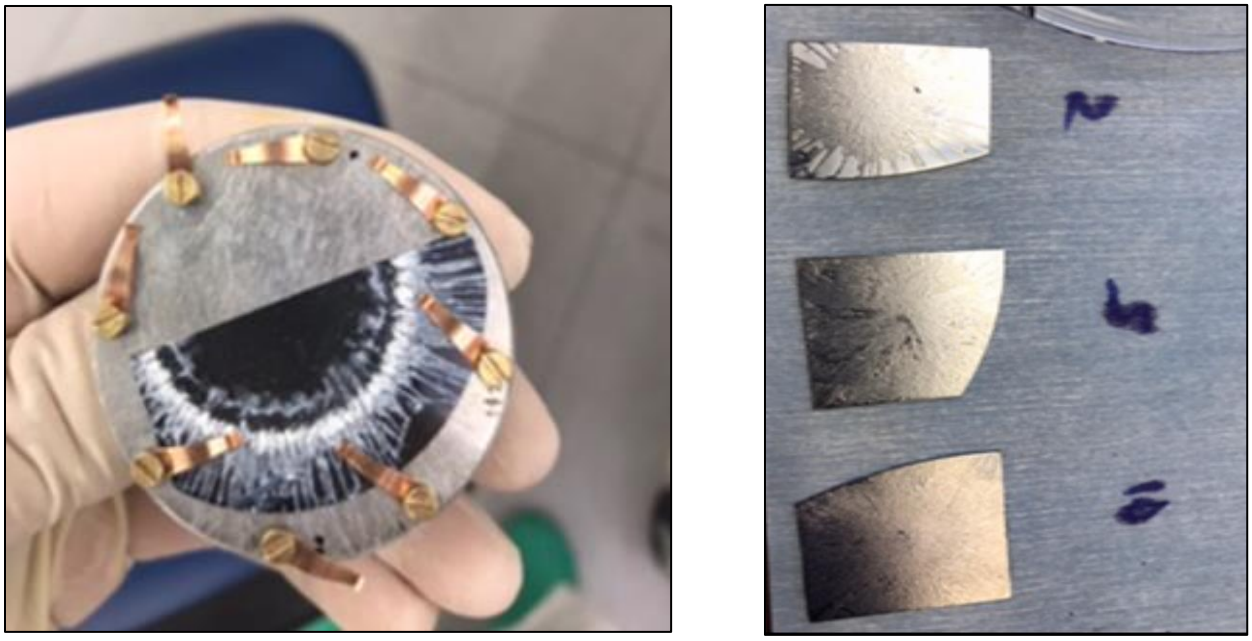

Figure 6.22. Deposition (left) insufficient solvent thickness vs. Depositions (right) with PEG

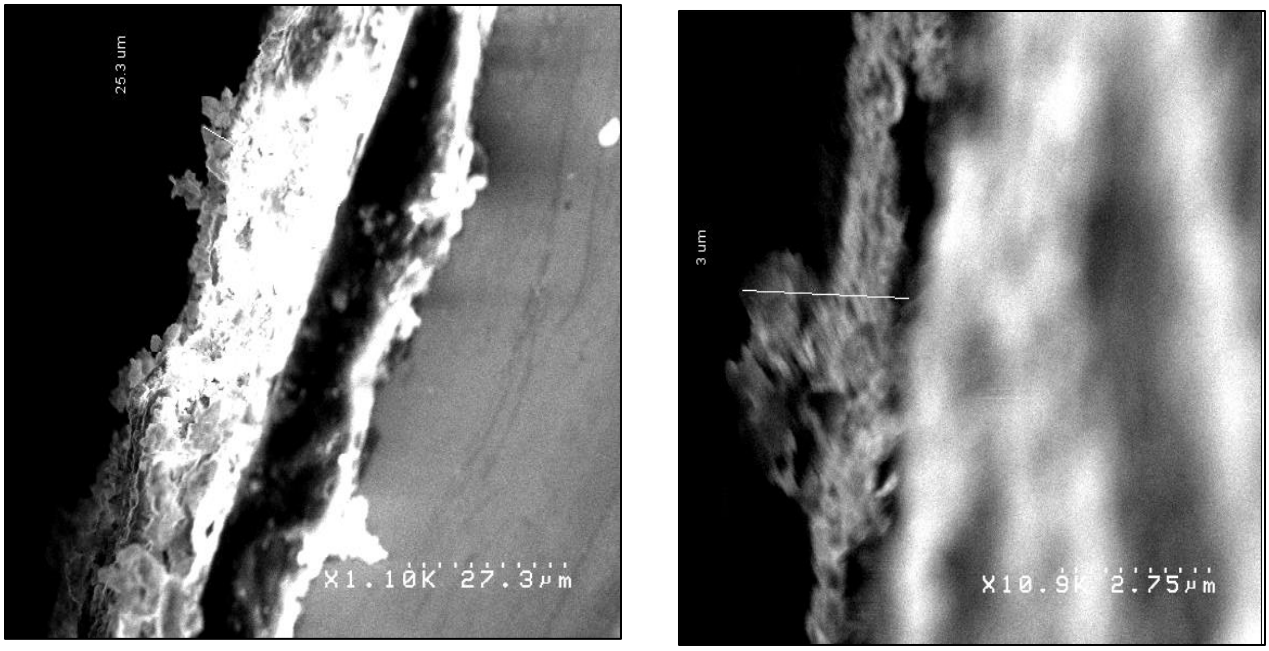

Figure 6.23. Left (0 RPM) vs. Right (3200 RPM) for 2 minute case

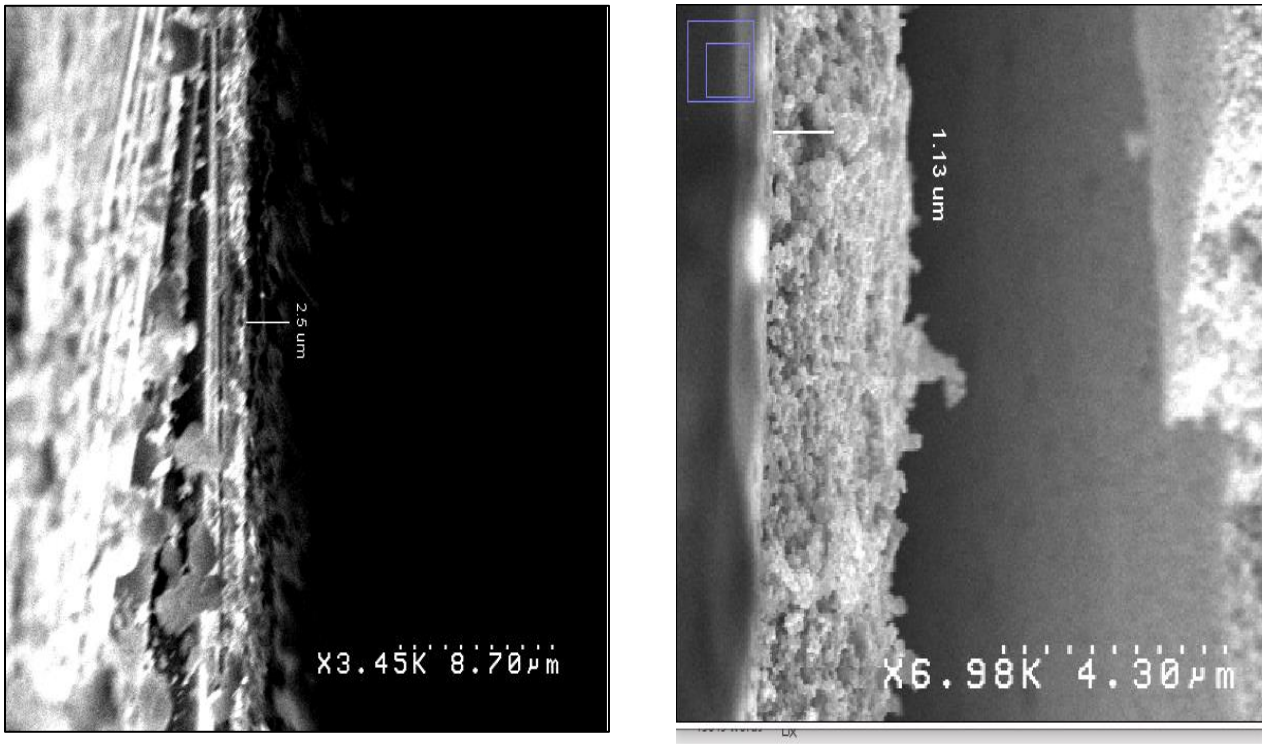

Figure 6.24. Left (5500 RPM) vs. Right (9000 RPM) for 2 minute case

From the above figures, it is noted that the average film thickness decreases with increases rotational velocity. The same dependency is also seen in the 5 minute and 10 minute cases as well. The following thickness vs. rpm plot was obtained (Figure 6.25).

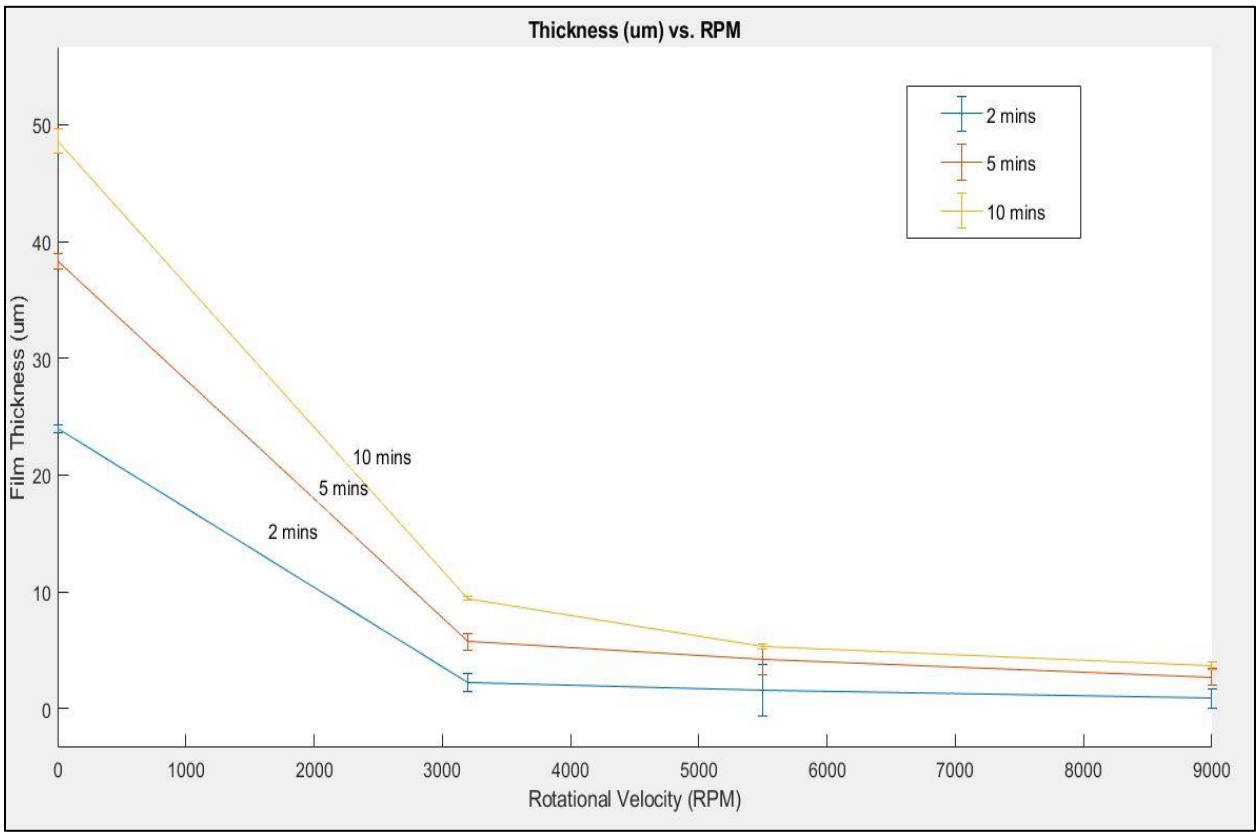

Figure 6.25. Film Thickness vs. RPM

Table 6.3. Thickness vs. RPM Data

RPM	**2 mins**	**5 mins**	**10 mins**
0	23.962 um	38.346 um	48.6 um
3200	2.212 um	5.731 um	9.426 um
5500	1.564 um	4.183 um	5.3 um
9000	0.877 um	2.68 um	3.674 um

6.6. Conclusion

In the work above, it has been demonstrated that Electrospray Deposition is a viable means for attaining ZnO thin and thick films. The effect of substrate rotation was thoroughly studied and quantified, demonstrating its profound affect on the thickness of ZnO depositions. The custom-made electrospray setup can be used for rapid and repeatable depositions onto silicon substrates. It was observed that the film thickness decayed exponentially with increase of rotational velocity. This trend was demonstrated for all the deposition times. In the instance of the 2 minute deposition time, sub-micron, thin-films were able to be obtained for rotational velocities approaching 9000 RPM. We have also developed a recipe for forming various sizes of ZnO nanoparticles and film thicknesses via control over the annealing times and durations. For decreased annealing temperatures observed at 30 minutes, 60 minutes, and 120 minutes, it was observed that the average nanoparticle size decreased by about 30-40 nm for the case of 30 and 60 minute with respect to the 120 minute anneal-time. A characterization of ZnO depositions via different electrospray modes was also conducted, showing the advantage of using the cone-jet mode over the dripping or microdripping modes.

The individual spray modes were characterized for various flow-rates to help determine what voltage was necessary to transition from mode to mode. All of the depositions above, unless otherwise noted, were carried out using the cone-jet mode which results in thinner attainable thicknesses in comparison with the other modes. In this work, we demonstrated a successful electrospray deposition technique from the characterization of these modes to the effect of annealing for nanostructure formation, to the quantification of the effect of RPM on the final thickness. These final thicknesses ranged from several tens of microns down to sub-micron

thicknesses. Overall, depositing ZnO through Electrospray is a low-cost, condition independent technique that can be utilized to achieve semiconducting films.

CHAPTER VII. SUMMARY AND RECOMMENDATIONS FOR FUTURE WORK

7.1. Recommendations for Future Work

Going forward, it would be advantageous to determine the absolute lower-limit on ZnO nanoparticle size that can be achieved while still sufficiently decomposing the precursor into the desired ZnO. This would allow for increased sensitivity for any future device applications such as gas-sensing technologies. In addition, a larger spanning profile on the effect of RPM should be carried out, with emphasis placed on the surface roughness in addition to the cross-sectional film thickness. This would allow for a more complete outlook on the scope of potential device level applications for the ZnO depositions.

APPENDIX. PERMISSION TO REPRINT FROM ACS PUBLICATIONS

1. Permission to use Figure 1.8 in the Thesis

JOHN WILEY AND SONS LICENSE TERMS AND CONDITIONS
Dec 01, 2020

This Agreement between Louisiana State University -- David Hooks ("You") and John Wiley and Sons ("John Wiley and Sons") consists of your license details and the terms and conditions provided by John Wiley and Sons and Copyright Clearance Center.

License Number	4950510081800
License date	Nov 15, 2020
Licensed Content Publisher	John Wiley and Sons
Licensed Content Publication	Wiley Books
Licensed Content Title	On the Mechanism of Electrospray Ionization Mass Spectrometry (ESIMS)
Licensed Content Author	Udo H. Verkerk, Paul Kebarle
Licensed Content Date	Nov 27, 2012
Licensed Content Pages	47
Type of use	Dissertation/Thesis
Requestor type	University/Academic
Format	Print and electronic
Portion	Figure/table
Number of figures/tables	1
Will you be translating?	No
Title	Electrospray Deposition of ZnO nanostructures and their Applications to Nanoscale Electronic Devices
Institution name	Louisiana State University
Expected presentation date	Nov 2020
Portions	Figure 1.8
Requestor Location	Louisiana State University 104 Downing St.

	LAFAYETTE, United Attn: Louisiana State University	LA	70506 States
Publisher Tax ID	EU826007151		
Total	0.00 USD		

Terms and Conditions

TERMS AND CONDITIONS

This copyrighted material is owned by or exclusively licensed to John Wiley & Sons, Inc. or one of its group companies (each a"Wiley Company") or handled on behalf of a society with which a Wiley Company has exclusive publishing rights in relation to a particular work (collectively "WILEY"). By clicking "accept" in connection with completing this licensing transaction, you agree that the following terms and conditions apply to this transaction (along with the billing and payment terms and conditions established by the Copyright Clearance Center Inc., ("CCC's Billing and Payment terms and conditions"), at the time that you opened your RightsLink account (these are available at any time at http://myaccount.copyright.com).

Terms and Conditions

- The materials you have requested permission to reproduce or reuse (the "Wiley Materials") are protected by copyright.

- You are hereby granted a personal, non-exclusive, non-sub licensable (on a stand-alone basis), non-transferable, worldwide, limited license to reproduce the Wiley Materials for the purpose specified in the licensing process. This license, **and any CONTENT (PDF or image file) purchased as part of your order,** is for a one-time use only and limited to any maximum distribution number specified in the license. The first instance of republication or reuse granted by this license must be completed within two years of the date of the grant of this license (although copies prepared before the end date may be distributed thereafter). The Wiley Materials shall not be used in any other manner or for any other purpose, beyond what is granted in the license. Permission is granted subject to an appropriate acknowledgement given to the author, title of the material/book/journal and the publisher. You shall also duplicate the copyright notice that appears in the Wiley publication in your use of the Wiley Material. Permission is also granted on the understanding that nowhere in the text is a previously published source acknowledged for all or part of this Wiley Material. Any third party content is expressly excluded from this permission.

- With respect to the Wiley Materials, all rights are reserved. Except as expressly granted by the terms of the license, no part of the Wiley Materials may be copied, modified, adapted (except for minor reformatting required by the new Publication), translated, reproduced, transferred or distributed, in any form or by any means, and no derivative works may be made based on the Wiley Materials without the prior permission of the respective copyright owner.**For STM Signatory Publishers**

clearing permission under the terms of the STM Permissions Guidelines only, the terms of the license are extended to include subsequent editions and for editions in other languages, provided such editions are for the work as a whole in situ and does not involve the separate exploitation of the permitted figures or extracts, You may not alter, remove or suppress in any manner any copyright, trademark or other notices displayed by the Wiley Materials. You may not license, rent, sell, loan, lease, pledge, offer as security, transfer or assign the Wiley Materials on a stand-alone basis, or any of the rights granted to you hereunder to any other person.

- The Wiley Materials and all of the intellectual property rights therein shall at all times remain the exclusive property of John Wiley & Sons Inc, the Wiley Companies, or their respective licensors, and your interest therein is only that of having possession of and the right to reproduce the Wiley Materials pursuant to Section 2 herein during the continuance of this Agreement. You agree that you own no right, title or interest in or to the Wiley Materials or any of the intellectual property rights therein. You shall have no rights hereunder other than the license as provided for above in Section 2. No right, license or interest to any trademark, trade name, service mark or other branding ("Marks") of WILEY or its licensors is granted hereunder, and you agree that you shall not assert any such right, license or interest with respect thereto

- NEITHER WILEY NOR ITS LICENSORS MAKES ANY WARRANTY OR REPRESENTATION OF ANY KIND TO YOU OR ANY THIRD PARTY, EXPRESS, IMPLIED OR STATUTORY, WITH RESPECT TO THE MATERIALS OR THE ACCURACY OF ANY INFORMATION CONTAINED IN THE MATERIALS, INCLUDING, WITHOUT LIMITATION, ANY IMPLIED WARRANTY OF MERCHANTABILITY, ACCURACY, SATISFACTORY QUALITY, FITNESS FOR A PARTICULAR PURPOSE, USABILITY, INTEGRATION OR NON-INFRINGEMENT AND ALL SUCH WARRANTIES ARE HEREBY EXCLUDED BY WILEY AND ITS LICENSORS AND WAIVED BY YOU.

- WILEY shall have the right to terminate this Agreement immediately upon breach of this Agreement by you.

- You shall indemnify, defend and hold harmless WILEY, its Licensors and their respective directors, officers, agents and employees, from and against any actual or threatened claims, demands, causes of action or proceedings arising from any breach of this Agreement by you.

- IN NO EVENT SHALL WILEY OR ITS LICENSORS BE LIABLE TO YOU OR ANY OTHER PARTY OR ANY OTHER PERSON OR ENTITY FOR ANY SPECIAL, CONSEQUENTIAL, INCIDENTAL, INDIRECT, EXEMPLARY OR PUNITIVE DAMAGES, HOWEVER CAUSED, ARISING OUT OF OR IN CONNECTION WITH THE DOWNLOADING, PROVISIONING, VIEWING OR USE OF THE MATERIALS REGARDLESS OF THE FORM OF ACTION, WHETHER FOR BREACH OF CONTRACT, BREACH OF WARRANTY, TORT,

NEGLIGENCE, INFRINGEMENT OR OTHERWISE (INCLUDING, WITHOUT LIMITATION, DAMAGES BASED ON LOSS OF PROFITS, DATA, FILES, USE, BUSINESS OPPORTUNITY OR CLAIMS OF THIRD PARTIES), AND WHETHER OR NOT THE PARTY HAS BEEN ADVISED OF THE POSSIBILITY OF SUCH DAMAGES. THIS LIMITATION SHALL APPLY NOTWITHSTANDING ANY FAILURE OF ESSENTIAL PURPOSE OF ANY LIMITED REMEDY PROVIDED HEREIN.

- Should any provision of this Agreement be held by a court of competent jurisdiction to be illegal, invalid, or unenforceable, that provision shall be deemed amended to achieve as nearly as possible the same economic effect as the original provision, and the legality, validity and enforceability of the remaining provisions of this Agreement shall not be affected or impaired thereby.

- The failure of either party to enforce any term or condition of this Agreement shall not constitute a waiver of either party's right to enforce each and every term and condition of this Agreement. No breach under this agreement shall be deemed waived or excused by either party unless such waiver or consent is in writing signed by the party granting such waiver or consent. The waiver by or consent of a party to a breach of any provision of this Agreement shall not operate or be construed as a waiver of or consent to any other or subsequent breach by such other party.

- This Agreement may not be assigned (including by operation of law or otherwise) by you without WILEY's prior written consent.

- Any fee required for this permission shall be non-refundable after thirty (30) days from receipt by the CCC.

- These terms and conditions together with CCC's Billing and Payment terms and conditions (which are incorporated herein) form the entire agreement between you and WILEY concerning this licensing transaction and (in the absence of fraud) supersedes all prior agreements and representations of the parties, oral or written. This Agreement may not be amended except in writing signed by both parties. This Agreement shall be binding upon and inure to the benefit of the parties' successors, legal representatives, and authorized assigns.

- In the event of any conflict between your obligations established by these terms and conditions and those established by CCC's Billing and Payment terms and conditions, these terms and conditions shall prevail.

- WILEY expressly reserves all rights not specifically granted in the combination of (i) the license details provided by you and accepted in the course of this licensing transaction, (ii) these terms and conditions and (iii) CCC's Billing and Payment terms and conditions.

- This Agreement will be void if the Type of Use, Format, Circulation, or Requestor Type was misrepresented during the licensing process.

- This Agreement shall be governed by and construed in accordance with the laws of the State of New York, USA, without regards to such state's conflict of law rules. Any legal action, suit or proceeding arising out of or relating to these Terms and Conditions or the breach thereof shall be instituted in a court of competent jurisdiction in New York County in the State of New York in the United States of America and each party hereby consents and submits to the personal jurisdiction of such court, waives any objection to venue in such court and consents to service of process by registered or certified mail, return receipt requested, at the last known address of such party.

WILEY OPEN ACCESS TERMS AND CONDITIONS

Wiley Publishes Open Access Articles in fully Open Access Journals and in Subscription journals offering Online Open. Although most of the fully Open Access journals publish open access articles under the terms of the Creative Commons Attribution (CC BY) License only, the subscription journals and a few of the Open Access Journals offer a choice of Creative Commons Licenses. The license type is clearly identified on the article.

The Creative Commons Attribution License

The Creative Commons Attribution License (CC-BY) allows users to copy, distribute and transmit an article, adapt the article and make commercial use of the article. The CC-BY license permits commercial and non-

Creative Commons Attribution Non-Commercial License

The Creative Commons Attribution Non-Commercial (CC-BY-NC)License permits use, distribution and reproduction in any medium, provided the original work is properly cited and is not used for commercial purposes.(see below)

Creative Commons Attribution-Non-Commercial-NoDerivs License

The Creative Commons Attribution Non-Commercial-NoDerivs License (CC-BY-NC-ND) permits use, distribution and reproduction in any medium, provided the original work is properly cited, is not used for commercial purposes and no modifications or adaptations are made. (see below)

Use by commercial "for-profit" organizations

Use of Wiley Open Access articles for commercial, promotional, or marketing purposes requires further explicit permission from Wiley and will be subject to a fee.

Further details can be found on Wiley Online Library http://olabout.wiley.com/WileyCDA/Section/id-410895.html

Other Terms and Conditions:

v1.10 Last updated September 2015

Questions? customercare@copyright.com or +1-855-239-3415 (toll free in the US) or +1-978-646-2777.

---

2. Permission to use Figure 1.1 in the Thesis

JOHN WILEY AND SONS LICENSE TERMS AND CONDITIONS
Dec 01, 2020

This Agreement between Louisiana State University -- David Hooks ("You") and John Wiley and Sons ("John Wiley and Sons") consists of your license details and the terms and conditions provided by John Wiley and Sons and Copyright Clearance Center.

License Number	4950510569513
License date	Nov 15, 2020
Licensed Content Publisher	John Wiley and Sons
Licensed Content Publication	Wiley Books
Licensed Content Title	General Properties of ZnO
Licensed Content Date	Sep 25, 2009
Licensed Content Pages	76
Type of use	Dissertation/Thesis
Requestor type	University/Academic
Format	Print and electronic
Portion	Figure/table

Number of figures/tables	1
Will you be translating?	No
Title	Electrospray Deposition of ZnO nanostructures and their Applications to Nanoscale Electronic Devices
Institution name	Louisiana State University
Expected presentation date	Nov 2020
Portions	Figure 1.1
Requestor Location	Louisiana State University 104 Downing St. LAFAYETTE, LA 70506 United States Attn: Louisiana State University
Publisher Tax ID	EU826007151
Total	0.00 USD

Terms and Conditions

TERMS AND CONDITIONS

This copyrighted material is owned by or exclusively licensed to John Wiley & Sons, Inc. or one of its group companies (each a"Wiley Company") or handled on behalf of a society with which a Wiley Company has exclusive publishing rights in relation to a particular work (collectively "WILEY"). By clicking "accept" in connection with completing this licensing transaction, you agree that the following terms and conditions apply to this transaction (along with the billing and payment terms and conditions established by the Copyright Clearance Center Inc., ("CCC's Billing and Payment terms and conditions"), at the time that you opened your RightsLink account (these are available at any time at http://myaccount.copyright.com).

Terms and Conditions

- The materials you have requested permission to reproduce or reuse (the "Wiley Materials") are protected by copyright.
- You are hereby granted a personal, non-exclusive, non-sub licensable (on a stand-alone basis), non-transferable, worldwide, limited license to reproduce the Wiley Materials for the purpose specified in the licensing process. This license, **and any CONTENT (PDF or image file) purchased as part of your order,** is for a one-time use only and limited to any maximum distribution number specified in the license. The first instance of republication or reuse granted by this license must be completed within two years of the date of the grant of this license (although copies prepared before the end date may be distributed thereafter). The Wiley Materials shall not be used in any other manner or for any other purpose, beyond what is granted in the license. Permission is granted subject to an appropriate acknowledgement given to the author, title of the material/book/journal and the publisher. You shall also duplicate the copyright notice that appears in the Wiley publication in your use of the Wiley

Material. Permission is also granted on the understanding that nowhere in the text is a previously published source acknowledged for all or part of this Wiley Material. Any third party content is expressly excluded from this permission.

- With respect to the Wiley Materials, all rights are reserved. Except as expressly granted by the terms of the license, no part of the Wiley Materials may be copied, modified, adapted (except for minor reformatting required by the new Publication), translated, reproduced, transferred or distributed, in any form or by any means, and no derivative works may be made based on the Wiley Materials without the prior permission of the respective copyright owner.**For STM Signatory Publishers clearing permission under the terms of the STM Permissions Guidelines only, the terms of the license are extended to include subsequent editions and for editions in other languages, provided such editions are for the work as a whole in situ and does not involve the separate exploitation of the permitted figures or extracts,** You may not alter, remove or suppress in any manner any copyright, trademark or other notices displayed by the Wiley Materials. You may not license, rent, sell, loan, lease, pledge, offer as security, transfer or assign the Wiley Materials on a stand-alone basis, or any of the rights granted to you hereunder to any other person.

- The Wiley Materials and all of the intellectual property rights therein shall at all times remain the exclusive property of John Wiley & Sons Inc, the Wiley Companies, or their respective licensors, and your interest therein is only that of having possession of and the right to reproduce the Wiley Materials pursuant to Section 2 herein during the continuance of this Agreement. You agree that you own no right, title or interest in or to the Wiley Materials or any of the intellectual property rights therein. You shall have no rights hereunder other than the license as provided for above in Section 2. No right, license or interest to any trademark, trade name, service mark or other branding ("Marks") of WILEY or its licensors is granted hereunder, and you agree that you shall not assert any such right, license or interest with respect thereto

- NEITHER WILEY NOR ITS LICENSORS MAKES ANY WARRANTY OR REPRESENTATION OF ANY KIND TO YOU OR ANY THIRD PARTY, EXPRESS, IMPLIED OR STATUTORY, WITH RESPECT TO THE MATERIALS OR THE ACCURACY OF ANY INFORMATION CONTAINED IN THE MATERIALS, INCLUDING, WITHOUT LIMITATION, ANY IMPLIED WARRANTY OF MERCHANTABILITY, ACCURACY, SATISFACTORY QUALITY, FITNESS FOR A PARTICULAR PURPOSE, USABILITY, INTEGRATION OR NON-INFRINGEMENT AND ALL SUCH WARRANTIES ARE HEREBY EXCLUDED BY WILEY AND ITS LICENSORS AND WAIVED BY YOU.

- WILEY shall have the right to terminate this Agreement immediately upon breach of this Agreement by you.

- You shall indemnify, defend and hold harmless WILEY, its Licensors and their respective directors, officers, agents and employees, from and against any actual or threatened claims, demands, causes of action or proceedings arising from any breach of this Agreement by you.

- IN NO EVENT SHALL WILEY OR ITS LICENSORS BE LIABLE TO YOU OR ANY OTHER PARTY OR ANY OTHER PERSON OR ENTITY FOR ANY SPECIAL, CONSEQUENTIAL, INCIDENTAL, INDIRECT, EXEMPLARY OR PUNITIVE DAMAGES, HOWEVER CAUSED, ARISING OUT OF OR IN CONNECTION WITH THE DOWNLOADING, PROVISIONING, VIEWING OR USE OF THE MATERIALS

REGARDLESS OF THE FORM OF ACTION, WHETHER FOR BREACH OF CONTRACT, BREACH OF WARRANTY, TORT, NEGLIGENCE, INFRINGEMENT OR OTHERWISE (INCLUDING, WITHOUT LIMITATION, DAMAGES BASED ON LOSS OF PROFITS, DATA, FILES, USE, BUSINESS OPPORTUNITY OR CLAIMS OF THIRD PARTIES), AND WHETHER OR NOT THE PARTY HAS BEEN ADVISED OF THE POSSIBILITY OF SUCH DAMAGES. THIS LIMITATION SHALL APPLY NOTWITHSTANDING ANY FAILURE OF ESSENTIAL PURPOSE OF ANY LIMITED REMEDY PROVIDED HEREIN.

- Should any provision of this Agreement be held by a court of competent jurisdiction to be illegal, invalid, or unenforceable, that provision shall be deemed amended to achieve as nearly as possible the same economic effect as the original provision, and the legality, validity and enforceability of the remaining provisions of this Agreement shall not be affected or impaired thereby.

- The failure of either party to enforce any term or condition of this Agreement shall not constitute a waiver of either party's right to enforce each and every term and condition of this Agreement. No breach under this agreement shall be deemed waived or excused by either party unless such waiver or consent is in writing signed by the party granting such waiver or consent. The waiver by or consent of a party to a breach of any provision of this Agreement shall not operate or be construed as a waiver of or consent to any other or subsequent breach by such other party.

- This Agreement may not be assigned (including by operation of law or otherwise) by you without WILEY's prior written consent.

- Any fee required for this permission shall be non-refundable after thirty (30) days from receipt by the CCC.

- These terms and conditions together with CCC's Billing and Payment terms and conditions (which are incorporated herein) form the entire agreement between you and WILEY concerning this licensing transaction and (in the absence of fraud) supersedes all prior agreements and representations of the parties, oral or written. This Agreement may not be amended except in writing signed by both parties. This Agreement shall be binding upon and inure to the benefit of the parties' successors, legal representatives, and authorized assigns.

- In the event of any conflict between your obligations established by these terms and conditions and those established by CCC's Billing and Payment terms and conditions, these terms and conditions shall prevail.

- WILEY expressly reserves all rights not specifically granted in the combination of (i) the license details provided by you and accepted in the course of this licensing transaction, (ii) these terms and conditions and (iii) CCC's Billing and Payment terms and conditions.

- This Agreement will be void if the Type of Use, Format, Circulation, or Requestor Type was misrepresented during the licensing process.

- This Agreement shall be governed by and construed in accordance with the laws of the State of New York, USA, without regards to such state's conflict of law rules. Any legal action, suit or proceeding arising out of or relating to these Terms and Conditions or the breach thereof shall be instituted in a court of competent jurisdiction in New York County in the

State of New York in the United States of America and each party hereby consents and submits to the personal jurisdiction of such court, waives any objection to venue in such court and consents to service of process by registered or certified mail, return receipt requested, at the last known address of such party.

WILEY OPEN ACCESS TERMS AND CONDITIONS

Wiley Publishes Open Access Articles in fully Open Access Journals and in Subscription journals offering Online Open. Although most of the fully Open Access journals publish open access articles under the terms of the Creative Commons Attribution (CC BY) License only, the subscription journals and a few of the Open Access Journals offer a choice of Creative Commons Licenses. The license type is clearly identified on the article.

The Creative Commons Attribution License

The Creative Commons Attribution License (CC-BY) allows users to copy, distribute and transmit an article, adapt the article and make commercial use of the article. The CC-BY license permits commercial and non-

Creative Commons Attribution Non-Commercial License

The Creative Commons Attribution Non-Commercial (CC-BY-NC)License permits use, distribution and reproduction in any medium, provided the original work is properly cited and is not used for commercial purposes.(see below)

Creative Commons Attribution-Non-Commercial-NoDerivs License

The Creative Commons Attribution Non-Commercial-NoDerivs License (CC-BY-NC-ND) permits use, distribution and reproduction in any medium, provided the original work is properly cited, is not used for commercial purposes and no modifications or adaptations are made. (see below)

Use by commercial "for-profit" organizations

Use of Wiley Open Access articles for commercial, promotional, or marketing purposes requires further explicit permission from Wiley and will be subject to a fee.

Further details can be found on Wiley Online Library http://olabout.wiley.com/WileyCDA/Section/id-410895.html

Other Terms and Conditions:

v1.10 Last updated September 2015

Questions? customercare@copyright.com or +1-855-239-3415 (toll free in the US) or +1-978-646-2777.

---

3. Permission to use Figure 1.8 in the Thesis

Rights DE <RIGHTS-and-LICENCES@wiley-vch.de>
Tue 12/1/2020 2:05 AM

Dear David,

About the Wiley-VCH Journal	
Journal Title	LSU Digital Commons
Year of Publication	2020
Volume and Issue Number	
Article Title (please include page numbers)	**Zinc Oxide: Fundamentals, Materials and Device Technology**
Author	- H. Morkoç, Ü. Özgür
Figure and Page Reference	1.1. (a, b., c.) pg. 2
Do you or your institute hold a current subscription to this journal?	yes
Are you the originial author of the requested material?	Yes

Where would you like to include our material?

About Your Publication	
Author / Editor	David Hooks/ Dr. Daniels-Race
Title of Publication	**Electrospray Deposition of ZnO Nanostructures for Future Nanoscale Electronic Applications**
Rights Required (eg. Print/ Electronic/ Translation, etc.)	Electronic/Print
Publisher	Louisiana State University
Publication Date	Dec-20
Medium (e.g. Book/Journal, Handout, CD Rom, Internet, etc.)	Internet/Paper Back

Print Run (hard back / paper back)	paper back
If Making Copies Please Include the Number of Copies You Wish to Make	
Retail Price	
Web address material will be posted on	LSU Digital Commons
Is the website password-protected?	yes

Tell us how to get in touch with you *(Please note that this will be where your invoice and/or permission will be addressed to. We are unable to send documents to more than one address):*

Please provide your full address details:

Name	David Hooks
Salutation	Mr.
Department	ECE
Job title	Graduate Student
Organisation	LSU
Street	104 Downing St.
Town	Lafayette
State / Province	Louisiana
Zip / Postal Code	70506
Country	United States
Telephone	337-308-7844
Fax	
Email	dhooks3@lsu.edu

We hereby grant permission for the requested use expected that due credit is given to the original source.

Any third party material is expressly excluded from this permission. If any of the material you wish to use appears within our work with credit to another source, authorization from that source must be obtained. Credit must include the following components:

- Books: Author(s)/ Editor(s) Name(s): Title of the Book. Page(s). Publication year. Copyright Wiley-VCH GmbH. Reproduced with permission.

This permission does not include the right to grant others permission to photocopy or otherwise reproduce this material except for accessible versions made by non-profit organizations serving the blind, visually impaired and other persons with print disabilities (VIPs).

Kind regards

Bettina Rights & **Loycke**
Senior Rights Manager
Rights Licenses

Wiley-VCH GmbH
Boschstraße 12
69469 Weinheim
Germany
www.wiley-vch.de

T +(49) 6201 606-280
F +(49) 6201 606-332
rightsDE@wiley.com

REFERENCES.

[1] Giessibl, F. J. (2003). "Advances in atomic force microscopy." Reviews of modern physics 75(3): 949

[2] Zhang, D. (1995). "Fast photoresponse and the related change of crystallite barriers for ZnO films deposited by RF sputtering." Journal of Physics D: Applied Physics 28(6): 1273.

[3] Vayssieres, L., Keis, K., Lindquist, S. E., & Hagfeldt, A. (2001). Purpose-built anisotropic metal oxide material: 3D highly oriented microrod array of ZnO. The Journal of Physical Chemistry B, 105(17), 3350-3352.

[4] Li, Z., Liu, P., Yun, G., Shi, K., Lv, X., Li, K., ... & Yang, B. (2014). 3D (Three-dimensional) sandwich-structured of ZnO (zinc oxide)/rGO (reduced graphene oxide)/ZnO for high performance supercapacitors. Energy, 69, 266-271.

[5] Tian, W., Zhang, C., Zhai, T., Li, S. L., Wang, X., Liu, J., ... & Golberg, D. (2014). Flexible ultraviolet photodetectors with broad photoresponse based on branched ZnS-ZnO heterostructure nanofilms. Advanced Materials, 26(19), 3088-3093.

[6] Zhang, H., Chen, W. G., Li, Y. Q., & Song, Z. H. (2018). Gas Sensing Performances of ZnO Hierarchical Structures for Detecting Dissolved Gases in Transformer Oil: A Mini Review. Frontiers in chemistry, 6, 508.

[7] Hosono, H., Ohta, H., Orita, M., Ueda, K., & Hirano, M. (2002). Frontier of transparent conductive oxide thin films. Vacuum, 66(3-4), 419-425.

[8] Xi, J., Zhang, Q., Myers, D., Cao, G., & Sun, Y. (2012). Hollow hemispherical titanium dioxide aggregates fabricated by coaxial electrospray for dye-sensitized solar cell application. Journal of Nanophotonics, 6(1), 063519.

[9] Yang, F., Wang, X., Fan, H., Tang, Y., Yang, J., & Yu, J. (2017). Effect of In Situ Annealing Treatment on the Mobility and Morphology of TIPS-Pentacene-Based Organic Field-Effect Transistors. Nanoscale Research Letters, 12(1), 1-7.

[10] Liu, L., Mei, Z., Tang, A., Azarov, A., Kuznetsov, A., Xue, Q. K., & Du, X. (2016). Oxygen vacancies: The origin of n-type conductivity in ZnO. Physical Review B, 93(23), 235305.

[11] Janotti, A. and C. G. Van de Walle (2009). "Fundamentals of zinc oxide as a semiconductor." Reports on progress in physics 72(12): 126501.

[12] Morkoç, H. and Ü. Özgür (2008). Zinc oxide: fundamentals, materials and device technology. 2. John Wiley & Sons.

[13] Pan, J., Chen, J., Huang, Q., Khan, Q., Liu, X., Tao, Z., ... & Nathan, A. (2016). Size tunable ZnO nanoparticles to enhance electron injection in solution processed QLEDs. *ACS photonics*, *3*(2), 215-222.

[14] Idriss, H. and M. Barteau (1992). "Photoluminescence from zinc oxide powder to probe adsorption and reaction of O {sub 2}, CO, H {sub 2}, HCOOH, and CH {sub 3} OH." Journal of Physical Chemistry 96(8).

[15] Clementi, C., Rosi, F., Romani, A., Vivani, R., Brunetti, B. G., & Miliani, C. (2012). Photoluminescence properties of zinc oxide in paints: a study of the effect of self-absorption and passivation. *Applied spectroscopy*, *66*(10), 1233-1241.

[16] Penfold, T. J., Szlachetko, J., Santomauro, F. G., Britz, A., Gawelda, W., Doumy, G., ... & Chergui, M. (2018). Revealing hole trapping in zinc oxide nanoparticles by time-resolved X-ray spectroscopy. *Nature communications*, *9*(1), 1-9.

[17] Jeong, S., Oh, S. K., Ryou, J. H., Ahn, K. S., Song, K. M., & Kim, H. (2018). Monolithic inorganic ZnO/GaN semiconductors heterojunction white light-emitting diodes. *ACS applied materials & interfaces*, *10*(4), 3761-3768.

[18] Zheng, G., Zhu, P., Sun, L., Jiang, J., Liu, J., Wang, X., & Li, W. (2016). Thin film zinc oxide gas sensor fabricated using near-field electrospray. *AIP Advances*, *6*(12), 125306.

[19] Borysiewicz, Michał A. "ZnO as a functional material, a review." *Crystals* 9.10 (2019): 505.

[20] Van de Walle, C. G. (2000). "Hydrogen as a cause of doping in zinc oxide." Physical review letters 85(5): 1012.

[21] Liu, X., Wu, X., Cao, H., & Chang, R. P. H. (2004). Growth mechanism and properties of ZnO nanorods synthesized by plasma-enhanced chemical vapor deposition. Journal of Applied Physics, 95(6), 3141-3147.

[22] Yang, J. L., An, S. J., Park, W. I., Yi, G. C., & Choi, W. (2004). Photocatalysis using ZnO thin films and nanoneedlesgrown by metal–organic chemical vapor deposition. Advanced materials, 16(18), 1661-1664.

[23] Zhang, B. P., Binh, N. T., Segawa, Y., Wakatsuki, K., & Usami, N. (2003).
Optical properties of ZnO rods formed by metalorganic chemical vapor deposition.
Applied Physics Letters, 83(8), 1635-1637.

[24] Deng, H., Russell, J. J., Lamb, R. N., Jiang, B., Li, Y., & Zhou, X. Y. (2004).
Microstructure control of ZnO thin films prepared by single source chemical vapor deposition.
Thin Solid Films, 458(1-2), 43-46.

[25] Hwang, N. M. (2016). Non-classical crystallization of thin films and nanostructures in CVD and PVD processes (Vol. 60). Springer

[26] Orton, J. W., & Foxon, T. (2015). Molecular beam epitaxy: a short history. Oxford University Press, USA..

[27] Ohgaki, T., Kawamura, Y., Kuroda, T., Ohashi, N., Adachi, Y., Tsurumi, T., ... & Haneda, H. (2003). Optical properties of heavily aluminum-doped zinc oxide thin films prepared by molecular beam epitaxy. In *Key Engineering Materials* (Vol. 248, pp. 91-94). Trans Tech Publications Ltd.

[28] Fischer, J., von Freymann, G., & Wegener, M. (2010). The materials challenge in diffraction-unlimited direct-laser-writing optical lithography. Advanced materials, 22(32), 3578-3582.

[29] Leskelä, M., & Ritala, M. (2003). Atomic layer deposition chemistry: recent developments and future challenges. *Angewandte Chemie International Edition*, *42*(45), 5548-5554.

[30] Johnson, R. W., Hultqvist, A., & Bent, S. F. (2014). A brief review of atomic layer deposition: from fundamentals to applications. *Materials today*, *17*(5), 236-246.

[31] Huby, N., Ferrari, S., Guziewicz, E., Godlewski, M., & Osinniy, V. (2008). Electrical behavior of zinc oxide layers grown by low temperature atomic layer deposition. *Applied Physics Letters*, *92*(2), 023502.

[32] J. Böhlmark, "Fundamentals of High Power Impulse Magnetron Sputtering," PhD dissertation, Institutionen för fysik, kemi och biologi, 2006.

[33] Park, K. C., Ma, D. Y., & Kim, K. H. (1997). The physical properties of Al-doped zinc oxide films prepared by RF magnetron sputtering. *Thin solid films*, *305*(1-2), 201-209.

[34] Saji, V. S., & Cook, R. M. (Eds.). (2012). *Corrosion protection and control using nanomaterials*. Elsevier.

[35] Lamia, Z. (2010). Sol–gel-deposited ZnO thin films. *Materials Science and Engineering B*, *174*, 18-30.

[36] García-Farrera, B., & Velásquez-García, L. F. (2019). Ultrathin ceramic piezoelectric films via room-temperature electrospray deposition of ZnO nanoparticles for printed GHz devices. *ACS applied materials & interfaces*, *11*(32), 29167-29176.\

[37] Mishra, Y. K., & Adelung, R. (2018). ZnO tetrapod materials for functional applications. *Materials Today*, *21*(6), 631-651.

[38] Ghosh, S., & Basak, D. (2017). A simple process step for tuning the optical emission and ultraviolet photosensing properties of sol–gel ZnO film. *RSC advances*, *7*(2), 694-703.

[39] Bah, A., Lim, K. Y., Wei, F., Khursheed, A., & Sow, C. H. (2019). Fluorescence Invigoration in Carbon-Incorporated Zinc oxide Nanowires from passage of Field emission electrons. *Scientific reports*, *9*(1), 1-12.

[40] Reimann, K., Steube, M., Fröhlich, D., & Clarke, S. J. (1998). Exciton binding energies and band gaps in GaN bulk crystals. *Journal of crystal growth*, *189*, 652-655.

[41] Janotti, A., & Van de Walle, C. G. (2009). Fundamentals of zinc oxide as a semiconductor. *Reports on progress in physics*, *72*(12), 126501.

[42] Chaudhary, S., Umar, A., Bhasin, K. K., & Baskoutas, S. (2018). Chemical sensing applications of ZnO nanomaterials. *Materials*, *11*(2), 287.

[43] Zhang, H., Chen, W. G., Li, Y. Q., & Song, Z. H. (2018). Gas Sensing Performances of ZnO Hierarchical Structures for Detecting Dissolved Gases in Transformer Oil: A Mini Review. *Frontiers in chemistry*, *6*, 508.

[44] Joshi, T., Kumar, A., Prakash, J., & Biradar, A. M. (2010). Low power operation of ferroelectric liquid crystal system dispersed with zinc oxide nanoparticles. *Applied Physics Letters*, *96*(25), 253109.

[45] Marinov, G., Lovchinov, K., Madjarova, V., Strijkova, V., Vasileva, M., Malinowski, N., & Babeva, T. (2019). Aluminum-doped zinc oxide thin films deposited by electrospray method. *Optical Materials*, *89*, 390-395.

[46] Hirao, T., Furuta, M., Furuta, H., Matsuda, T., Hiramatsu, T., Hokari, H., ... & Kakegawa, M. (2007). Novel top-gate zinc oxide thin-film transistors (ZnO TFTs) for AMLCDs. *Journal of the Society for Information Display*, *15*(1), 17-22.

[47] Barquinha, P., Pimentel, A., Marques, A., Pereira, L., Martins, R., & Fortunato, E. (2006). Influence of the semiconductor thickness on the electrical properties of transparent TFTs based on indium zinc oxide. *Journal of non-crystalline solids*, *352*(9-20), 1749-1752.

[48] Park, K., Lee, D. K., Kim, B. S., Jeon, H., Lee, N. E., Whang, D., ... & Ahn, J. H. (2010). Stretchable, transparent zinc oxide thin film transistors. *Advanced Functional Materials*, *20*(20), 3577-3582.

[49] Stadler, A. (2012). Transparent conducting oxides—an up-to-date overview. *Materials*, *5*(4), 661-683.

[50] Transparent Conducting Oxides. Materion. https://materion.com/-/media/files/advanced-materials-group/me/technicalpapers/transparentconductiveoxidethinfilms.pdf

[51] Rahman, F. (2019). Zinc oxide light-emitting diodes: a review. *Optical Engineering*, *58*(1), 010901.

[52] Zhang, S. G., Zhang, X. W., Yin, Z. G., Wang, J. X., Dong, J. J., Wang, Z. G., ... & Chow, P. P. (2011). Improvement of electroluminescent performance of n-ZnO/AlN/p-GaN light-emitting diodes by optimizing the AlN barrier layer. *Journal of Applied Physics*, *109*(9), 093708.

[53] Fan, J. C., Chang, S. L., & Xie, Z. ZnO-Based Light-Emitting Diodes Optoelectronics-Advanced Materials and Devices.

[54] Mosca, M., Macaluso, R., Caruso, F., Muzzo, V. L., Calì, C., Adorno, D. P., & Pokutnyi, S. (2015). The p-type doping of ZnO: Mirage or reality?. In *Advances in semiconductor research: physics of nanosystems, spintronics and technological applications* (pp. 245-282). Nova Science Publishers.

[55] To, C. K., Yang, B., Su, S. C., Ling, C. C., Beling, C. D., & Fung, S. (2011). Post-growth annealing induced change of conductivity in As-doped ZnO grown by radio frequency magnetron sputtering. *Journal of Applied Physics*, *110*(11), 113521.

[56] Liu, K., Sakurai, M., & Aono, M. (2010). ZnO-based ultraviolet photodetectors. *Sensors*, *10*(9), 8604-8634.

[57] Khokhra, R., Bharti, B., Lee, H. N., & Kumar, R. (2017). Visible and UV photo-detection in ZnO nanostructured thin films via simple tuning of solution method. *Scientific reports*, *7*(1), 1-14.

[58] Ghosh, S. P., Das, K. C., Tripathy, N., Bose, G., Kim, D. H., Lee, T. I., ... & Kar, J. P. (2016, February). Ultraviolet photodetection characteristics of Zinc oxide thin films and nanostructures. In *IOP Conf. Ser. Mater. Sci. Eng* (Vol. 115, No. 1, p. 25).

[59] Qin, L., Shing, C., & Sawyer, S. (2010). Metal–semiconductor–metal ultraviolet photodetectors based on zinc-oxide colloidal nanoparticles. *IEEE electron device letters*, *32*(1), 51-53.

[60] Seiler, H. (1983). Secondary electron emission in the scanning electron microscope. *Journal of Applied Physics*, *54*(11), R1-R18.

[61] Howell, P. G. T., Davy, K. M. W., & Boyde, A. (1998). Mean atomic number and backscattered electron coefficient calculations for some materials with low mean atomic number. *Scanning: The Journal of Scanning Microscopies*, *20*(1), 35-40.

[62] De Vlaemynck, T. (2018). Study of the effect of solvent and molecular weight of TQ1 on the morphology of TQ1: PC60BM and TQ1: PC70BM spin coated systems.

[63] Snow, E. S., Park, D., & Campbell, P. M. (1996). Single-atom point contact devices fabricated with an atomic force microscope. *Applied Physics Letters*, *69*(2), 269-271.

[64] Giessibl, F. J. (2003). Advances in atomic force microscopy. *Reviews of modern physics*, *75*(3), 949.

[65] Eaton, P., & West, P. (2010). *Atomic force microscopy*. Oxford university press.

[66] Meyer, E. R. N. S. T. (1992). Atomic force microscopy. Progress in surface science, 41(1), 3-49.

[67] Barron, A. R. (2015). Physical methods in chemistry and nano science.

[68] Dumont, Q., & Cole, R. B. (2014). Jean-Antoine Nollet: The father of experimental electrospray. *Mass spectrometry reviews*, *33*(6), 418-423.

[69] Meher, A. K., & Chen, Y. C. (2017). Electrospray modifications for advancing mass spectrometric analysis. *Mass Spectrometry*, *6*(2), S0057-S0057.

[70] Rayleigh, L. (1882). XX. On the equilibrium of liquid conducting masses charged with electricity. *The London, Edinburgh, and Dublin Philosophical Magazine and Journal of Science*, *14*(87), 184-186.

[71] Wang, X., Lin, J., Jiang, J., Guo, S., Li, W., & Zheng, G. (2018). Continuous Near-Field Electrospraying Using a Glass Capillary Nozzle. *Micromachines*, *9*(2), 56.

[72] Thompson, J. W., Eschelbach, J. W., Wilburn, R. T., & Jorgenson, J. W. (2005). Investigation of electrospray ionization and electrostatic focusing devices using a three-dimensional electrospray current density profiler. *Journal of the American Society for Mass Spectrometry*, *16*(3), 312-323.

[73] Jaworek, A. (2007). Electrospray droplet sources for thin film deposition. *Journal of materials science*, *42*(1), 266-297.

[74] Dole, M., Cox Jr, H. L., & Gieniec, J. (1973). Electrospray mass spectroscopy.

[75] Iribarne, J. V., & Thomson, B. A. (1976). On the evaporation of small ions from charged droplets. *The Journal of chemical physics*, *64*(6), 2287-2294.

[76] Kebarle, P., & Verkerk, U. H. (2000). A Brief Overview of the mechanisms involved in electrospray mass spectrometry. *Reactive Intermediates: MS Investigations in Solution (Ed. Santos, LS)*, 1-35.

[77] Jaworek, A. T. S. A., & Sobczyk, A. T. (2008). Electrospraying route to nanotechnology: An overview. *Journal of electrostatics*, *66*(3-4), 197-219.

[78] Kebarle, P., & Verkerk, U. H. (2010). On the mechanism of electrospray ionization mass spectrometry (ESIMS). *Electrospray and MALDI mass spectrometry: fundamentals, instrumentation, practicalities, and biological applications*, 1-48.

[79] Jaworek, A., & Krupa, A. (1998, June). Main modes of electrohydrodynamic spraying of liquids. In *Third International Conference on multiphase Flow* (pp. 8-12).

[80] Park, I., Kim, W., & Kim, S. S. (2011). Multi-jet mode electrospray for non-conducting fluids using two fluids and a coaxial grooved nozzle. *Aerosol Science and Technology*, *45*(5), 629-634.

[81] Duby, M. H., Deng, W., Kim, K., Gomez, T., & Gomez, A. (2006). Stabilization of monodisperse electrosprays in the multi-jet mode via electric field enhancement. *Journal of Aerosol Science*, *37*(3), 306-322.

[82] Morad, M. R., Rajabi, A., Razavi, M., & Sereshkeh, S. P. (2016). A very stable high throughput Taylor cone-jet in electrohydrodynamics. *Scientific reports*, *6*, 38509.

[83] Gan, Y., Jiang, Z., Li, H., Luo, Y., Chen, X., Shi, Y., ... & Yan, Y. (2019). A comparative study on droplet characteristics and specific charge of ethanol in two small-scale electrospray systems. *Scientific Reports*, *9*(1), 1-12.

[84] Sun, D., Chang, C., Li, S., & Lin, L. (2006). Near-field electrospinning. *Nano letters*, *6*(4), 839-842.

[85] Zheng, G., Zhu, P., Sun, L., Jiang, J., Liu, J., Wang, X., & Li, W. (2016). Thin film zinc oxide gas sensor fabricated using near-field electrospray. *AIP Advances*, *6*(12), 125306.

[86] Li, W., Zheng, G., Xu, L., & Wang, X. (2016). Fabrication of micro-patterns via near-field electrospray. *AIP Advances*, *6*(11), 115002.

[87] Jiang, J., Zheng, G., Zhu, P., Liu, J., Liu, Y., Wang, X., ... & Guo, S. (2018). Controlling of Electrospray Deposition for Micropatterns. *Micromachines*, *9*(2), 72.

[88] Song, W., & Shumlak, U. (2010). Ultrasonically aided electrospray source for charged particles approaching monodisperse distributions. *Journal of Propulsion and Power*, *26*(2), 353-363.

[89] Yang, F., Wang, X., Fan, H., Tang, Y., Yang, J., & Yu, J. (2017). Effect of In Situ Annealing Treatment on the Mobility and Morphology of TIPS-Pentacene-Based Organic Field-Effect Transistors. *Nanoscale Research Letters*, *12*(1), 1-7.

[90] Pitsalidis, C., Pappa, A. M., Hunter, S., Laskarakis, A., Kaimakamis, T., Payne, M. M., ... & Logothetidis, S. (2016). High mobility transistors based on electrospray-printed small-molecule/polymer semiconducting blends. *Journal of Materials Chemistry C*, *4*(16), 3499-3507.

[91] Mahmood, K., Mehran, M. T., Rehman, F., Zafar, M. S., Ahmad, S. W., & Song, R. H. (2018). Electrosprayed polymer-hybridized multidoped ZnO mesoscopic nanocrystals yield highly efficient and stable perovskite solar cells. *ACS omega*, *3*(8), 9648-9657.

[92] Bu, I. Y., Fu, Y. S., Li, J. F., & Guo, T. F. (2017). Large-area electrospray-deposited nanocrystalline Cu XO hole transport layer for perovskite solar cells. *RSC advances*, *7*(74), 46651-46656.

[93] Xi, J., Zhang, Q., Myers, D., Cao, G., & Sun, Y. (2012). Hollow hemispherical titanium dioxide aggregates fabricated by coaxial electrospray for dye-sensitized solar cell application. *Journal of Nanophotonics*, *6*(1), 063519.

[94] Jiang, Y., Wu, C., Li, L., Wang, K., Tao, Z., Gao, F., ... & Deng, W. (2018). All electrospray printed perovskite solar cells. *Nano energy*, *53*, 440-448.

[95] Li, W., Zheng, G., Xu, L., & Wang, X. (2016). Fabrication of micro-patterns via near-field electrospray. *AIP Advances*, *6*(11), 115002.

[96] Li, W., Lin, J., Wang, X., Jiang, J., Guo, S., & Zheng, G. (2018). Electrospray deposition of ZnO thin films and its application to gas sensors. *Micromachines*, *9*(2), 66.

[97] Jasek, K., Pasternak, M., Grabka, M., Neffe, S., & Zasada, D. (2017). Deposition of Polymer Sensor Films on SAW Surface by Electrospraying Technology. *Archives of Acoustics*, *42*(3), 507-513.

[98] Maulik, S. (2018). Voltage-Controlled Deposition of Nanoparticles for Next Generation Electronic Materials.

[99] Go, D. B., Atashbar, M. Z., Ramshani, Z., & Chang, H. C. (2017). Surface acoustic wave devices for chemical sensing and microfluidics: a review and perspective. *Analytical methods*, *9*(28), 4112-4134.

VITA

David Hooks was born in November 1994 in Opelousas, Louisiana, which is located in southwestern Louisiana. He finished his bachelors degree in December, 2017 from the University of Louisiana at Lafayette in Electrical Engineering with a minor in Mathematics. He has been enrolled in the ECE graduate program at LSU since January 2018 where he set out to achieve a Masters in Electrical Engineering, studying semiconductor materials. The focus of his research was in the deposition and characterization of Zinc Oxide Nanostructures for future electronic applications. He plans on receiving his M.S. in Electrical Engineering in May of 2021.